

PhD thesis

School of Chemistry

Cardiff University



**From glucose to γ -valerolactone: development
of novel catalytic methodologies**

Thesis submitted in accordance with the requirements of Cardiff

University for the degree of Doctor of Philosophy by

Igor Aleksander Orłowski

2019

Summary

The body of work presented in this thesis focuses on the conversion pathway from glucose to γ -valerolactone (GVL). GVL has been identified as a potential fuel additive, and the developments in this thesis contribute towards making it a more sustainable process.

There are two results chapters in this thesis, chapter 3 and 4s; the first one explores the dehydration of glucose to methyl levulinate. A range of solid acid catalysts was evaluated. Efforts were taken to limit the polymerisation side reaction by changing reaction conditions and introducing methanol as a solvent, as opposed to the typically used water. It was found that the polymerisation greatly depends on the concentration of substrate. Reducing the polymerisation is crucial, as they not only reduce the carbon balance, but adsorb on the catalyst surface, reducing re-usability.

The second results chapter tackles the hydrogenation of levulinic acid to γ -valerolactone with the use of Cu-ZrO₂ catalysts. A novel catalyst preparation method was developed which allowed to reduce the copper loading from 50% mol. to 30% while retaining high activity. The surface species were investigated and it was found that well-dispersed copper particles with strong metal-support interactions are the most active for this reaction. Steps were taken to maximise the number of those sites, such as optimising the reduction conditions and acid washing the labile copper off the surface. Mechanistic studies were also carried out to prove that H₂O from the solvent is critically involved in the hydrogenation mechanism.

Acknowledgments

Firstly, I would like to thank Professor Graham Hutchings for giving me the opportunity to conduct this research as part of the Cardiff Catalysis Institute. His guidance throughout the project was of great help. I would like to acknowledge every member of the international NOVACAM team – specifically Daniel Jones, Mark Douthwaite, Jun Hirayama, Satoshi Ishikawa. They all had immense input into making the project as successful as it was.

I would like to thank all my supervisors and colleagues who helped me improve as a chemist and as a person. Dr David Willock, Dr James Hayward, Dr Thomas Davies, Dr Samuel Pattison, Dr Ewa Nowicka, Dr Richard Lewis. Your help was invaluable. A thank you to the workshop and departmental staff who made the labs run smoothly and fixed all our issues on time.

I would like to extend a very special thanks to Mark Douthwaite, without who this thesis would not have been possible.

I would like to thank all of the members of CCI “rigade” who made my time at the institution fun.

I would like to thank Leah Williams who made me a better person and got me through the worst days; my friends and family who always supported me in everything I do.

Declarations

STATEMENT 1

This thesis is being submitted in partial fulfilment of the requirements for the degree of PhD.

Signed _____

Date _____

STATEMENT 2

This work has not been submitted in substance for any other degree or award at this or any other university or place of learning, nor is it being submitted concurrently for any other degree or award (outside of any formal collaboration agreement between the University and a partner organisation)

Signed _____

Date _____

STATEMENT 3

I hereby give consent for my thesis, if accepted, to be available in the University's Open Access repository (or, where approved, to be available in the University's library and for inter-library loan), and for the title and summary to be made available to outside organisations, subject to the expiry of a University-approved bar on access if applicable.

Signed _____

Date _____

DECLARATION

This thesis is the result of my own independent work, except where otherwise stated, and the views expressed are my own. Other sources are acknowledged by explicit references. The thesis has not been edited by a third party beyond what is permitted by Cardiff University's Use of Third Party Editors by Research Degree Students Procedure.

Signed _____

Date _____

WORD COUNT _____

(Excluding summary, acknowledgments, declarations, contents pages, appendices, tables, diagrams and figures, references, bibliography, footnotes and endnotes)

Table of contents

1.1. An introduction to catalysis	1
1.2. Biomass.....	3
1.3. Dehydration of glucose	4
1.4. Hydrogenation of levulinic acid.....	7
1.5. Aims of the thesis.....	11
1.6. References.....	12
2.1. Materials	17
2.2. Catalyst preparation	18
2.2.1. Preparation of Cu-ZrO ₂ catalysts	18
2.2.1.1. Co-precipitation	18
2.2.1.2. Oxalate gel precipitation	19
2.2.1.2.1. Doping Cu-ZrO ₂ catalysts with manganese	20
2.2.1.3. pH gradient precipitation	20
2.2.1.4. Preparation of SO ₄ -ZrO ₂ catalysts	21
2.2.1.5. Treatment of zeolites.....	22
2.2.1.6. Silylation of zeolites	22
2.2.1.7. Preparation of phosphated zirconia.....	22
2.2.1.8. Preparation of CeO ₂	23
2.2.1.9. Preparation of SO ₄ -CeO ₂	23
2.2.1.10. Preparation of 15% WO ₃ -ZrO ₂	23
2.3. Catalyst testing.....	23
2.3.1. Hydrogenation of levulinic acid to γ -valerolactone	23
2.3.2. Conversion of glucose and methyl glucosides to methyl levulinate	24
2.3.3. Re-use testing of Cu-ZrO ₂ catalysts.....	24
2.3.4. Re-use testing of zeolites	25
2.4. Analytical techniques.....	25
2.4.1. Gas chromatography	25
2.4.2. High Performance Liquid Chromatography (HPLC).....	30
2.4.3. Nuclear magnetic resonance (NMR) spectroscopy.....	33
2.4.4. Gas chromatography-mass spectrometry (GC-MS).....	34
2.4.5. Calculation of yields and conversions	35
2.5. Catalyst characterisation	36
2.5.1. Bruanuer-Emmett-Teller (BET) surface area analysis.....	36
2.5.2. X-ray diffraction	38

2.5.3. Temperature-programmed reduction	39
2.5.4. Diffuse reflectance infrared fourier transform (DRIFTS) analysis	39
2.5.5. Microwave plasma atomic emission spectroscopy (MPAES)	40
2.5.6. Scanning electron microscopy (SEM)	40
2.5.7. Copper surface area measurement by N ₂ O titration.....	41
2.5.8. Ammonia temperature programmed desorption	41
2.5.9. References.....	42
3.1. Introduction.....	43
3.2. Results and discussion	44
3.2.1. Conversion of glucose to methyl glucoside	44
3.2.2. Dehydration of methyl glucoside using solid acids	49
3.2.3. Dehydration of methyl glucoside using zeolites	62
3.2.4. Humins and reaction optimisation	69
3.2.5. Conclusions.....	82
3.2.6. References.....	85
4.1. Introduction.....	91
4.2. Results and discussion	92
4.2.1. Manual preparation	92
4.2.2. Automated preparation.....	101
4.2.3. Acid wash of the catalyst	109
4.2.4. Effect of reduction treatment on catalyst activity	113
4.2.4. Kinetic analysis of 30% Cu-ZrO ₂	120
4.2.5. Mechanistic studies	122
4.3. Conclusions.....	138
4.4. References.....	140
5.1. Conversion of methyl glucoside to methyl levulinate using solid acid catalysts	143
5.2. Conversion of levulinic acid to γ -valerolactone using Cu-ZrO ₂ catalysts	146
5.3. Future work.....	147
5.4. References.....	151
<i>Chapter 1</i>	1
<i>Chapter 2</i>	17
<i>Chapter 3</i>	43
<i>Chapter 4</i>	91
<i>Chapter 5</i>	143

Chapter 1

Introduction

All references are self-contained to within this chapter, and do not refer to any other chapters.

1.1. An introduction to catalysis

The term “catalysis” has been first coined by Jacob Berzelius, a 19th century Swedish chemist. He initially called it “catalytic power”, referring to phenomena by which new compounds are formed.¹ However, catalysis has been unknowingly used by mankind for centuries before that. The fermentation of sugar to alcohol is a catalytic process in which yeast is the enzyme catalyst, and sugar is the substrate. In the modern world, catalysis underlines every aspect of modern living. It is used extensively in polymer synthesis of polyethylene using the Ziegler-Natta catalysts.² Perhaps the most significant catalytic process to date is the Haber-Bosch process, where an iron catalyst facilitates the formation of ammonia from nitrogen and hydrogen.³ The ammonia is chiefly used in fertilisers, without which current world food demands would not have been met.

Catalysts are usually fall into three categories: homogeneous, heterogeneous, and enzymatic. Homogeneous catalysts are in the same phase as the reactants. These catalysts are generally very effective as each molecule possesses an active site for catalysis, maximising the contact with the substrate; but they are also difficult to separate from the product mixture, and therefore their re-use is problematic. Heterogeneous catalysts are found in a phase different the reactants, typically solid powders (which can also be pressed and shaped into pellets). They can have lower

activities than their homogeneous counterparts; homogeneous catalysts are predominately more selective than heterogeneous catalysts, as they have very well-defined active sites. However, the latter can be easily separated from the reaction mixture, and typically feature consistent re-use cycles, making them incredibly valuable in the industry. Indeed, the majority of catalysts used commercially are heterogeneous in nature. Enzymes are large organic molecules with active centres specifically tailored to carry out a small set of functions. Because of this, they are incredibly effective at what they do, however their scope of use is limited. Because of their biological nature, they are also only usually useful in a narrow range of conditions. The catalysts featured in this thesis are exclusively heterogeneous.

A catalyst can be described as a substance which lowers the activation energy (E_a) for a reaction by offering an alternate pathway. A catalyst changes the kinetic properties of a reaction without altering the thermodynamics of it. In other words, it does not alter the energy states of the reactants or products, and has no effect on the position of the equilibrium in a given reaction. Figure 1 illustrates a graphic representation of how a catalyst influences a reaction.

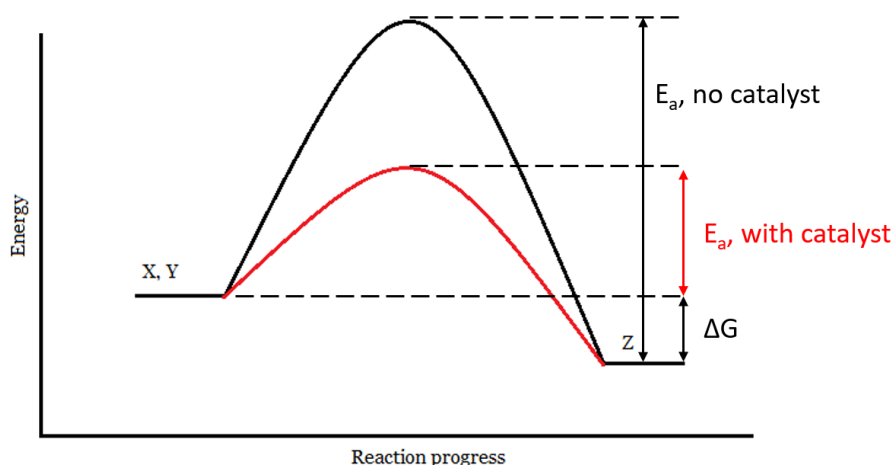


Figure 1. An energy diagram for a given reaction which compares reaction profile with catalyst and without catalyst. The energy states at the start and end of the reaction remain unchanged.

The activation energy can be calculated from the Arrhenius equation:

$$k = Ae^{-\frac{Ea}{RT}}$$

Where k is the reaction constant; A is the pre-exponential factor; Ea is the activation energy; R is the gas constant; and T is the temperature in Kelvin.

Thus it can be deduced that the smaller the activation energy, the larger the reaction constant, k – indicating faster rate of reaction.

1.2. Biomass

Biomass is an all-encompassing term, used to define animal or plant matter, and is the most abundant raw material on earth. Most common usage of it refers to dead plant matter such as wood residues or waste from food crops. The application of biomass has evolved over the years, and can be classified into three major categories: first, second, and third generation. First generation biomass refer to biomass derived from food crops such as sugar cane or oil crops.⁴ Second generation biomass describes biomass from non-food sources, for example agricultural waste or wood residue. It is therefore much more attractive than first generation biomass as it does not compete with food crops for arable land. Third generation biomass refers to biofuels such as bioethanol produced with the use of algae.⁵

As the global demand for energy continues to increase every year,⁶ and global petroleum reserves are in finite supply, there is much need for the development of new and renewable sources of energy. Additionally, there is need for new bio-derived platform chemicals and to source existing commodity chemicals from biomass. Therefore, there is a growing interest in biomass valorisation. Lignocellulose is a promising biomass source due to its abundance.⁷

For the purposes of this thesis, biomass refers to lignocellulosic biomass. Lignocellulose has three main components: cellulose (35 - 50%), hemicellulose (20 - 35%) and lignin (10 – 25%).⁸ While all three can be valorised to various products, such as 5-HMF, toluene (and other aromatic compounds), furans, levulinic acid, and others,⁸⁻¹¹ this thesis focuses on the chemistry of glucose and its derivatives.

1.3. Dehydration of glucose

With cellulose being the major component of biomass, it is made up of $\beta(1\rightarrow4)$ linked glucose molecules. This means that each glucose molecule is bonded to another through an equatorially-oriented C-O bond from first carbon on the first molecule, to the fourth carbon on the second molecule (using IUPAC nomenclature; hence 1 \rightarrow 4). Glucose is therefore the most common naturally occurring monosaccharide and is a highly attractive target for valorisation due to its renewable nature. It can be extracted from biomass using various strategies, such as chemical or enzymatic hydrolysis,^{12,13} heterogeneous catalysis,¹⁴ or simply through the use of mineral acids.¹⁵ The dehydration reaction of glucose produces chiefly two compounds of interest: 5-hydroxymethylfurfural (5-HMF) and levulinic acid (LA). 5-HMF can be converted into a multitude of chemicals through catalytic means, including levulinic acid.¹⁶ LA is also considered a platform chemical, due to its reactive carbonyl functional groups allowing it to be derived into many other compounds, like γ -valerolactone or 2-methyltetrahydrofuran (2-MTHF).^{17,18}

One of the biggest issues to overcome with this reaction is the formation of humins, furan-based polymers that are produced from some of the reaction intermediates. One of the ways to limit this process is to carry the reaction out in methanol.¹⁹ As most compounds in the mixture will rapidly form methyl esters, the ester acts as a protecting group, slowing down the rate of side-reactions. Depending on the alcohol solvent used, a corresponding levulinate ester will form as a product, for example methyl levulinate (ML). The most commonly used catalysts for the

dehydration are zeolites and sulfated metal oxides. Zeolite types β and Y have been shown to give good yields of levulinate esters in methanol at 160 °C (47% and 49%, respectively), however under long reaction times (20 hours) and with low carbon mass balance of approximately 50%.²⁰ ZSM-5 was also tested, however it only yielded 8% of the desired product after 20 hours. Xu *et al.* also reported very poor yields of methyl levulinate with ZSM-5, 0.3% after 150 minutes.²¹ They speculate that this difference in activity between zeolites is likely due to the inability of ZSM-5 to facilitate the isomerisation of glucose to fructose effectively, however there is very little evidence that isomerisation to fructose happens in methanol. Indeed, the catalytic performance is most likely to be associated with the corresponding pore sizes of these materials.²² Aside from zeolites, sulfated metal oxides such as $\text{SO}_4\text{-ZrO}_2$ and $\text{SO}_4\text{-TiO}_2$ are also a popular choice of catalyst for this reaction. Jiang *et al.* reported moderate yield of 18% ML from glucose using $\text{SO}_4\text{-ZrO}_2$; this yield increased to 49% upon addition of a Sn-Beta co-catalyst.²³ Peng *et al.* showed $\text{SO}_4\text{-TiO}_2$ yield as high as 45% ML after one-hour reaction time, however they used 50 wt.% catalyst loading with respect to substrate.²⁴ They also correlated the turn over number with amount of acid sites on the catalyst and their density, demonstrating the importance of acid sites for this dehydration reaction.

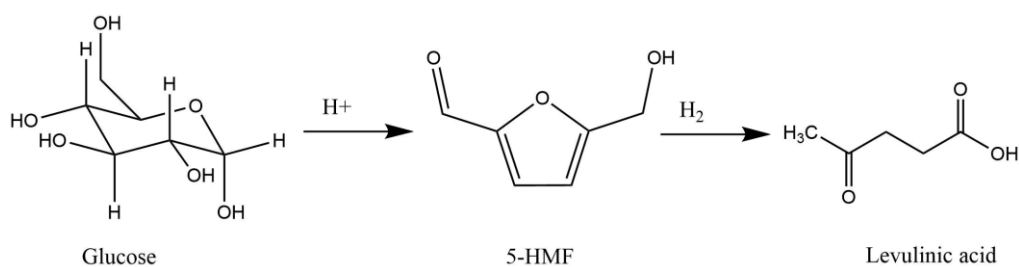


Figure 2. A simplified reaction scheme showing transformation of glucose to levulinic acid

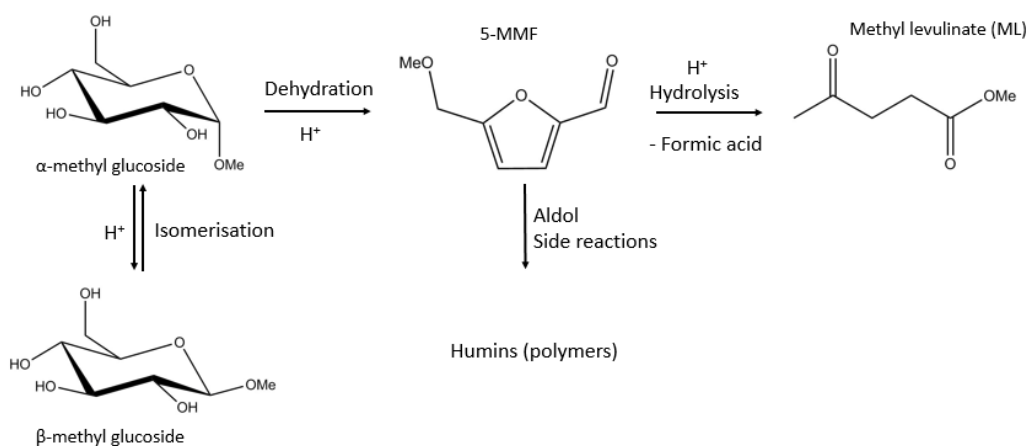


Figure 3. A more detailed reaction scheme of the reaction in methanol solvent. Methanol reacts with all the substrates, intermediates and products to form methyl esters.

There are several industrial processes available for the production of levulinic acid, such as the Biofine process. This process utilises wood pulp as a feedstock and in the presence of dilute acids, LA yields of 57% can be achieved.²⁵ Another patented process published in 1953 focuses on levulinic acid production from corn.²⁶ More recent process patents from 2013²⁷ and 2014²⁸ are also available, indicating that this is an area of active interest. In 2015, “GFBiochemicals” opened a pilot plant which produces levulinic acid from biomass. LA yields in excess of 8,000 MT/year are reported. However, details on their production process are somewhat elusive. Global production and market size statistics are not widely available, as the current interest in LA is chiefly academic, predominately due to the cost of its production when compared to alternatives such as bioethanol. Most industrial processes utilise mineral acids to convert biomass into LA. In fact, mineral acids remain to be the best performing acids for this reaction; yields vary depending on the temperature, reaction time, flow or batch conditions, type of mineral acid used – however, mineral acids generally outperform solid acids. Qi *et al.* reported LA yield of 51% with H_2SO_4 after 2 hours at 130 °C.²⁹ Szabolcs *et al.* reported 49% yield of LA with HCl after 30 minutes at 170 °C – interestingly, HCl outperformed H_2SO_4 by approximately 8%, but environmental concerns were expressed about using a

chlorinated chemical.³⁰ The maximum theoretical yield of LA from hexose was speculated to not exceed 70%.³¹ Therefore, any yield approaching this value is significant. Dumesic group approached this theoretical maximum reporting a 63% yield of LA using 0.05M H₂SO₄ at 160 °C for 4 hours.³² Impressively, they achieved 59% yield under identical conditions when using solid acid Amberlyst 70. They found that 90% GVL solvent aided the reaction, likely by solubilizing humins and cellulose. This is important because neither cellulose nor humins are soluble in most solvents. Solubilizing cellulose allows it to reach the catalyst more easily; solubilizing humins is important as they often stick to, and solidify on the catalyst, covering the active sites and reducing catalyst activity. Mineral acids are hard to recover from the reactant mixture and are non-reusable. Extraction of LA from different solvents, specifically alcohols, is possible with the use of Amberlite LA-2.³³ With LA prices approximately \$5-8 per kilogram, levulinic acid stands to compete with ethanol as a fuel additive (approximately \$5 per kilogram) if a more economic process is found. A heterogeneously catalysed process could potentially be more economical due to easier reuse of catalyst, and easier separation of catalyst from reactant mixture.

1.4. Hydrogenation of levulinic acid and methyl levulinate

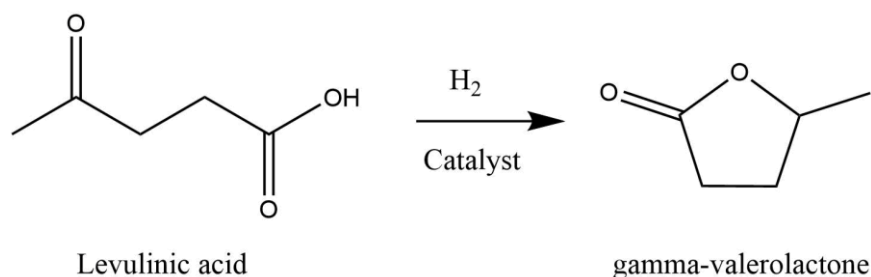


Figure 4. Reaction scheme for the hydrogenation of levulinic acid.

Many catalytic systems have been reported for the conversion of levulinic acid (LA) to γ -valerolactone (GVL) in the literature, both homogeneous and heterogeneous. Supported ruthenium catalysts are popular for this reaction due to

their consistently excellent GVL yields (>95%) under relatively mild conditions (e.g. 130 °C, 30 minutes, 40 bar H₂). Various supports such as carbon, silica or alumina have been reported, and Ru-based catalysts are generally accepted as an activity benchmark for this reaction, with typical metal loadings of 0.5 – 2% Ru.^{34–37} Other noble metals have also been studied, such as palladium,^{38,39} gold⁴⁰ or platinum³⁶. However, due to the relatively high costs associated with noble metals stemming from their low natural abundance and their use on an industrial scale, there is a drive to develop hydrogenation catalysts using cheap, non-noble metals. Copper has been explored as an alternative to ruthenium for this reaction, and is one of the more abundant metals. Hengne and Rode were one of the first groups to utilise 50% Cu-ZrO₂ and 50% Cu-Al₂O₃ for hydrogenation of LA with complete conversion.⁴¹ Samadhan *et al.*⁴² use 6 wt. % CuO-SiO₂ with formic acid as a hydrogen source, demonstrating versatility of the metal. Kai *et al.*¹⁷ show successful synthesis of GVL using a 1:1 Cu-Fe material prepared by forming a hydrotalcite precursor and calcining it at high temperature (950 °C), obtaining 90% yield after 10 hours. Jun Hirayama *et al.* noted excellent yields of GVL exceeding 80% after just 30 minutes by doping a 50%Cu-ZrO₂ catalyst with 1% wt. manganese.⁴³

Methyl levulinate (ML) is an ester derivative of levulinic acid, similar to ethyl levulinate (EL)⁴⁴ and butyl levulinate (BL),⁴⁵ both of which have been explored in literature and can be prepared readily from levulinic acid in yields exceeding 90% in as little as 30 minutes.⁴⁶ Similarly to levulinic acid, alkyl levulinates can be used as fuel additives or as platform chemicals,^{47,48} as they undergo similar chemistry as levulinic acid. This means lower sulfur emissions than ethanol-based additives, and much better relative engine efficiency.⁴⁷ The longer-chain alkyl levulinates such as butyl levulinate are functionally similar as fuel additives to shorter chain compounds, however they can form polymers (humins) in their production, and potentially form more carbon deposits once combusted in the engine.⁴⁹ Typically, ethyl levulinate has

been considered over the other levulinates as a fuel additive due to its better mixing with certain diesel blends.^{47,50} Li *et al.* has used sulfated ZrO₂/TiO₂ nanocomposite to obtain 90% conversion of levulinic acid to ethyl levulinate after 180 minutes at 105 °C.⁵¹ Nandiwale *et al.* reached 95% yield of EL at 120 °C by after 5 hours by using de-silicated H-ZSM-5.⁵² In fact, the industrial Biofine process poses that the levulinic acid is esterified downstream, rather than adding alcohol solvent at an earlier stage.⁴⁷ Production of methyl levulinate can be achieved through the same means as production of levulinic acid or indeed any alkyl levulinate – the addition of methanol (or other alcohol) as a solvent during the dehydration of hexoses in the presence of an acid can cause esterification of most reaction intermediates and products. For example, Wilson and co-workers obtained yields of approximately 25% alkyl levulinate using both methanol and ethanol with sulfated zirconia grafted onto SBA-15 at 140 °C for 24 hours.⁵³ Peng *et al.* reported 33 mol% yield of ML from glucose using SO₄-TiO₂ at 2 hours, however using a 50:50 mass ratio of catalyst:substrate.⁵⁴ Ding *et al.* achieved approximately 45% ML yield from methyl glucoside using a niobium-phosphate catalyst after 24 hours at 180 °C.⁵⁵ A relatively high ML yield of 51% from glucose was reported in 2018 by the Xu group, by combining Amberlyst-15 with Sn-Beta at 160 °C for 5 hours.⁵⁶

As most of the academic and industrial spotlight is focused on the use of ethyl levulinate or levulinic acid, and current industrial applications do not utilise heterogeneous catalysts, there is currently a gap in research on heterogeneous solutions for formation of methyl levulinate. A lot of current literature on the subject does not tackle the formation of humins (polymers) and mechanistic pathways in detail, a subject which is discussed in this work. Additionally, as part of the aims set out for this work, our research partners were working on the extraction of cellulose and hexoses from biomass using methanol as solvent – therefore work presented in chapter 3 was a continuation of that process.

The hydrogenation of levulinic acid and its corresponding esters can result in the formation of γ -valerolactone (GVL). The generally accepted mechanism for this reaction can be seen in Figure 5. Levulinic acid is hydrogenated to 4-hydroxypentanoic acid (4-HPA), which then undergoes a spontaneous cyclisation reaction to form GVL. The presence of an ester group on LA does not affect this mechanism, however it may have an effect on the rate of reaction. Therefore, many of the same catalysts can be used for the hydrogenation of ML to GVL as LA to GVL, provided they are not sensitive to methanol. In fact, certain copper catalysts such as CuO⁵⁷ or Cu-Cr⁵⁸ oxide material are capable of decomposing MeOH into H₂ *in situ*, removing the need to supply gaseous H₂. The resulting hydrogenation reaction reached yields of 89% after 4 hours at 250 °C. Another pathway is also possible, with LA forming an enol form and dehydrating to form angelica lactone, which then hydrogenates to GVL – though this pathway is rarely observed.⁵⁹ As discussed in chapter 4 of this thesis, the LA enolate formation is a spontaneous event which happens at higher reaction temperatures – however dehydration into angelica lactone requires presence of a weak acid, for example SiO₂.⁶⁰

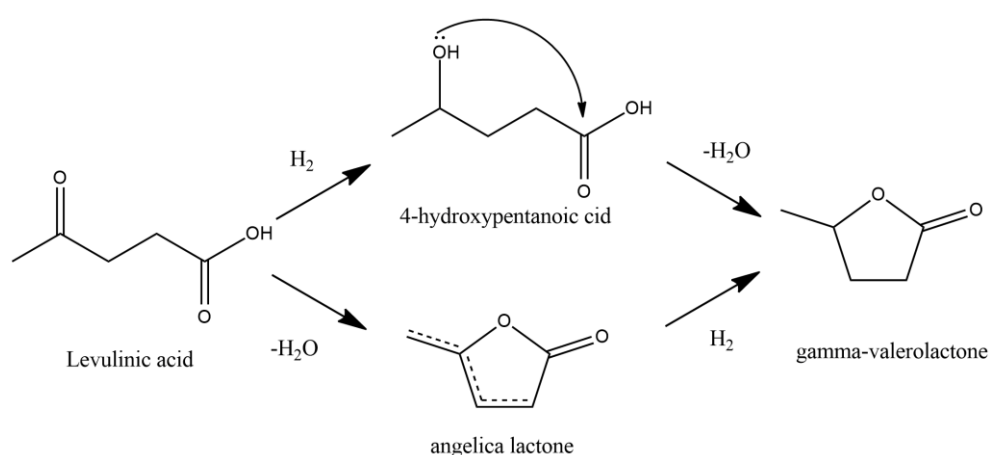


Figure 5. Possible reaction pathways of LA to GVL.

Like LA, GVL has several applications which make it a desirable molecule. Both molecules are non-toxic and renewable. GVL can be used as a solvent, as mentioned previously in the formation of LA from cellulose;^{32,61} it can be used as a

non-toxic replacement to solvents such as chloroform or ethyl acetate in the production of phosphatidylserine (drug supporting healthy brain function).⁶² Likely, there are many reactions for which GVL could potentially replace toxic solvents. It could also have applications in polymer chemistry, forming monomers such as α -methylene- γ -valerolactone.⁶³ GVL can also be used as a fuel source and fuel additive, similarly to levulinic acid and ethanol. Horvath *et al.* has shown that a mixture of 10% GVL and 90% 95-octane gasoline not only has similar properties to 10% ethanol 90% 95-octane mix, it also featured a lower vapour pressure, ranking it favourably.⁶⁴ GVL retains 97% of the energy stored in glucose, and can be broken down further to form various hydrocarbons.⁶⁵ Priced at approximately \$10-20 per kilogram, it is not only economically favourable to upgrade from levulinic acid, it can also enable high-volume industrial processes such as production of jet fuel range alkenes.⁶⁶ However, while industrial production of both LA and GVL is possible, it is often the issue that their “competitors” such as ethanol are cheaper. Therefore, there is need for development of cheaper, optimised processes. A twofold approach can be taken to this problem: research of cheaper ways of extracting hexoses from biomass, which would reduce price of the feedstock; and innovation of the conversion of biomass into LA and GVL to make it less expensive. Currently, the benchmark catalysts for hydrogenation of LA to GVL are ruthenium based,³⁴ which is a relatively expensive and scarce metal. Development of a novel catalytic system which makes use of more abundant and cheaper materials could reduce the cost of GVL production and make it more economically viable on an industrial scale.

1.5. Aims of the thesis

This work is part of the international NOVACAM project supported by the European Union and Japan Science and Technology Agency. The overall aims of the NOVACAM project were to develop novel catalysts based on non-critical metals to facilitate the conversion of lignocellulose to useful chemicals and biofuels. The

group at Cardiff University focused on the valeric platform – efficient formation of γ -valerolactone from cellulose and glucose. The objectives of this body of work were not to find the strictly best performing catalysts for these reactions; it was to synthesise relatively inexpensive catalysts, optimise their activity and gain a deeper insight into how these reactions take place. The goals can be outlined:

1. To develop a methodology for the production of levulinic acid from glucose. To gain an insight into the methodology and limit the polymerisation side reactions.
2. To develop a novel material from non-critical metals for the hydrogenation of levulinic acid to γ -valerolactone.
3. To incorporate the “catalysis by design” approach. Thorough examination of the catalytic systems is required in order to drive future catalyst design.
4. The catalysts should be active in water or methanol, as these are the two most common solvents for industrial processing of biomass.

1.6. References

- 1 J. J. Berzelius, *Edinburgh New Philos. J.*, 1836, **XXI**, 223.
- 2 I. Prefecture and K. Prefecture, *Ziegler–Natta Catal. Polym.*, 2016, **22**, 1503–1546.
- 3 B. Lindström and L. J. Pettersson, *Cattech*, 2003, **7**, 130–138.
- 4 M. A. Martin, *N. Biotechnol.*, 2010, **27**, 596–608.
- 5 O. Fenton and D. Ó hUallacháin, *Algal Res.*, 2012, **1**, 49–56.
- 6 British Petroleum, *BP Statistical Review of World Energy 2017*, 2017.
- 7 C.-H. Zhou, X. Xia, C.-X. Lin, D.-S. Tong and J. Beltramini, *Chem. Soc. Rev.*, 2011, **40**, 5588.
- 8 J. Wang, J. Xi and Y. Wang, *Green Chem.*, 2015, **17**, 737–751.

- 9 I. Delidovich, K. Leonhard and R. Palkovits, *Energy Environ. Sci.*, 2014, **7**, 2803–2830.
- 10 S. Ur-Rehman, Z. Mushtaq, T. Zahoor, A. Jamil and M. A. Murtaza, *Crit. Rev. Food Sci. Nutr.*, 2015, **55**, 1514–1528.
- 11 C. V. T. Mendes, M. G. V. S. Carvalho, C. M. S. G. Baptista, J. M. S. Rocha, B. I. G. Soares and G. D. A. Sousa, *Food Bioprod. Process.*, 2009, **87**, 197–207.
- 12 K. Przybysz Buzafa, H. Kalinowska, P. Przybysz and E. Małachowska, *Wood Sci. Technol.*, 2017, **51**, 873–885.
- 13 J. B. Binder and R. T. Raines, *Proc. Natl. Acad. Sci.*, 2010, **107**, 4516–4521.
- 14 B. Qi, A. Vu, S. R. Wickramasinghe and X. Qian, *Biomass and Bioenergy*, 2018, **117**, 137–145.
- 15 A. L. Stern, *J. Chem. Soc. Trans.*, 1895, 74–90.
- 16 Z. Xue, M. G. Ma, Z. Li and T. Mu, *RSC Adv.*, 2016, **6**, 98874–98892.
- 17 K. Yan and A. Chen, *Fuel*, 2014, **115**, 101–108.
- 18 J. J. Bozell, L. Moens, D. C. Elliott, Y. Wang, G. G. Neuenschwander, S. W. Fitzpatrick, R. J. Bilski and J. L. Jarnefeld, *Resour. Conserv. Recycl.*, 2000, **28**, 227–239.
- 19 S. Kang and J. Yu, *Ind. Eng. Chem. Res.*, 2015, **54**, 11552–11559.
- 20 S. Saravanamurugan and A. Riisager, *ChemCatChem*, 2013, **5**, 1754–1757.
- 21 J. Xu, Y. Su, L. Wu, T. Lu, H. Zou, J. Nan, X. Yang and L. Zhou, *Catal. Commun.*, 2014, **50**, 13–16.
- 22 M. Moliner, Y. Roman-Leshkov and M. E. Davis, *Proc. Natl. Acad. Sci.*,

- 2010, **107**, 6164–6168.
- 23 L. Jiang, L. Zhou, J. Chao, H. Zhao, T. Lu, Y. Su, X. Yang and J. Xu, *Appl. Catal. B Environ.*, 2018, **220**, 589–596.
- 24 L. Peng, J. Zhuang and L. Lin, *J. Nat. Gas Chem.*, 2012, **21**, 138–147.
- 25 K. C. C. G.G. Liversidge J.F. Bishop, D.A. Czekai, 1980, **96**, 62–66.
- 26 US Patent 2,813,900, 1953.
- 27 US Patent 9,073,841, 2013.
- 28 Patent WO2014087016A1, 2014.
- 29 L. Qi, Y. F. Mui, S. W. Lo, M. Y. Lui, G. R. Akien and I. T. Horváth, *ACS Catal.*, 2014, 1–11.
- 30 Á. Szabolcs, M. Molnár, G. Dibó and L. T. Mika, *Green Chem.*, 2013, **15**, 439–445.
- 31 R. H. Leonard, *Ind. Eng. Chem.*, 1956, **48**, 1330–1341.
- 32 D. M. Alonso, J. M. R. Gallo, M. A. Mellmer, S. G. Wettstein and J. A. Dumesic, *Catal. Sci. Technol.*, 2013, **3**, 927–931.
- 33 H. Uslu, Ş. I. Kirbaşlar and K. L. Wasewar, *J. Chem. Eng. Data*, 2009, **54**, 712–718.
- 34 J. Tan, J. Cui, T. Deng, X. Cui, G. Ding, Y. Zhu and Y. Li, *ChemCatChem*, 2015, **7**, 508–512.
- 35 Z. Yan, L. Lin and S. Liu, *Energy & Fuels*, 2009, **23**, 3853–3858.
- 36 P. P. Upare, J. M. Lee, D. W. Hwang, S. B. Halligudi, Y. K. Hwang and J. S. Chang, *J. Ind. Eng. Chem.*, 2011, **17**, 287–292.
- 37 S. Cao, J. R. Monnier, C. T. Williams, W. Diao and J. R. Regalbuto, *J. Catal.*,

- 2015, **326**, 69–81.
- 38 K. Yan, T. Lafleur, C. Jarvis and G. Wu, *J. Clean. Prod.*, 2014, **72**, 230–232.
- 39 K. Yan, T. Lafleur, G. Wu, J. Liao, C. Ceng and X. Xie, *Appl. Catal. A Gen.*, 2013, **468**, 52–58.
- 40 K. Mustafin, F. Cárdenas-Lizana and M. A. Keane, *J. Chem. Technol. Biotechnol.*, 2017, **92**, 2221–2228.
- 41 A. M. Hengne and C. V. Rode, *Green Chem.*, 2012, **14**, 1064.
- 42 S. Lomate, A. Sultana and T. Fujitani, *Catal. Sci. Technol.*, 2017, **7**, 3073–3083.
- 43 J. Hirayama, I. Orłowski, S. Iqbal, M. Douthwaite, S. Ishikawa, P. J. Miedziak, J. K. Bartley, J. Edwards, Q. He, R. L. Jenkins, T. Murayama, C. Reece, W. Ueda, D. J. Willock and G. J. Hutchings, *J. Phys. Chem. C*, 2018, **123**, 7879–7888.
- 44 F. Wang, Z. Chen, H. Chen, T. A. Goetjen, P. Li, X. Wang, S. Alayoglu, K. Ma, Y. Chen, T. Wang, T. Islamoglu, Y. Fang, R. Q. Snurr and O. K. Farha, *ACS Appl. Mater. Interfaces*, 2019, **11**, 32090–32096.
- 45 H. J. Bart, J. Reidetschläger, K. Schatka and A. Lehmann, *Ind. Eng. Chem. Res.*, 1994, **33**, 21–25.
- 46 S. Quereshi, E. Ahmad, K. K. Pant and S. Dutta, *Ind. Eng. Chem. Res.*, 2019, **58**, 16045–16054.
- 47 D. J. Hayes, S. Fitzpatrick, M. H. B. Hayes and J. R. H. Ross, *Biorefineries-Industrial Process. Prod. Status Quo Futur. Dir.*, 2008, **1**, 139–164.
- 48 U.S. Patent, 4,364,743, 1982.
- 49 X. Hu, L. Wu, Y. Wang, D. Mourant, C. Lievens, R. Gunawan and C. Z. Li,

- Green Chem.*, 2012, **14**, 3087–3098.
- 50 E. Ahmad, M. I. Alam, K. K. Pant and M. A. Haider, *Green Chem.*, 2016, **18**, 4804–4823.
- 51 Z. Li, R. Wnetrzak, W. Kwapinski and J. J. Leahy, *ACS Appl. Mater. Interfaces*, 2012, **4**, 4499–4505.
- 52 K. Y. Nandiwale, P. S. Niphadkar, S. S. Deshpande and V. V. Bokade, *J. Chem. Technol. Biotechnol.*, 2014, **89**, 1507–1515.
- 53 G. Morales, A. Osatiashtiani, B. Hernández, J. Iglesias, J. A. Melero, M. Paniagua, D. Robert Brown, M. Granollers, A. F. Lee and K. Wilson, *Chem. Commun.*, 2014, **50**, 11742–11745.
- 54 L. Peng, L. Lin, H. Li and Q. Yang, *Appl. Energy*, 2011, **88**, 4590–4596.
- 55 D. Ding, J. Xi, J. Wang, X. Liu, G. Lu and Y. Wang, *Green Chem.*, 2015, **17**, 4037–4044.
- 56 L. Jiang, L. Zhou, J. Chao, H. Zhao, T. Lu, Y. Su, X. Yang and J. Xu, *Appl. Catal. B Environ.*, 2018, **220**, 589–596.
- 57 X. Tang, Z. Li, X. Zeng, Y. Jiang, S. Liu, T. Lei, Y. Sun and L. Lin, *ChemSusChem*, 2015, **8**, 1601–1607.
- 58 Z. Li, X. Tang, Y. Jiang, Y. Wang, M. Zuo, W. Chen, X. Zeng, Y. Sun and L. Lin, *Chem. Commun.*, 2015, **51**, 16320–16323.
- 59 M. Sudhakar, V. V. Kumar, G. Naresh, M. L. Kantam, S. K. Bhargava and A. Venugopal, *Appl. Catal. B Environ.*, 2016, **180**, 113–120.
- 60 D. Sun, Y. Takahashi, Y. Yamada and S. Sato, *Appl. Catal. A Gen.*, 2016, **526**, 62–69.
- 61 D. Fegyverneki, L. Orha, G. Láng and I. T. Horváth, *Tetrahedron*, 2010, **66**,

1078–1081.

- 62 Z. Q. Duan and F. Hu, *Green Chem.*, 2012, **14**, 1581–1583.
- 63 L. E. Manzer, *Appl. Catal. A Gen.*, 2004, **272**, 249–256.
- 64 I. T. Horváth, H. Mehdi, V. Fábos, L. Boda and L. T. Mika, *Green Chem.*, 2008, **10**, 238–242.
- 65 N. Savage, *Nature*, 2011, **474**, S9–S11.
- 66 J. Han, *J. Ind. Eng. Chem.*, 2017, **48**, 173–179.

Chapter 2

Experimental

All references are self-contained to within this chapter, and do not refer to any other chapters.

2.1. Materials

Table 1. Chemical materials used in this thesis

Material	Supplier	Purity
$\text{Cu}(\text{NO}_3)_2 \cdot 3\text{H}_2\text{O}$	Acros Chemicals	99%
$\text{ZrO}(\text{NO}_3)_2 \cdot 6\text{H}_2\text{O}$	Acros Chemicals	98%
$\text{Mn}(\text{NO}_3)_2 \cdot 4\text{H}_2\text{O}$	Sigma Aldrich	99%
$\text{Ce}(\text{NO}_3)_3$	Sigma Aldrich	99%
Zeolites β	Alfa Aesar	n/a
Zeolites ZSM-5	Alfa Aesar	n/a
K_2CO_3	Sigma Aldrich	99%
Oxalic acid	Sigma Aldrich	99%

NH ₄ OH solution (25-28% conc.)	Sigma Aldrich	99%
H ₂ SO ₄	Sigma Aldrich	95%
H ₃ PO ₄	Sigma Aldrich	85%
Methanol	Sigma Aldrich	99%
Ethanol	Sigma Aldrich	99%
Levulinic acid	Sigma Aldrich	99%
γ -valerolactone	Sigma Aldrich	99%
α -D-methyl glucopyranoside	Sigma Aldrich	99%
β -D-methyl glucopyranoside	Sigma Aldrich	99%
5-Hydroxymethylfurfural	Sigma Aldrich	99%
Methyl levulinate	Sigma Aldrich	99%
Formic acid	Sigma Aldrich	99%
Methyl formate	Sigma Aldrich	99%
Ammonium metatungstate	Sigma Aldrich	99%
Mesitylene	Sigma Aldrich	98%

2.2. Catalyst preparation

2.2.1. Preparation of Cu-ZrO₂ catalysts

2.2.1.1. Co-precipitation

Co-precipitation is a catalyst synthesis technique, in which two or more metals are precipitated out of solution simultaneously. Changing preparation variables such as temperature, aging time, or metal source can have significant effects on the final catalyst, and therefore need to be controlled carefully; it is also necessary to identify the optimal conditions and timings to use for each step of the preparation. It is important that any catalyst synthesis and pre-conditioning methods lead to reproducible materials.

The co-precipitation of Cu-ZrO₂ is reported in literature, as follows: Cu(NO₃)₂·3H₂O (0.01 mol) and ZrO(NO₃)₂ (0.01 mol) are dissolved in separate solutions of water (100 mL each). Both solutions are then added together and stirred in a beaker at room temperature for 5 minutes. Once homogenous mixing is achieved, K₂CO₃ is added to the solution dropwise (0.2 M) to raise the pH to 9. The mixture is then aged for 6 hours, filtered on a Buchner funnel, and washed with hot deionised water (1 L). The catalyst is then dried for 16 hours at 110 °C. After drying, the precursor is ground to a fine powder using a mortar and pestle, and calcined under static air at 550 °C, 10 °C min⁻¹ for 2 hours. After calcination the catalyst is reduced under flowing 5% H₂/Ar (200 mL min⁻¹) at 300 °C, 10 °C min⁻¹ for 2 hours.

2.2.1.2. Oxalate gel precipitation

Oxalate gel precipitation is a catalyst synthesis method similar to co-precipitation, however the pH of the solution is not intentionally adjusted, and instead the catalyst is precipitated out of reaction by the formation of an alcohol insoluble CuZr-oxalate gel (og).

The co-precipitation of Cu-ZrO₂ (og) is reported in literature, as follows: Cu(NO₃)₂·3H₂O (0.01 mol) and ZrO(NO₃)₂ (0.01 mol) are dissolved in separate solutions of ethanol (100 mL each). Both solutions are then added together and stirred in a beaker at room temperature for 5 minutes. Once homogenous mixing is achieved, oxalic acid (0.024 mol) is added, causing the metals to precipitate out of solution. The mixture is aged for 2 hours at room temperature, and filtered on a Bucher funnel. The catalyst is then dried for 16 hours at 110 °C. After drying, the catalyst is subject to the same calcination and reduction treatment as co-precipitation catalysts.

2.2.1.2.1. Doping Cu-ZrO₂ catalysts with manganese

Doping of Cu-ZrO₂ catalyst with manganese is achieved using the wet impregnation method. In order to achieve 1% wt. doping, Mn(NO₃)₂·4H₂O (0.0231 g, 0.00009 mol) is dissolved in 3 mL ethanol by sonication. Then, the calcined Cu-ZrO₂ (0.5 g) is dispersed in the metal salt solution, and the resulting slurry is dried under vigorous stirring and heating (100 °C). After that, the solid was re-calcined at 550 °C for 2 h with a 10 °C min⁻¹ ramp under static air, and reduced at 300 °C for 2 h with a 10 °C min⁻¹ ramp under 5% H₂/Ar mixture gas (200 mL min⁻¹).

2.2.1.3. pH gradient precipitation

Another method of catalyst preparation used in this thesis is pH gradient precipitation. It is a catalyst synthesis method derived from co-precipitation. The main aim of the pH gradient method is reduction in the amount of metal loading while retaining high activity. This is achieved by taking advantage of the fact that certain metals precipitate out of solution at different pH values. One of the main catalysts used in this thesis is CuZrO₂; in the standard, non-gradient co-precipitation method, both metals are precipitated at the same time, which leads to a lot of copper being locked in the bulk lattice of zirconia, where it is inactive, and therefore wasted. Zirconia starts to precipitate at around pH 4.5, whereas copper precipitates around pH 5.5. By creating a pH gradient over time, a layered catalyst can theoretically be synthesised, with zirconia at the core and most of the copper on the outside.

In a typical synthesis, calculated amounts of Cu(NO₃)₂·3H₂O and ZrO(NO₃)₂·6H₂O are dissolved in separate solutions of deionised water (100 mL). The solutions are then mixed together and stirred for 5 minutes to achieve thorough mixing. The starting pH of the solution is measured to be around 1.7, depending on the total amount of nitrates used (higher copper loading catalyst require more Cu(NO₃)₂·3H₂O, which in turn lowers the pH of solution), and the mixture is kept at

25 °C with a heated water bath. The pH of the solution is then adjusted to 4.5 by a slow and controlled addition of K₂CO₃ solution (0.2 M). Initially, the addition of base was carried out by hand, using either a burette or a pipette; however use of an autotitrator proves to be much more consistent as manual preparation is prone to errors. A value of pH 4.5 was chosen as the starting point due to the very slow rate of precipitation of nitrates at pH values lower than 4.5. Once pH 4.5 was achieved, the mixture is aged for 30 minutes. After 30 minutes, pH is adjusted to 5.5 and the mixture is left to age for another 30 minutes. The process is repeated again for pH setpoints of 6.5, 7.5, and 9.5. These setpoints were selected basing on experimental data gathered when evaluating this preparation method, discussed in chapter 4. Once pH of 9.5 is reached, the mixture is aged for 4 hours. After aging, catalyst is recovered by vacuum filtration and washed with room temperature deionised water (1 L). The precursor is then dried at 110 °C for 16 hours. After drying, catalyst was ground to a fine powder using mortar and pestle and calcined under static air at 400 °C, 20 °C min⁻¹ for 4 hours. A range of catalysts denoted xCuZrO₂ was prepared this way, where x = 10%, 20%, 30%, 40% and 50%.

Reduction treatment

Some catalysts were subjected to reduction treatment (after calcination) under 5% H₂/Ar, at 300 °C for 2 hours with a ramp rate of 10 °C/min.

2.2.1.4. Preparation of SO₄-ZrO₂ catalysts

Preparation of SO₄-ZrO₂ catalysts utilised a standard precipitation method, followed by acid treatment, as described below.

ZrO(NO₃)₂.6H₂O (0.03 mol, 10 g) is dissolved in deionised water (200 mL). A solution of ammonium hydroxide (25-28%) is then slowly added under constant stirring until pH 9 is reached. White sol appears. The mixture is then aged for an hour at room temperature, filtered under vacuum and dried at 110 °C for 16 hours.

After drying, the white powder is ground using mortar and pestle and stirred at room temperature in a solution of sulfuric acid (0.5 M, 20 mL g⁻¹) for an hour. Catalyst is then recovered by filtration, dried at 110 °C for 16 hours and calcined under static air at 550 °C for 4 hours, with a ramp rate of 10 °C min⁻¹.

2.2.1.5 Treatment of zeolites

Commercial zeolites β and ZSM-5 (NH₄-form) were obtained from Alfa Aesar. Zeolites are calcined before use under flowing N₂ at 550 °C for 4 hours, with a ramp rate of 5 °C/min. Treatment was done in order to convert the zeolites from NH₄-form into the H-form.

2.2.1.6. Silylation of zeolites

A silylation procedure has been adapted from literature.¹ Zeolite β (38) (2 g) was added to hexane (50 mL) and heated under stirring until reflux. Tetraethylorthosilicate (TEOS, 0.3 mL) was then added into the mixture and it was stirred under reflux for an hour. The mixture was then cooled down and solvent was evacuated using a rotary evaporator. The resulting zeolite was then dried at 110 °C for 16 hours, and subsequently calcined at 500 °C for 4 hours in flowing air.

2.2.1.7. Preparation of phosphated zirconia

ZrO(NO₃)₂ (10 g) was dissolved in 200ml of deionised water. 25% NH₄OH was added dropwise to the solution until pH 9 was reached and white precipitate appeared. The mixture was left to stir for an hour at room temperature. It was then filtered and dried at 110 °C for 16 hours. The dried powder was ground, stirred in 0.5M H₃PO₄ for an hour, filtered and dried at 110 °C for 16 hours. The dried powder was calcined at 550 °C under static air for 3 hours (10 °C/min).

2.2.1.8. Preparation of CeO₂

Ce(NO₃)₃ (10 g) was dissolved in 200ml of deionised water. 25% NH₄OH was added dropwise to the solution until pH 9 was reached and beige precipitate appeared. Solution was left to stir for an hour at room temperature. It was then filtered and dried at 110 °C for 16 hours. The dried powder was calcined at 450 °C under static air for 4 hours (10 °C/min).

2.2.1.9. Preparation of SO₄-CeO₂

The dried, pre-calcination material prepared in 2.2.1.8 was ground, stirred in 0.5M H₂SO₄ for an hour, filtered and put in an oven overnight. The dried powder was calcined at 450 °C under static air for 4 hours (10 °C/min).

2.2.1.10. Preparation of 15% WO₃-ZrO₂

Solutions of ammonium metatungstate (0.00038 mol, 1.1 g) and ZrO(NO₃)₂.6H₂O (0.03 mol, 10 g) in de-ionised water (200 mL) were prepared separately. Ammonium metatungstate was added to zirconyl nitrate; white precipitate was observed immediately, and 28% NH₄OH was then slowly added to the solution until pH ~9.5 was reached. The catalyst was then put in an autoclave and heated to 180 °C under autogenous pressure for 18h. The catalyst was then filtered, dried at 110 °C for 16 hours and calcined under flowing air at 800 °C, 10 °C/min, 4h.

2.3. Catalyst testing

2.3.1. Hydrogenation of levulinic acid to γ -valerolactone

Catalytic testing of xCu-ZrO₂ catalysts for the conversion of levulinic acid was carried out using a 50 mL, Parr Instruments 5500 stainless steel stirred autoclave. A Teflon liner is used to hold the reactants. The liner was loaded with 5% levulinic acid solution (10 g) and catalyst (0.05 g); the autoclave is then sealed, and purged with H₂ three times to remove any residual atmospheric gases. The autoclave is then

heated to 200 °C under 200 rpm stirring. Once reaction temperature was reached, the autoclave is charged with 35 barg H₂ and stirring rate is increased to 2000 rpm. This is considered to be t₀ for the reaction, and the reactor is then left for a desired amount of time. After reaction has finished, the reactor is cooled on ice, gasses are vented once the reactor has cooled below 15 °C. Reaction solution is then recovered by filtration and analysed using GC equipped with a HP-5ms boiling point column.

2.3.2. Conversion of glucose and methyl glucosides to methyl levulinate

Catalytic testing of solid acid catalysts and zeolites was carried out using a 50 mL, Parr Instruments 4957 stainless steel stirred autoclave equipped with a Teflon liner. The liner is loaded with a desired amount of substrate, methanol (7.85 g), catalyst (0.08 g) and mesitylene (0.1 g, used as internal standard). The reactor is then sealed, purged three times with N₂ to remove any residual atmospheric gases, and charged with 10 bar of N₂. The reactor is kept under inert pressure in order to prevent evaporation of the solvent at high temperatures, and to avoid any oxidation side reactions. The autoclave is then heated to the desired temperature under 600 rpm stirring. After the reaction, the autoclave is cooled on ice and gasses are vented once the reactor has cooled below 15 °C. Reaction solution is then recovered by filtration and analysed using GC and HPLC.

2.3.3. Re-use testing of Cu-ZrO₂ catalysts

Catalyst reuse testing was carried out by running a reaction with large amount of catalyst (0.25 g) under standard conditions. The catalyst was then filtered, washed with deionised water (100 mL) and dried at 110 °C for 16 h. From the used catalyst, 50 mg was taken, and a standard reaction was carried out. However, since catalyst recovery rates were only ~60%, it was necessary to combine the used catalysts of more than one reaction to generate the required 50 mg. Two approaches were used. In one, a large batch of catalyst (0.25 g) was synthesised and all initial catalysts were

taken from this single batch. In the other, multiple smaller batches (0.05 g) were used for the initial catalysts. In both cases the recovered catalysts from multiple runs were combined to generate the catalyst for the next set of reuse tests.

No difference in results was observed between these methods, and as such the single-batch method was used for consistency.

2.3.4. Re-use testing of zeolites

Catalyst reuse testing was carried out by running a reaction with large amount of catalyst (0.25 g) under standard conditions. The catalyst was then filtered, washed with deionised water (100 mL) and dried at 110 °C for 16 h. The zeolite was then subject to calcination procedure decompose any humins adsorbed on the surface. The zeolite was calcined before use under flowing N₂ at 550 °C for 4 hours, with a ramp rate of 5 °C/min. From the used catalyst, 80 mg was taken, and a standard reaction was carried out. However, since catalyst recovery rates were only ~50%, it was necessary to combine the used catalysts of more than one reaction to generate the required 80 mg. In a fashion identical to Cu-ZrO₂ reuse, two approaches were used, one utilising large batch (0.25 g) and one utilising multiple smaller batches (0.08 g). No difference in results was observed between these methods, and as such the single-batch method was used for consistency.

2.4. Analytical techniques

2.4.1. Gas chromatography

Gas chromatography (GC) is an analytical technique which is able to separate a chemical mixture into individual substances in the gas phase. The separation is achieved by utilising the interaction of the injected gas with both mobile phase (mixture) and stationary phase (column). A typical gas chromatograph is built of several distinct parts, listed in order in which a sample goes through them:

1. Injector port – this port is kept at a temperature sufficiently high to vapourise the injected sample. The injector port is important, as the whole analytical technique relies on the sample being evaporated into gas phase.
2. Column – a key component in a GC; a column contains the stationary phase, which defines how an analyte mixture (mobile phase) interacts with it and therefore dictates how the output chromatogram will look (signal separation, intensity, and retention time). A column is placed inside an oven, in order to keep the sample temperature high and prevent condensation, which can lead to analytical errors. Liquid samples in this thesis were analysed using a GC equipped with a HP-5ms column, which separates components based on their boiling points.
3. Detector – Like with columns, there are many different types of detectors available to use in GCs. The detector used in this thesis was a Flame Ionisation Detector (FID). The sample is carried from the column into the FID, where it is pyrolysed by a hydrogen/air flame. The ionised carbons generate a signal with the detector electrodes and a detector output is produced. FIDs are often used to analyse hydrocarbon mixtures, because they are easily ionised. It is a destructive technique of analysis.
4. Data collection – signal is collected from the FID, processed and plotted by a computer.
5. Carrier gas – carrier gas is, alongside the injected sample, part of mobile phase and accompanies every step of the analytical process. It carries the analyte mixture from the injector port into the detector. Typically, helium, nitrogen or argon are chosen as the carrier gas because of their inert nature.

Samples analysed by GC in chapter 4 were liquid samples prepared by mixing 0.9 mL of the reaction mixture with 0.1 mL acetonitrile (AcCN) or mesitylene standard. A standard was used in order to minimise any errors associated with injection of the

sample, and all other signals were normalised to it. Calibration curves used for measurement of conversions and yields are shown in figures 6 – 12.

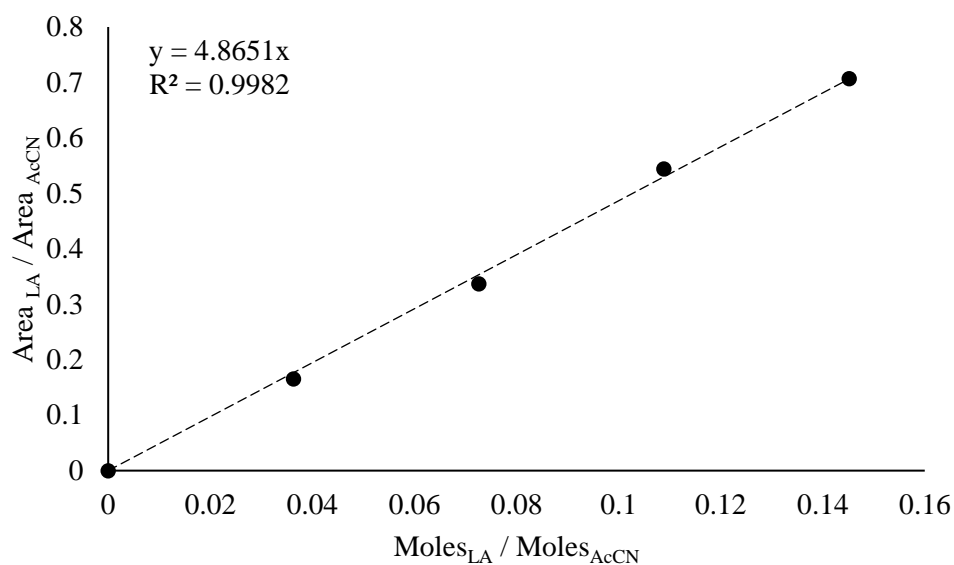


Figure 6. Calibration curve used for measuring levulinic acid with GC for chapter 4. Response factor of 4.8651 was obtained. Acetonitrile was used as external standard.

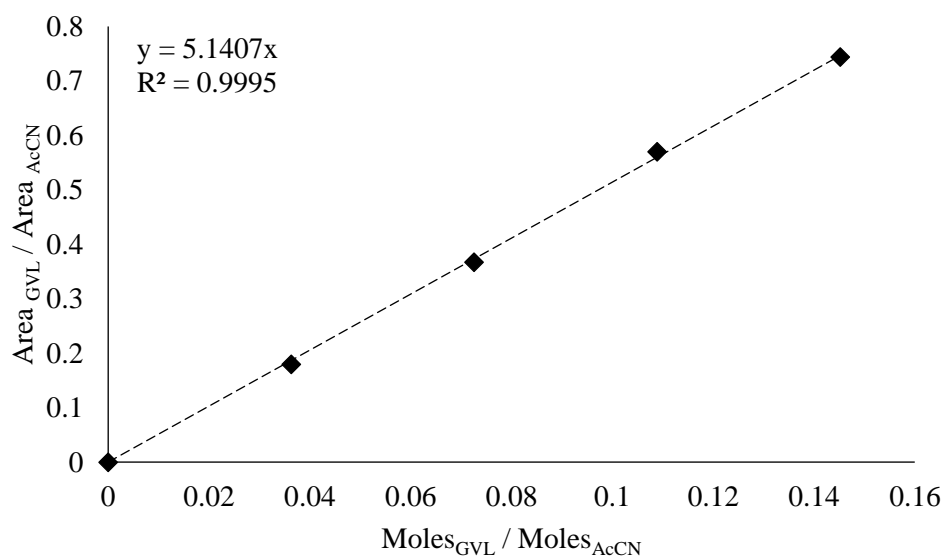


Figure 7. Calibration curve used for measuring GVL yield with GC for chapter 4. Response factor of 5.1407 was obtained. Acetonitrile was used as external standard.

For experiments in chapter 3 when mesitylene was used as an internal standard, the calibration curves used are shown in figures 8 – 12.

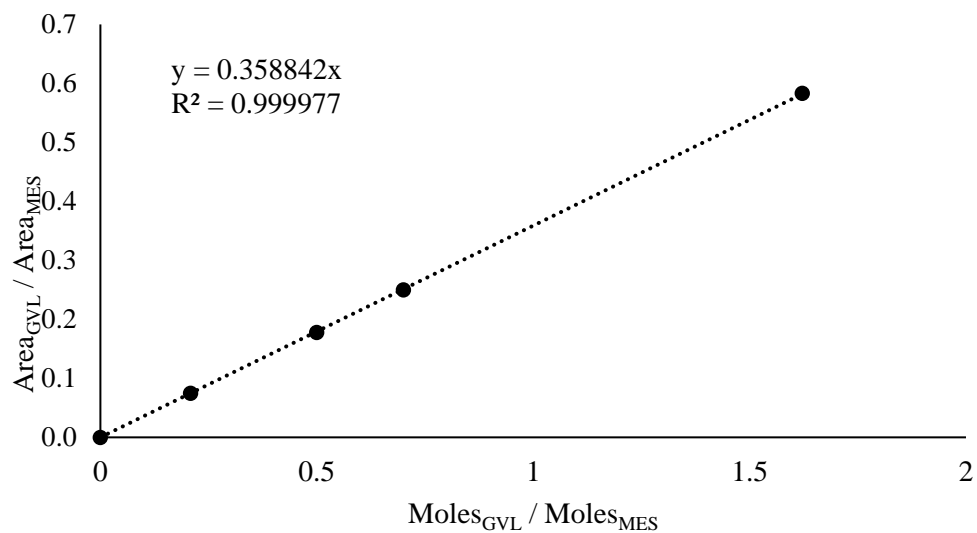


Figure 8. Calibration curve used for measuring GVL with GC for chapter 3. Response factor of 0.3588 was obtained. Mesitylene was used as internal standard.

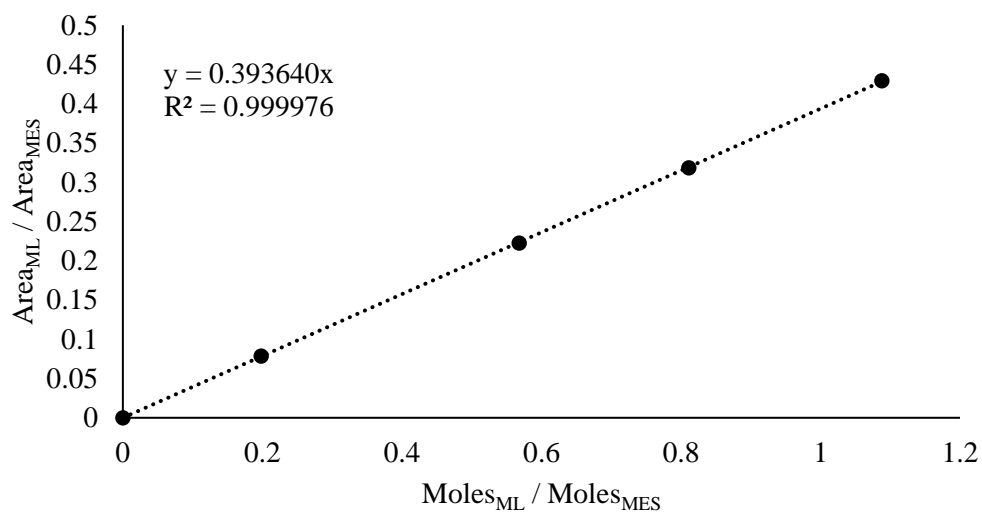


Figure 9. Calibration curve used for measuring methyl levulinate with GC for chapter 3. Response factor of 0.3936 was obtained. Mesitylene was used as internal standard.

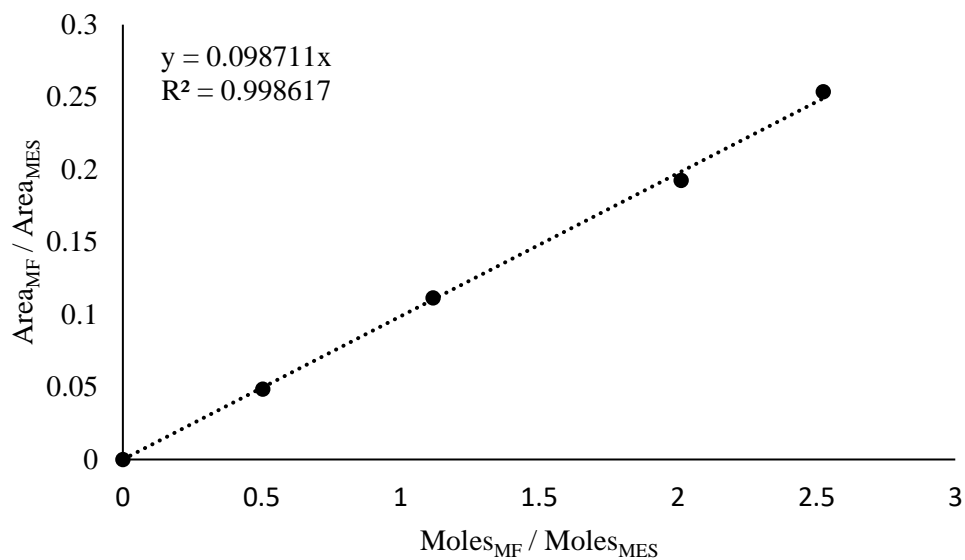


Figure 10. Calibration curve used for measuring methyl formate with GC for chapter 3. Response factor of 0.0987 was obtained. Mesitylene was used as internal standard.

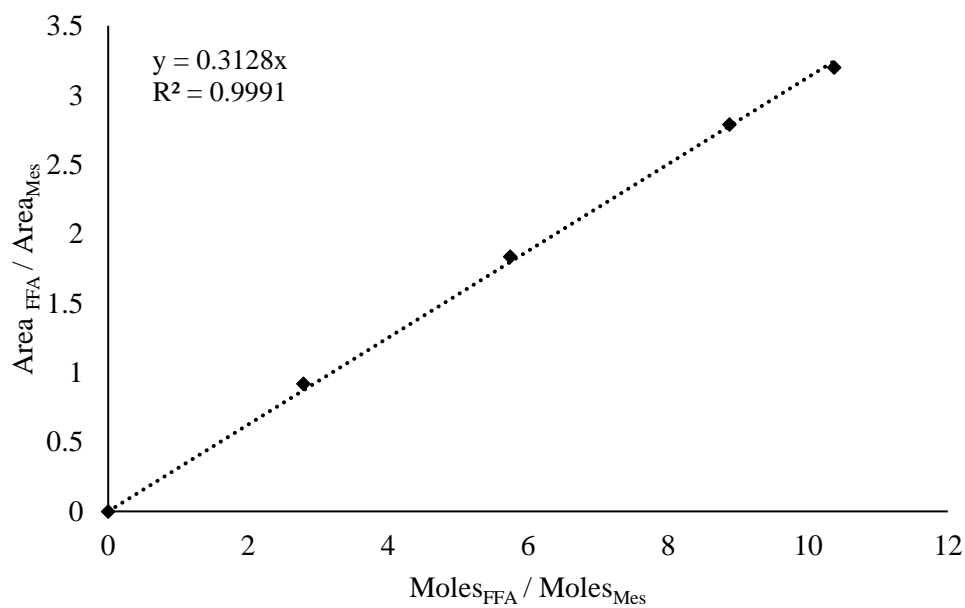


Figure 11. Calibration curve used for measuring furfural alcohol with GC for chapter 3. Response factor of 0.3128 was obtained. Mesitylene was used as internal standard.

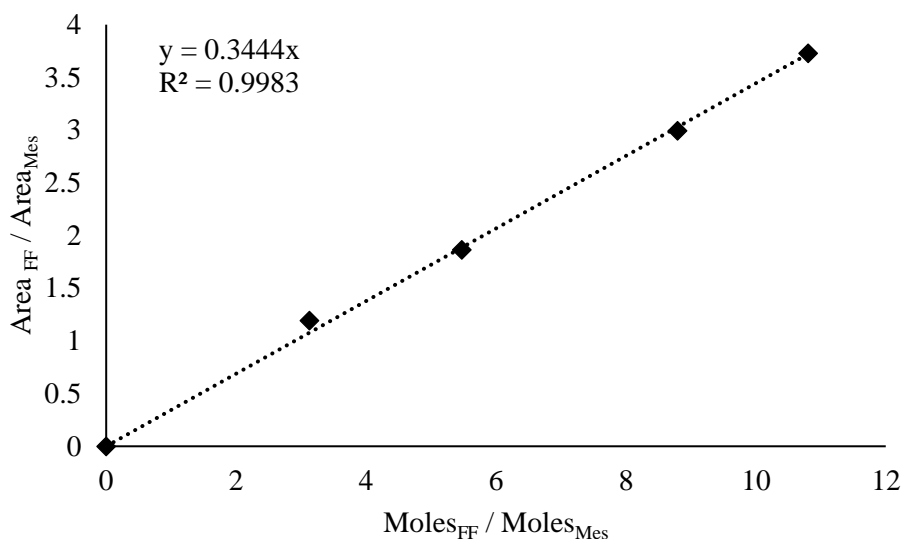


Figure 12. Calibration curve used for measuring furfural (FF) with GC for chapter 3. Response factor of 0.3444 was obtained. Mesitylene was used as internal standard.

2.4.2. High Performance Liquid Chromatography (HPLC)

HPLC works on an identical basis to GC, however the samples are injected as liquid, and remain liquid for the duration of analysis. A typical HPLC machine consists of several components:

1. Pump – the pump is responsible for maintaining a constant flow of mobile phase throughout the instrument. It is capable of delivering high pressures (typically 50 – 300 bar) at high-precision flow rates. A pump takes mobile phase from the solvent reservoir, takes it to the degasser where atmospheric gasses are removed and then flows it to the rest of the instrument. A pump is a very important component of any HPLC, as variations in flow rates will affect the output signal retention times and strength.
2. Injector valve – the injector valve introduces the analyte sample into the mobile phase.
3. Column – similarly to a GC, the role of a column is separation of chemicals. Column is packed with porous adsorbate material (stationary phase) which interacts with the injected chemicals and changes their individual flow rates

throughout the column, thus achieving signal separation. The column used for analysis of liquid samples in this thesis was MetaCarb 67H.

4. Detector – typically, two types of detectors are used in a HPLC – Refractory Index Detector (RID) and UV/Vis absorbance detector. UV/Vis detector can scan a range of UV values at once, however it is best applied to systems with unsaturated bonds present, as saturated hydrocarbons might be undetected or produce weak signals. An RID detector is considered to be a universal detector, because it detects changes in refractive index with relation to the mobile phase. RID was used for analysis of post-reaction mixtures in this thesis.
5. Data collection – raw signal from the RID was collected, processed and plotted by a computer.
6. Mobile phase – the mobile phase used in this thesis was 0.1% H_3PO_4 . Many different mobile phases can be used in HPLC analysis, and they are picked appropriately to fit the chemicals analysed and the column used.

All samples analysed by HPLC in this thesis were 1 mL liquid samples of the reaction mixture. Calibration curves used for measurement of conversions and yields are shown in figures 13-16.

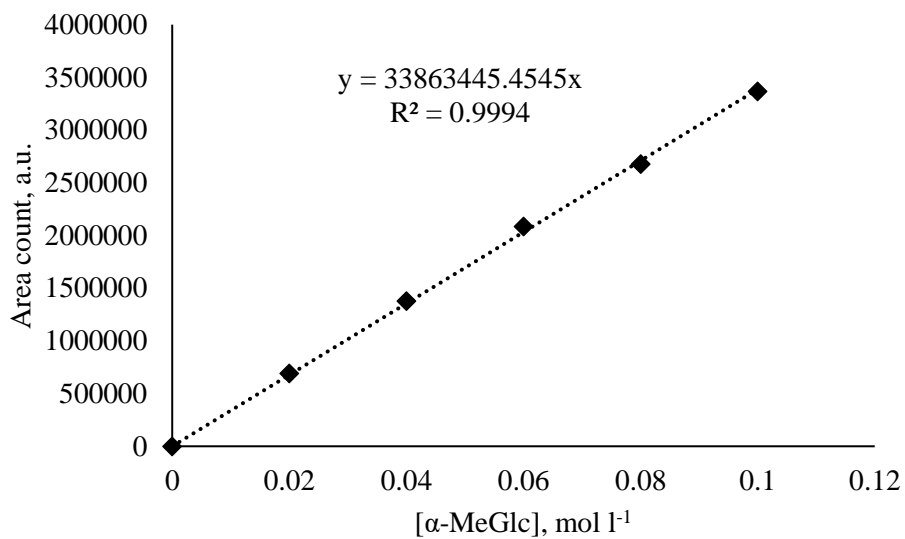


Figure 13. Calibration curve for α -MeGlc with HPLC for chapter 3. Response factor of 33863445.4545 was obtained.

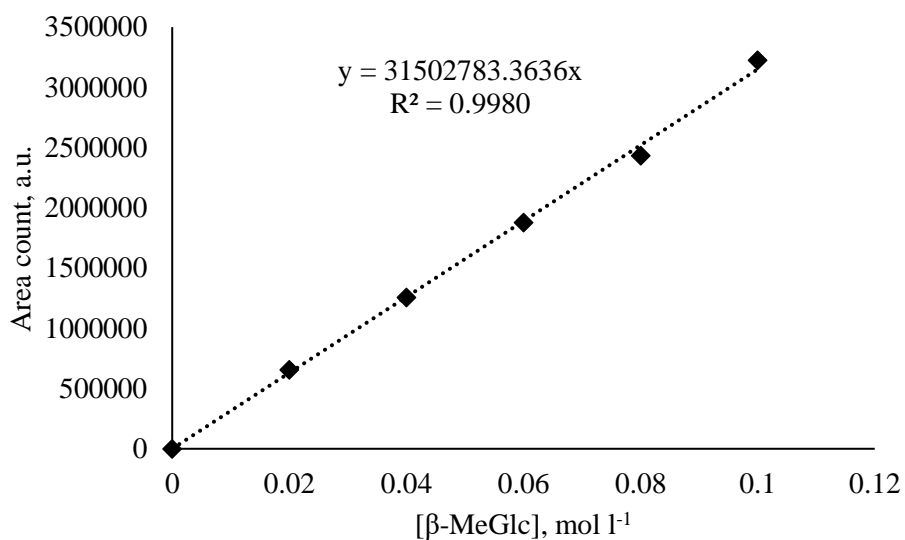


Figure 14. Calibration curve for β -MeGlc with HPLC for chapter 3. Response factor of 31502783.3636 was obtained.

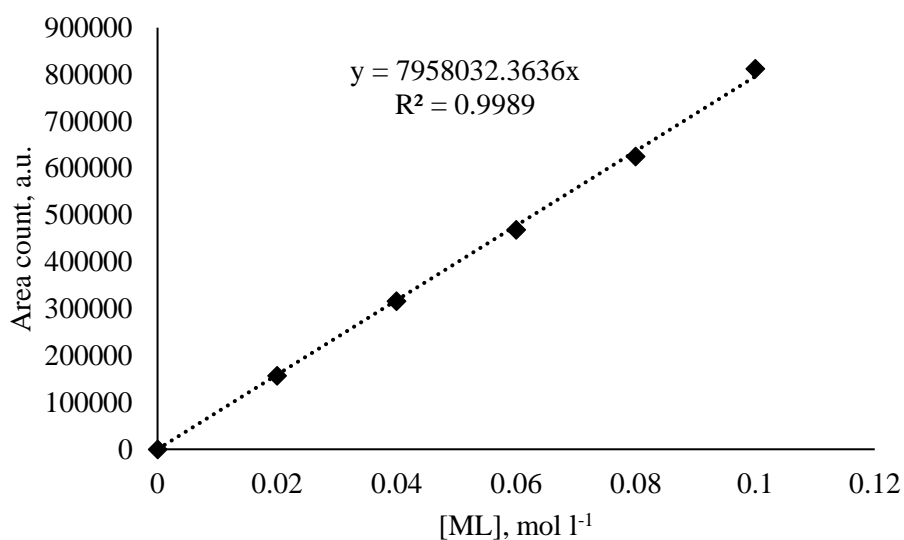


Figure 15. Calibration curve for methyl levulinate with HPLC for chapter 3. Response factor of 7958032.3636 was obtained.

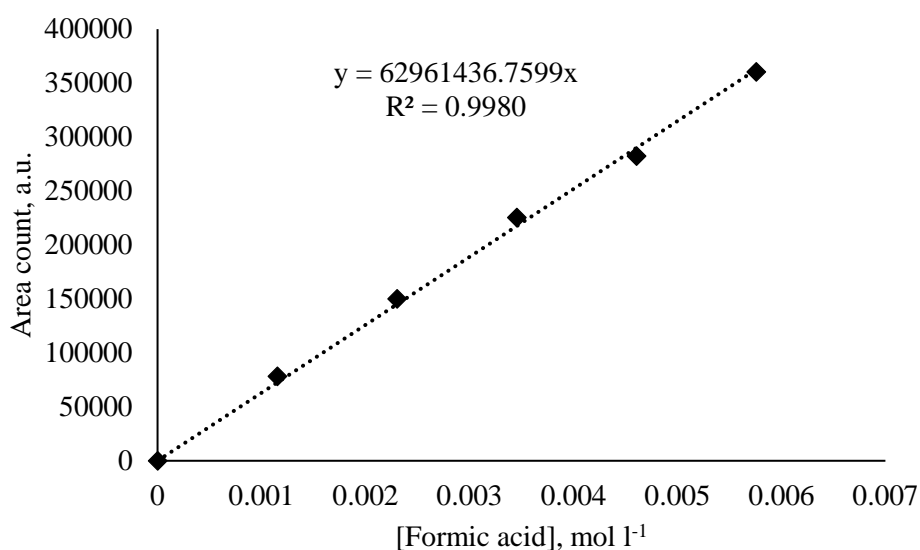


Figure 16. Calibration curve for formic acid with HPLC for chapter 3. Response factor of 62961436.7599 was obtained.

2.4.3. Nuclear magnetic resonance (NMR) spectroscopy

NMR is a non-destructive spectroscopic technique used to identify molecules present in a sample. Various types of NMR analysis exists, such as ¹H and ¹³C, both of which were used in this thesis. The technique can be applied to any atom which has a spin value of ½. A sample of analyte was prepared by mixing known quantities of the sample solution and D₂O. A deuterated solvent is necessary for NMR analysis, as

the machine locks on to the signal of the pre-configured deuterated compound. This is done to compensate for any drift in magnetic field. An internal standard (tetramethylsilane, TMS) of known quantity was sealed in a glass tube and added to the vial, so that quantitative analysis could be carried out. A strong magnetic field (B_0) is then applied to the sample, which causes the $\frac{1}{2}$ spin nuclei to separate into two energy states: the lower $+\frac{1}{2}$ and the excited $-\frac{1}{2}$. The energy of the spin state becomes excited, after which it relaxes to the original state; as part of this process, energy is given emitted at a specific wavelength which can then be measured and interpreted by the instrument.

2.4.4. Gas chromatography-mass spectrometry (GC-MS)

GC-MS is an analytical method which combines gas chromatography and mass spectrometry in tandem for a more complete analysis. GC-MS assigns mass fragments detected to each peak in the GC spectrum, making positive identification of a chemical possible. The prepared sample is injected into the GC instrument, as described in section 2.4.1. However, at the end of the column, the sample is then carried over into a mass spectrometer.

Mass spectrometry is an analytical technique which ionises the compounds in the sample and outputs a report of ions present and their charge/mass ratio. The sample is first vapourised at the injector, and ionised by being bombarded with electrons. Organic molecules break down into identifiable fragments. The fragments are then accelerated and a magnetic field is applied to deflect them. The amount by which a fragment is deflected depends on their charge/mass ratio; lighter fragments will be deflected more by the magnetic field. As the ions are sorted by their mass/charge ratio, they hit the detector which analyses the relative abundances of the ions. GC-MS was utilised in chapter 4 of this thesis. A gas chromatograph Shimadzu GC-2010 Plus was paired with a Shimadzu GCMS-QP2010 SE mass spectrometer.

2.4.5. Calculation of yields and conversions

Yields and conversions were calculated using calibrated response factors for both GC and HPLC machines. Typically, calibrations were carried out by preparing five solutions containing the desired chemicals, at a range of concentrations spanning values typically seen in reactions. If a standard (internal or external) was used for calibration, then two values were calculated for each solution: a) molecule peak area divided by standard peak area and b) moles of molecule, divided by moles of standard. The obtained values were plotted on an area vs. moles graph and the resulting plots' gradient was taken as the response factor ($R^2 \geq 0.99$).

If no standard was used for calibration (i.e. HPLC analysis), then peak area vs. moles graph was plotted for each chemical and the gradient was taken to as the response factor ($R^2 \geq 0.99$).

The amount of chemical, x , in the sample could then be calculated as such from GC or HPLC data using equations 2.1 – 2.4.

Equation 2.1.

$$\text{moles } x = \left(\frac{\left(\frac{\text{peak area of } x}{\text{peak area standard}} \right)}{\text{Response factor of } x} \right) * \text{moles standard}$$

Knowing the amount of moles in a sample, conversion could be calculated:

Equation 2.2.

$$\text{Conversion of } x = \frac{x_0 - x_f}{x_0} * 100\%$$

Where x_0 is the starting moles of the substrate x and x_f is the moles of the substrate x after a reaction.

Yields of product, m , were calculated from moles:

Equation 2.3.

$$\text{Yield of } m = \frac{m_f}{x_0} * 100\%$$

Where m_f is the moles of m after a reaction, and x_0 is the starting moles of a substrate x .

For the conversion of α -D-methyl glucopyranoside to methyl levulinate, where both α and β anomers are present in the reaction, x_f is taken to be the sum of moles of α and β anomers at the end of a reaction as their reactivity profiles are very similar and there is an equilibrium established between the two molecules.

Finally, carbon balance was calculated from moles of carbon of identified products:

Equation 2.4.

$$\text{Carbon balance} = \frac{C_{final}}{C_0} * 100\%$$

Where C_{final} is the total moles of carbon in known products after a reaction, and C_0 is the total moles of carbon before a reaction.

2.5. Catalyst characterisation**2.5.1. Bruanuer-Emmett-Teller (BET) surface area analysis**

Determination of surface area is one of the primary characterisation techniques for many catalysts, as surface area can often be correlated to catalytic activity. The BET model is commonly used for surface area analysis, and it's based on the Langmuir model for monolayer molecule adsorption. The BET model features several assumptions to allow it to be applied to surface area analysis:

1. Gas molecules adsorb on a solid surface in infinite layers.
2. There is no interaction between each adsorbed layer.
3. The Langmuir model can be applied to each layer.

BET surface area can be calculated by using the following BET equations:

Equation 2.5.

$$\frac{1}{v\left[\left(\frac{p_0}{p}\right) - 1\right]} = \frac{c - 1}{v_m c} \left(\frac{p}{p_0}\right) + \frac{1}{v_m c}$$

Where v is the quantity of gas adsorbed, p_0 is the saturation pressure of adsorbed gas at adsorption temperature, p is the equilibrium pressure of adsorbed gas at adsorption temperature, v_m is the quantity of a gas adsorbed needed for a monolayer, and c is a BET constant, which is calculated from the heat of adsorption. Equation 2.5 can then be plotted on a graph where $x = (p/p_0)$ and $y = 1/v[(p/p_0) - 1]$. Slope and the intercept can be used to calculate v_m , from which total surface area, S_{total} , can be calculated.

Equation 2.6.

$$S_{total} = \frac{(v_m N s)}{V}$$

Where S_{total} is the total surface area, N is the Avogadro's number, s is the adsorption cross section of the adsorbed gas, and V is the molar volume of the gas adsorbed.

From total surface area S_{total} , specific surface area, S_{BET} , is calculated.

Equation 2.7.

$$S_{BET} = \frac{S_{total}}{m}$$

Where m is the mass of the sample or adsorbent used.

All surface areas for in this thesis were determined using a 5-point adsorption method performed at liquid nitrogen temperature (-196 °C) on a Micromeritics Gemini 2360 using the BET model. Each sample was subject to a degass procedure at 120 °C for 2 hours under flowing N₂ before analysis, to remove any adsorbed species.

2.5.2. X-ray diffraction

X-ray diffraction (XRD) is one of the most popular techniques for characterisation of heterogeneous catalysts. It is a non-destructive, crystallographic technique which allows for the determination of crystallites present and their size, phases or unit size. However, it is only useful for crystalline materials, where atoms are regularly spaced. Amorphous materials will not produce useful information with this technique.

XRD works on the basis of measuring the constructive interference stemming from elastic scattering of the x-rays as the incident beam hits the atoms of a measured material. Elastic scattering means that the scattered x-rays is of the same wavelength as the source x-rays. As the incoming x-ray beam hits the atoms, it is scattered in a specular (mirror-like) fashion, and depending on the diffraction angle θ , the interference of the outgoing radiation can be either constructive or destructive; a constructive interference will produce a signal, and therefore a peak in XRD, whereas destructive interference will not. Constructive interferences can be described by Bragg's law (equation 2.8).

Equation 2.8.

$$2d \sin \theta = n\lambda$$

Where d is the inter-planar spacing, θ is the diffraction angle, n is a positive integer, and λ is the wavelength of incoming x-rays.

Powder XRD was used for all XRD analysis in this thesis. A PANalytical X'Pert Pro diffractometer equipped with a CuK α source operated at 40 kV and 40 mA was used for data collection, with 2θ range of 10-80°. Analysis of data was carried out by comparison of data to a PDF library of XRD patterns.

2.5.3. Temperature-programmed reduction

Temperature-programmed reduction (TPR) is a catalyst characterisation technique where hydrogen is passed over a heated sample in order to identify the oxidation state of a metal and its reducibility. Optimal reduction temperature for a catalyst can also be determined from TPR. As the catalyst is reduced during TPR, it consumes hydrogen, which produces a signal and results can be plotted on a graph.

TPR was carried out using a Thermo 1100 TPDRO instrument. Samples (0.25 g) were pre-treated at 110 °C, with 20 °C/min heating rate, for 1 hour under flow of helium (20 mL/min) in order to clean the catalyst surface. The sample was then cooled to room temperature, and subject to reduction under 10% H₂/Ar (20 mL/min), heating to 350 °C at 1 °C/min.

2.5.4. Diffuse reflectance infrared fourier transform (DRIFTS) analysis

DRIFTS is a technique which analyses the diffuse infrared reflection of a solid sample. In this thesis, pyridine DRIFTS was used as a way of measuring acidity of a catalyst. Pyridine is absorbed onto the catalyst, and interacts with acid sites. Bronsted-acid sites protonate pyridine, producing an IR absorption at around 1540 cm⁻¹. Lewis acid sites form a complex with pyridine, giving an IR absorption at around 1445 cm⁻¹. There are also several other IR adsorption bands that can be attributed to either Bronsted sites (B), Lewis sites (L), or both; these bands can be found around 1635 cm⁻¹ (B), 1610 cm⁻¹ (L) and 1488 cm⁻¹ (L+B). Quantification of acid site strength is difficult, but possible with this technique. It is mainly used as a qualitative tool.

Pyridine DRIFTS was carried out using Bruker Tensor 27 instrument. The sample cuvette was filled with catalyst and the sample chamber was sealed. Nitrogen was bubbled through pyridine and carried through a heated steel line (120 °C), and passed over the sample at 60 mL/min for 5 minutes at room temperature. Once the surface

of the catalyst has been saturated with pyridine, flow of nitrogen was stopped and the catalyst was exposed to a vacuum line. The sample was then heated to pre-determined set points and IR measurements were taken. The temperature was ramped in stages until a maximum of 550 °C, in order to desorb pyridine off the surface of the catalyst.

2.5.5. Microwave plasma atomic emission spectroscopy (MPAES)

MPAES is an elemental analysis technique which can be used to analyse the specific metal content in solution. For example, a catalyst can be digested in aqua regia, and the solvated metal content can be analysed to give an accurate metal loading on the catalyst. MPAES can also be used to find the amount of metal leached into the reaction solution.

The technique is based on passing a nebulized sample over a nitrogen plasma, heated to 5000K with the use of microwave radiation and magnetic fields. Electrons in the metal atoms in the sample are excited into higher energy states as they pass over the plasma, followed by a relaxation into lower energy. As the electrons relax, they give off photons of defined wavelengths which are specific to certain elements, due to the fact that energy levels are quantized. The photons are then detected and the response can be quantified using a calibrated response curve made up from stock solutions.

Solution samples from reactions using CuZrO₂ catalysts were checked for copper metal leaching using an Agilent MP-AES 4100 instrument.

2.5.6. Scanning electron microscopy (SEM)

SEM is a powerful surface analysis technique which uses a focused beam of electrons originating from a LaB₆ filament to scan the surface of a sample with a raster pattern. As the electron beam interacts with the surface of the catalyst, several types of radiation are generated, including backscattered electrons (BSE), x-ray (EDX), and secondary electrons (SE). Secondary electrons are emitted from the

sample due to high energy of the beam. The SE are detected and an image can be generated from the data. As electrons are emitted off the sample, electron holes may form; in order to fill these electron holes, electrons from higher energy levels may fill the hole, and in the process give off x-rays correspondent to the difference in energy between the two levels. The x-rays can be detected by SEM and a map of elements and their positions can be generated, giving the composition of the surface.

Samples were prepared for SEM by sonicating a small amount of catalyst in ethanol and depositing them onto a carbon-supported, 300-mesh copper grid, and drying any excess solvent. SEM was then carried out using a Tescan MAIA3 Triglav FEG-SEM, with the beam operating at 15 kV.

2.5.7. Copper surface area measurement by N₂O titration

Aside from total surface area, normally measured by BET method, the specific surface area of a metal can also be measured by using N₂O titration. N₂O is capable of oxidising copper particles to cuprous oxide. A known quantity of N₂O is passed over the catalyst, where the redox reaction happens ($2\text{Cu} + \text{N}_2\text{O} \rightarrow \text{N}_2 + \text{Cu}_2\text{O}$). Any excess N₂O is captured by a molecular sieve, and the produced N₂ is carried to the detector. The specific copper surface area can be calculated by comparing the N₂ output of the catalyst to a N₂ calibration peak.

N₂O titration experiments were carried out using a Quantachrome ChemBet Pulsar instrument. Prior to analysis, the catalyst was reduced inside the instrument under flow of 10% H₂/Ar at 280 °C. Once reduced, the catalyst was cooled under a flow of He to 70 °C. The instrument was then injected with 12 pulses of 113 μL N₂O and 4 pulses of N₂ for calibration.

2.5.8. Ammonia temperature programmed desorption

Ammonia temperature programmed desorption (TPD) is an analytical technique which allows for quantitative measurement of acid sites present on a material.

Ammonia is a small molecule which can penetrate most pores and therefore a good choice for a probe molecule. The probe molecule adsorbs onto acid sites on the material. The sample is then heated; depending on the strength of the adsorption, the probe molecule will desorb at different temperatures. As the ammonia desorbs and passes through TCD, it generates a signal which is then recorded on a computer. The signal can then be plotted and used for qualitative and quantitative analysis of acid sites on the catalyst.

NH₃ TPD experiments were carried out using a Quantachrome ChemBet instrument. Prior to analysis, the catalyst was subject to pre-treatment to remove any adsorbed water on the surface by heating it under flowing helium for an hour (130 °C, 15 °C min⁻¹). Sample was then cooled to room temperature, and ammonia gas was passed over it at approximately 50 ml min⁻¹ for 15 minutes to saturate the surface. Any physisorbed ammonia was then removed by heating the sample under flowing helium for 1 hour (100 °C, 15 °C min⁻¹). Once ready, TPD was performed by heating the sample to 900 °C, ramp rate 15 °C min⁻¹.

2.5.9. References

- 1 S. Zheng, H. R. Heydenrych, A. Jentys and J. A. Lercher, *J. Phys. Chem. B*, 2002, **106**, 9552–9558.

Chapter 3

Conversion of methyl glucoside to methyl levulinate using solid acid catalysts

All references are self-contained to within this chapter, and do not refer to any other chapters.

3.1. Introduction

Methyl glucoside (MeGlc) is a methyl ester derivative of glucose, the most common monosaccharide on the planet. As a renewable chemical, glucose can be derived from lignocellulosic biomass; more specifically cellulose, which makes up to 50% of biomass.¹ Glucose can be converted into a wide range of useful chemicals, such as 5-HMF, fructose, furfural, and levulinic acid amongst others.² Levulinic acid (LA) has been identified by the US Department of Energy as one of the top ten high-value target molecules derived from biomass.³ Levulinic acid can be industrially extracted from cellulose using the Biofine process with sulfuric acid.⁴ While comparatively inexpensive, use of a mineral acid has several disadvantages: additional costs in the recovery of acid from mixture, lack of control over selectivity, lack of control over polymerisation side reactions, potential equipment corrosion.⁵ Because of this, there is an interest in developing a heterogeneous catalysis approach to this issue.

There are numerous examples in literature of heterogeneous materials applied to this reaction, as discussed in chapter 1. There is a range of conditions reported, varying in catalysts, temperature, solvents used, etc. One unifying factor is that vast majority of these materials are Brønsted acidic, meaning they are proton

donors. The dehydration reaction from glucose to levulinic acid requires acidic conditions to take place, somewhat limiting the scope of materials available. Further, acidity of a catalyst can be difficult to control and tailor; zeolites are customisable in that the Si:Al ratio and pore size can be modified as necessary, however on most other materials the acidity is poorly controlled.

While most of the catalysts used in this chapter are not novel, the goal was not to develop new materials, but rather to gain a better understanding of the dehydration reaction. The aims of this chapter are to carry out a study on the production of methyl levulinate from methyl glucoside with heterogeneous catalysts; assess the relationship between acidity of the material and activity; gain a better understanding of how humins are produced and how to optimise the reaction conditions to limit their formation.

3.2. Results and discussion

3.2.1. Conversion of glucose to methyl glucoside

The main substrate used in this chapter was methyl glucoside (MeGlc). The methylated version was used because of two reasons; firstly, the work in this chapter was carried out as part of an EU-Japan collaboration. The glucose extraction from biomass sources was initially reported to have been carried out in methanol as solvent by our partners. Therefore, methylated glucose was the product of the reaction. Secondly, use of alcohols as solvents for the dehydration of glucose has been reported in literature to limit the formation of humins, the polymer side-products.^{6,7} As a first step in this reaction, the ease of conversion of glucose into methyl glucoside was assessed.

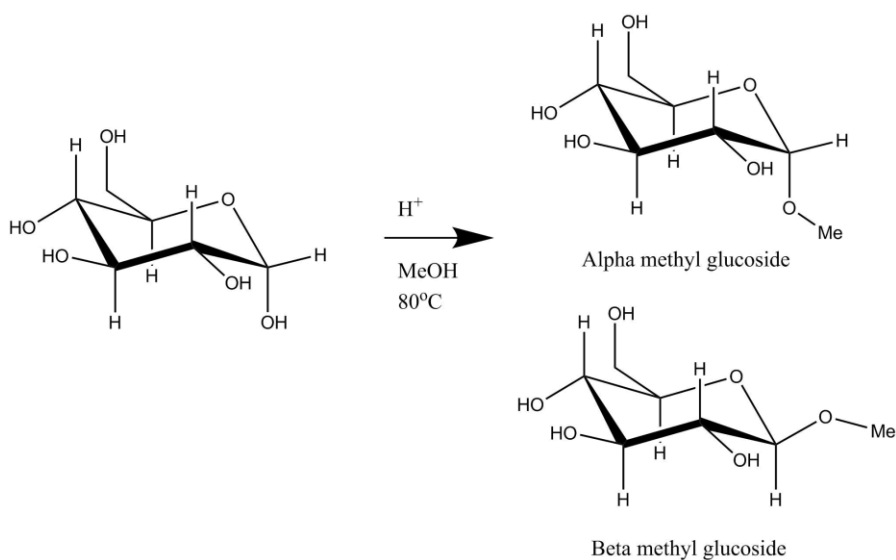


Figure 17. Reaction scheme for methylation of glucose.

Methylation of glucose is an esterification reaction. Esterifications are catalysed by acids, and therefore sulfuric acid was selected as one of the most common and simple acids. Varying amounts of conc. H_2SO_4 were used – 1 mmol, 3 mmol and 5 mmol, seen in Figure 18. This was done in order to determine whether any side reactions took place when more acid was used. It was found that 100% conversion was reached at 1 mmol acid, which was a stoichiometric amount; conversion and selectivity did not change with increasing acid concentrations. It is known that glucose can undergo dehydration reactions, resulting in a myriad of products, ranging from polymers, lactones to simple acids.⁸⁻¹¹ However, only two products were observed in this reaction, α -MeGlc and β -MeGlc. This is most likely because temperature at which this reaction was carried out at was too low to initiate the dehydration reactions. The selectivity for α -MeGlc and β -MeGlc was 70% and 30%, respectively, despite the fact that the beta anomer is slightly less sterically hindered. This is in agreement with known glucose chemistry – for a large number of glucose derivatives, the alpha anomer is more stable than the beta anomer.¹² This is because of the anomeric effect, which has several causes: there is good orbital overlap between the ring-oxygen lone pairs and the δ^* orbital of the axial ester

(hyperconjugation); the dipoles of these oxygens point in opposite directions when in the axial position. The effect was significant enough so that α -MeGlc was the major product.

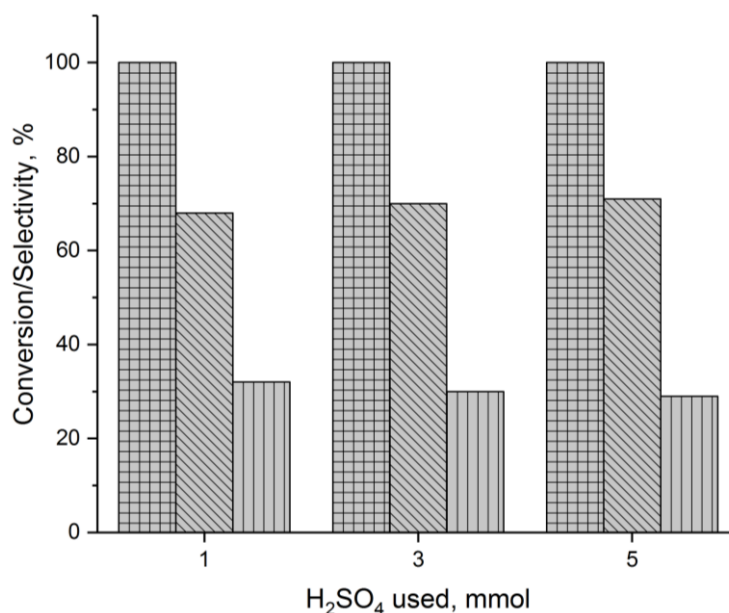


Figure 18. Methylation of glucose using different amounts of acid. Squares: conversion; slanted lines: α -MeGlc selectivity; vertical lines: β -MeGlc selectivity. Reaction conditions: Glucose 1 mmol, Methanol 20 mL, H₂SO₄ 1-3 mmol, temp. 80 °C (reflux), time 16 hours.

It is clear that 16-hour reaction time was sufficient to carry the reaction to full conversion. As such, shorter reaction times were explored, shown in Figure 19. After 2 hours, 77% conversion was observed, with selectivity for α -MeGlc and β -MeGlc of 40% and 60%, respectively. This is in contrast to the 16 hour reaction, where the selectivities were essentially reversed. This means that β -MeGlc was a kinetic product, and α -MeGlc was a thermodynamic one. The beta anomer, with the methyl group in equatorial position, is less sterically hindered; the alpha anomer is thermodynamically more stable because of the anomeric effect. Typically, the beta anomer is the thermodynamic product when the 2-substituent includes a positively charged N⁺ ion. This is known as a reverse anomeric effect; it appears to be exclusive to nitrogen-containing compounds, and is a rare occurrence.¹² The conversion after 4 hours reached 80%, a marginal improvement over the 2 hour reaction. However,

the selectivity towards α -MeGlc and β -MeGlc were different, at 47% and 53% respectively. The data suggests that the esterification reaction proceeded quickly, and much of the reaction time was spent on isomerisation between the two anomers, to reach an equilibrium. Roughly 80% of glucose was converted within the first 2 hours, whereas the remaining 12 hour period accounted for 20% conversion.

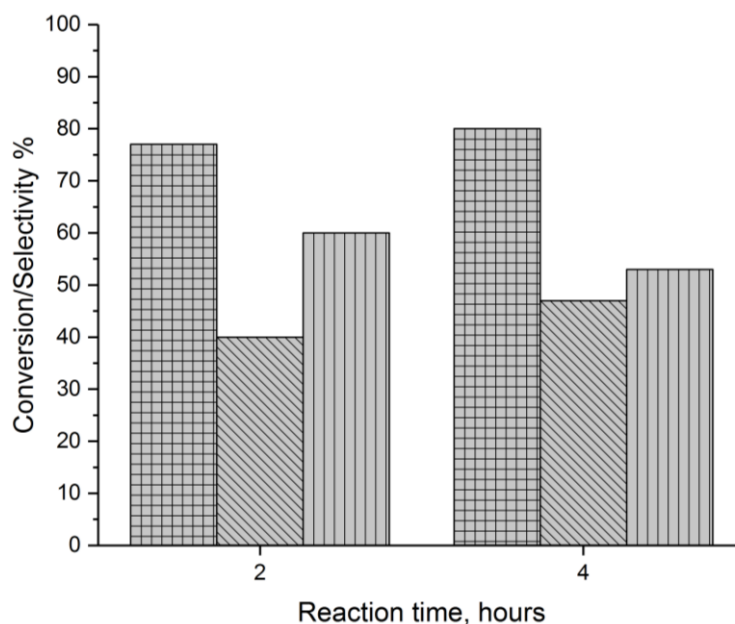


Figure 19. Methylation of glucose at different reaction times. Squares: conversion; slanted lines: α -MeGlc selectivity; vertical lines: β -MeGlc selectivity. Reaction conditions: Glucose 1 mmol, Methanol 20 mL, H_2SO_4 1 mmol, temp. 80 °C (reflux).

Considering that methylation of glucose appeared to happen readily even at short reaction times, a comparison was made between homogenous and heterogeneous acids (Figure 20). A common, commercial solid acid was used - Amberlyst-15 (wet). The amount of glucose was increased tenfold from 1 mmol to 10 mmol, as 1 mmol of substrate proved to be too low at the time frame of a 16 hour reaction. Ideally, the conversion will not reach 100% for either heterogeneous or homogenous catalysts, so that their activity can be compared effectively. Under these conditions, sulfuric acid gave 92% conversion, with 55% and 45% selectivities towards α -MeGlc and β -MeGlc, respectively. The slightly lower than expected ratio of alpha to beta anomers suggests that the reaction was not finalised even after 16

hours. The equilibrium ratio was expected to be around 70:30. When the heterogeneous catalyst was used, a slightly lower conversion of 76%, with selectivities of 43% and 57% towards α -MeGlc and β -MeGlc, respectively. The lower conversion when compared to the mineral acid was not unexpected. Despite the fact that 1 mmol of both was used, H_2SO_4 had a higher concentration of acid sites at 20 meq H^+ /g, compared to 4.8 meq H^+ /g.¹³ At the same time, Amberlyst is considered a superacid thanks to its much lower pKa value of -6.5 compared to approximately -3 for H_2SO_4 .¹³ Any acid stronger than concentrated H_2SO_4 is considered a superacid. The low ratio of alpha to beta anomers, and conversion of roughly 80% indicated that the reaction was at similar stage after 16 hours as the homogenous reaction was after 2 hours, shown in Figure 19 (despite slightly different conditions). This shows that the heterogeneous material catalysed the reaction much more slowly. Aside from acid strength and quantity, this was likely due to sterics. Amberlyst-15 has a polymer structure. Glucose had to be transported to the acid sites before any methylation could take place and was therefore subject to mass transfer limitations. Sulfuric acid was fully dissolved, and each molecule was a single active site because it is a homogenous acid. Additionally, each sulfuric acid molecule can potentially donate two protons.

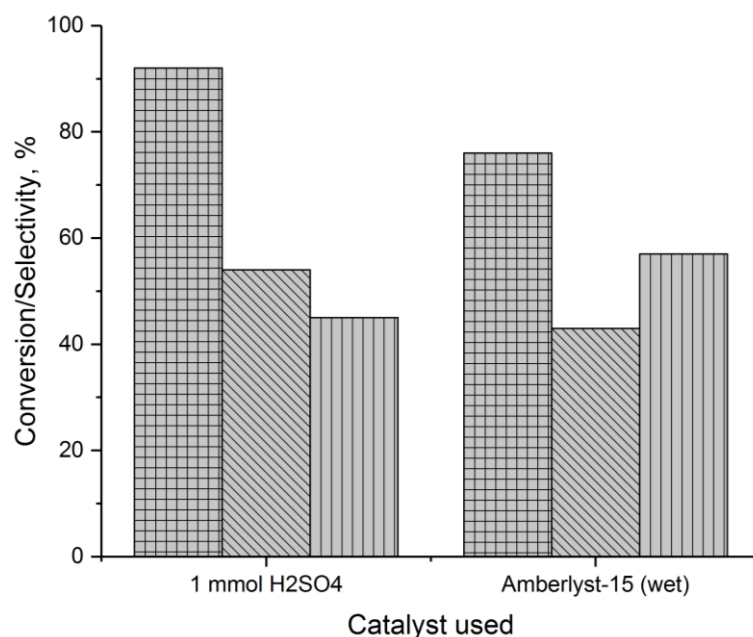


Figure 20. Methylation of glucose using homogenous and heterogeneous acid. Squares: conversion; slanted lines: α -MeGlc selectivity; vertical lines: β -MeGlc selectivity. Reaction conditions: Glucose 10 mmol, Methanol 20 mL, acid 1 mmol, temp. 80 °C (reflux), time 16 hours.

Overall, the esterification process was easy to achieve. It occurred at temperatures much lower than most dehydration reactions, and there was no side-products. Both heterogeneous and homogeneous acids were capable of carrying out the methylation. It was assumed that this part of the reaction would not be a rate-limiting step, especially at higher temperatures. It was therefore acceptable to use methyl glucoside as the starting substrate for future reactions. Specifically, the alpha anomer was chosen due to its natural abundance and much lower cost.

3.2.2. Dehydration of methyl glucoside using solid acids

Several metal oxides were prepared and tested for the dehydration of α -MeGlc. The target molecule was levulinic acid (LA), or a levulinate ester. Initially, the focus was some of the most commonly used oxides – titania and zirconia. Both oxides were tested on their own, and were subject to a sulfation procedure, which added Brønsted functionality to them. The results can be seen in Table 2. The reaction was monitored for levulinic acid, and any levulinate esters. Since the

reaction was carried out in methanol, methyl levulinate (ML) was a possible product. In fact, no LA was observed in any of the reactions, and only ML was present. Nearly all of the catalysts isomerised the starting material between alpha and beta anomers, however the beta anomer was not treated as a product and was considered as unreacted substrate for the purpose of calculations. This is because both the anomers are extremely similar, and their isomerisation was assumed to be a rapid process – the results presented in section 3.2.1. showed that

When titania or zirconia (both prepared in-house) were tested, no ML was produced. This was also the case for P25, a commercially available form of titania. However, all three materials did convert the starting material into 5-methoxymethylfurfural (5-MMF). 5-MMF is a methylated version of a common glucose product, 5-hydroxymethylfurfural (5-HMF). Yields in this case were estimated based on 5-HMF calibrations, since no commercial 5-MMF was available for purchase at the time of these experiments and synthesis of a pure compound proved difficult. The presence of 5-MMF was confirmed through ^1H NMR studies, shown in (Figure 21). The post-reaction NMR spectrum can be compared to commercially available 5-HMF (spectrum obtained from Sigma-Aldrich) in Figure 22. Two characteristic alkene hydrogen doublets can be identified in those spectra.

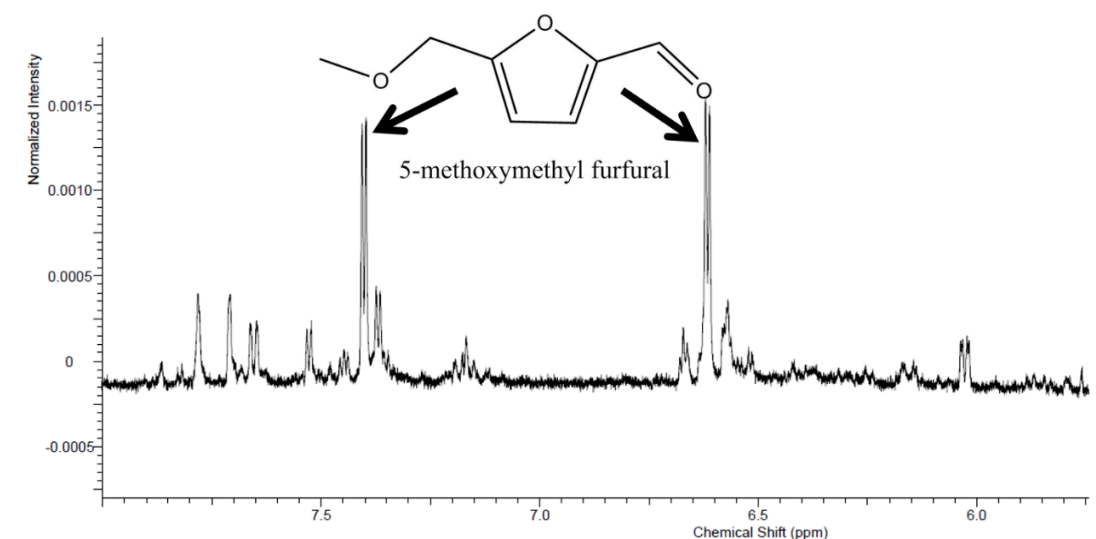


Figure 21. ¹H NMR of the post-reaction mixture. D₂O was used as solvent

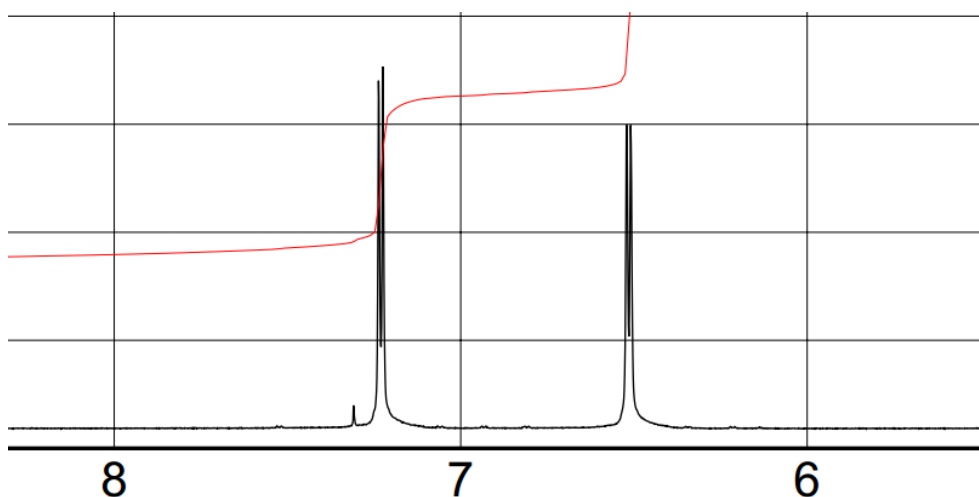


Figure 22. NMR of commercial 5HMF. The corresponding peaks are identical in 5-MMF as these are the alkene hydrogens. Solvent used = CDCl₃

The oxides on their own did not yield any levulinate species. Literature shows that Brønsted acidity is a desired functionality for glucose dehydration and production of levulinate molecules.^{14–16} Therefore, a simple sulfation procedure was carried out on the metal oxides; the materials were immersed in 0.5M H₂SO₄, dried and calcined, in order to add –SO₃H group functionality. Upon sulfation, both titania

and zirconia became active towards the formation of methyl levulinate. The conversion has more than doubled for both materials. $\text{SO}_4\text{-ZrO}_2$ yielded more ML than $\text{SO}_4\text{-TiO}_2$, with yields of 24% and 14%, respectively. The maximum theoretical yield of levulinic acid from glucose has been calculated to be 64.5% in water, however realistically yields as low as 43.0% can be expected due to propagation of side reactions and formation of insoluble humins.^{16,17} Indeed, no higher yield than approximately 24% has been measured in this thesis, which could range anywhere from 37% to 56% of the maximum yield. Isolated examples of literature listing yields higher than 64.5% exist, but it is not clear if their yields are normalised, or listed as a weight fraction.¹⁸

As ML was produced, formic acid was also produced. For $\text{SO}_4\text{-TiO}_2$, the amount of formic acid was stoichiometric with ML. When $\text{SO}_4\text{-ZrO}_2$ was used, a slight excess of formic acid was produced. This is not unexpected, as production of ML is not the only pathway for formic acid formation in this reaction.^{10,19-21} The traditional assumption in portion of the literature is that levulinate species (depending on the solvent) and formate species are produced in stoichiometric amounts. In fact, a great number of publications do not even try to quantify the formic acid in their reactions, either assuming it is formed in 1:1 ratio to levulinic acid or ignoring it altogether. However, several pathways to formic acid exist, and it is common for the ratio of formic acid to levulinic acid to exceed 1 – majority of the reactions in this chapter exceeded that ratio. This is because not every converted molecule of substrate will form the desired product. Aside from the pathway to methyl levulinate which results in one equivalent of methyl formate, there are furfuryl intermediates formed during the dehydration which are capable of producing formate species but do not lead to methyl levulinate/levulinic acid; formic acid could be produced during polymerisation of humins; yet undiscovered pathways could be taking place; methyl levulinate could be getting adsorbed and trapped on the humins; another possible

pathway is through D-erythrose,¹⁹ which can reportedly form from glucose.²²⁻²⁴ Erythrose is a possible product in this reaction, however due to the sheer amount of by-products and intermediates formed, not every single compound was identified by chromatographic techniques. The pathways are illustrated in Figure 23.

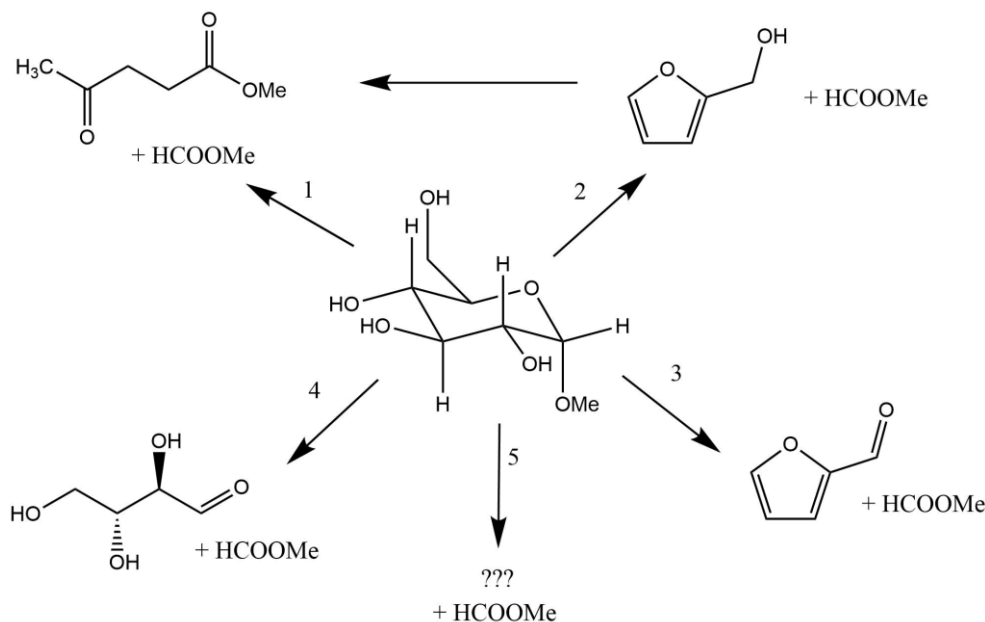


Figure 23. A non-exhaustive list of pathways to formic acid or methyl formate in the dehydration of methyl glucoside. Pathways are not direct, only end-product is shown. 1). Formation of methyl levulinate. 2). Formation of furfuryl alcohol derivative, which can further form levulinate species. 3). Formation of Furfural species. 4). Production of D-Erythrose. 5). Other unknown pathways

Ceria, sulfated ceria and sulfated P25 did not yield any ML. Ceria has been demonstrated to display Lewis acidity,^{25,26} however the data suggests that both acid and base sites are needed. Zirconia and titania are known amphoteric materials (they have both acidic and basic properties), whereas ceria is not. Perhaps it is this amphotericism which drives the reaction. Sulfated ceria and titania did convert the starting material, but they failed to yield any ML. This is likely because of weaker Brønsted acid sites, and lack of amphoteric character of the support. However, without any measurements made, no definite conclusion can be made. The only material other than titania or zirconia which produced ML was $\text{WO}_3\text{-ZrO}_2$. Tungsten was considered as its acidic properties have been shown before.²⁷⁻²⁹ The theory

proved correct and the tungsten oxide-enriched zirconia yielded 1.5% ML. The result is significant for two reasons; the data shows that production of ML simply does not happen without an appropriate catalyst, so even a low yield is statistically important; the result also demonstrates that my understanding of the reaction requirements is correct, and Brønsted acidity is crucial; despite this, the material was not followed further as sulfated zirconia and titania were significantly more active, easier to prepare, and comparatively cheaper. Additionally, 0.5 CuZrO₂ prepared in house was tested for this reaction (last two entries in the table). This catalyst is further explored in chapter 4 of this thesis. Copper zirconia was tried because of its ability to hydrogenate levulinic acid and its esters to gamma-valerolactone. This entire thesis has the premise of converting glucose into gamma-valerolactone; both catalysts are active under the same regimes, with the same solvents, temperatures and pressures, therefore a one-pot process was tested. The copper catalyst on its own did not yield any conversion. This is because CuZrO₂ contains no Brønsted acid sites, despite the amphoteric character of ZrO₂. In order to add Brønsted functionality to the system, SO₄-ZrO₂ was added. Both catalysts were used in equal amounts. Surprisingly, the mixed-catalyst system resulted in 0% conversion of the substrate. Even though SO₄-ZrO₂ performed well in previous tests, with significant yields of ML and formic acid, when paired with Cu-ZrO₂ its activity was inhibited. This was likely caused by poisoning of the catalysts, as sulfur is a known poison for many metals, forming metal sulfides on the surface.^{30,31} It therefore became apparent that a one-pot process might not be possible with this configuration of catalysts, and focus was put on understanding and refining the individual processes.

Table 2. Initial results of dehydration of α -MeGlc. Reaction conditions: 0.62 g α -MeGlc, 0.31 g catalyst, 8 g MeOH, 5 bar N₂, temp 180 °C, time 1 hour. Error margins on all the results are within \pm 5%.

Catalyst	Conversion, %	ML yield, %	5MMF yield, %	Formic acid yield, %	LA yield, %
TiO ₂	19	0	19	0	0
SO ₄ -TiO ₂	54	15	23	15	0
SO ₄ -TiO ₂ (2 hours)	91	35	29	23	0
ZrO ₂	25	0	25	0	0
SO ₄ -ZrO ₂	56	24	0	31	0
Phosphated ZrO ₂	0	0	0	0	0
15% WO ₃ -ZrO ₂	25	1.5	0	15	0
P25	23	0	23	0	0
SO ₄ /P25	37	0	37	0	0
CeO ₂	0	0	0	0	0
SO ₄ -CeO ₂	10	0	10	0	0
0.5 Cu-ZrO ₂	0	0	0	0	0
0.5 Cu-ZrO ₂ + SO ₄ -ZrO ₂	0	0	0	0	0

Sulfated zirconia proved to be more selective towards the levulinate ester than sulfated titania, an effect possibly associated with higher Brønsted acidity. The relative strength of the sulfate group on the surface of these catalysts can be visualised by TGA analysis in Figure 24. The region of interest is above 500°C, where the sulfate species break down from a -SO₄ bound to the metal surface, down to SO₃ and zirconia, and subsequently into SO₂.³² It was observed that the sulfate species on SO₄-ZrO₂ remained bonded to the zirconia at temperatures approximately 100°C higher than SO₄-TiO₂. This indicates that SO₄-ZrO₂ featured stronger sulfate-zirconia interactions, and therefore higher acidity than SO₄-TiO₂.

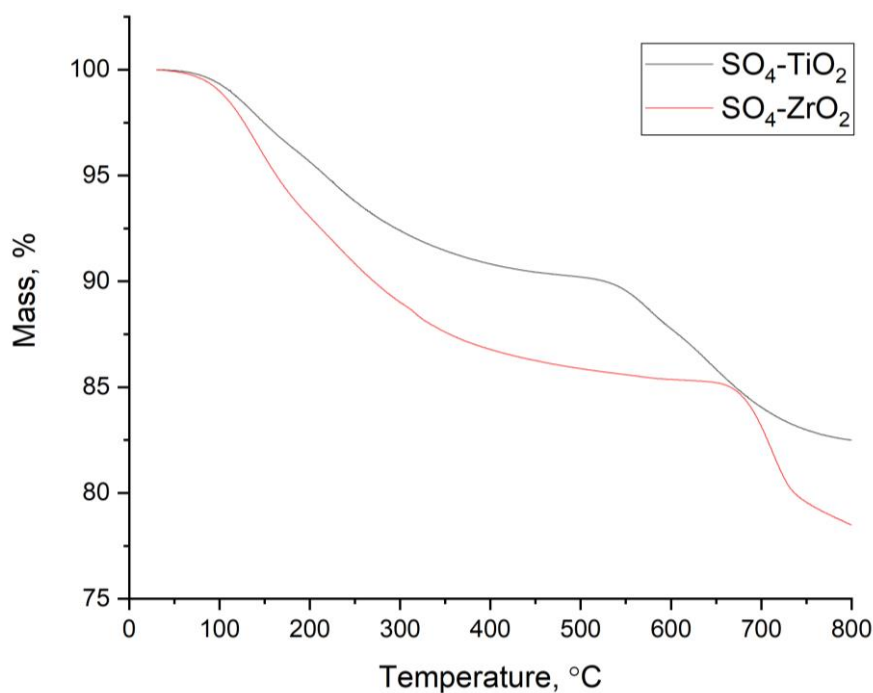


Figure 24. TGA profiles for sulfated catalysts. Red = SO₄/TiO₂, Black = SO₄/ZrO₂

Quantifiable acidity profiles for these catalysts were measured using ammonia TPD (Figure 25). Zirconia-based catalyst had comparatively much stronger acid sites. The total surface acidity of SO₄-ZrO₂ was measured at 0.76 mmol/g, and SO₄-TiO₂ at 0.33 mmol/g. The acidity of these materials is comparable to similar catalysts reported in literature, with acidity values in the region of approximately 0.1-0.7 mmol/g.³³⁻³⁶ These findings strongly correlate several pieces of data obtained for the sulfated catalyst, such as XPS, surface area and activity. XPS data (Table 3) showed that the zirconia catalyst had approximately 2.85 times the amount of sulfur atom concentration of titania catalyst; ammonia TPD revealed that SO₄-ZrO₂ was approximately 2.30 times more acidic on the surface compared to SO₄-TiO₂; BET surface area of these catalysts showed that zirconia-based material had comparatively much higher surface area roughly 157 m²g⁻¹, approximately a factor of 2 higher than titania-based material which was measured at roughly 80 m²g⁻¹. Activity data followed suit, as SO₄-ZrO₂ yielded approximately 1.6 times the amount of ML as SO₄-TiO₂ at the same conversion. Higher surface area catalysts are able to

contain more active sites per area of catalysts. Therefore, it is possible that $\text{SO}_4\text{-ZrO}_2$ was overall more acidic and more active than $\text{SO}_4\text{-TiO}_2$ due to the increased surface area. The increase in yield was not proportional to the increase in acidity, however it was not expected to be. It is likely that not every acid (active) site was available for the reaction to take place. For example, some sites could have been located in small pores where the substrate cannot reach, or be located too close to another active site for two ML molecules to fit in.

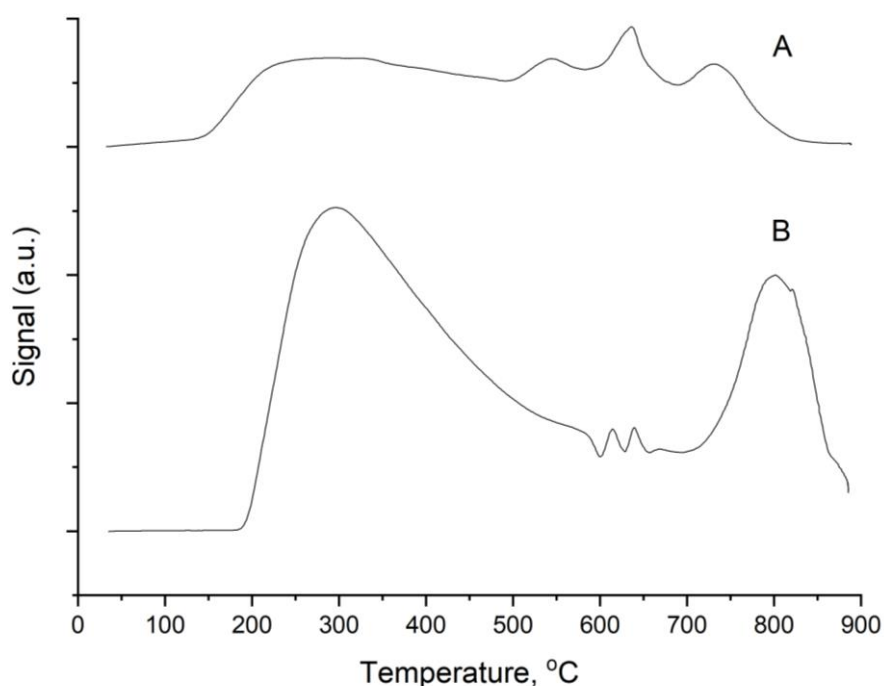


Figure 25. Ammonia TPD patterns for sulfated titania (A) and sulfated zirconia (B).

Table 3. Surface atom concentrations derived from XPS data for sulfated catalysts.

Catalyst	Surface concentration / at.%				
	Zr (3d) / Ti (2p)	S (2p)	O (1s)	C (1s)	N (1s)
$\text{SO}_4\text{-TiO}_2$	19.13	1.19	53.48	23.34	1.16
$\text{SO}_4\text{-ZrO}_2$	17.39	3.40	52.30	26.91	n/a

Table 4. BET surface areas for the sulfated catalysts. Margin of error is approximately $\pm 5\%$, based on commonly accepted errors on BET surface area measurements; still, multiple measurements were taken for consistency.

Catalyst	BET surface area (m^2g^{-1})
$\text{SO}_4\text{-TiO}_2$	80
$\text{SO}_4\text{-ZrO}_2$	157

The ammonia TPD profiles for both catalysts feature at least two relatively distinct peaks, which can be attributed to weak and strong acid sites. The weak acid site peak is located at approximately 300 °C for both catalysts; the strong acid site at approx. 800 °C for $\text{SO}_4\text{-ZrO}_2$, and 740 °C for $\text{SO}_4\text{-TiO}_2$. Another prominent feature of the ammonia TPD profiles is the irregularity in the spectra for both catalysts at 510 °C and 640 °C for $\text{SO}_4\text{-TiO}_2$ and $\text{SO}_4\text{-ZrO}_2$, respectively. These temperatures correlate with significant weight loss events in TGA (Figure 24) and are likely present due to desorption of and breakdown of weakly bound sulfate species on the catalysts.³² There is a small temperature delta between these events in TGA and TPD spectra of about 20 °C, with TGA event recorded at the higher temperatures. The heating ramp rate used for both measurements was identical at 5 °C min^{-1} , however the TGA was carried out in a static air environment, whereas NH_3 TPD was measured in flowing helium. The flow of room-temperature gas over a hot catalyst likely eliminated hot spots and had a small, but measurable effect on the ramp rate. In any case, 20 °C can be considered within margin of error given that the events measured happen over the range of nearly 100 °C (or approximately 20 minutes).

While the difference between Lewis and Brønsted acid sites cannot be discerned from ammonia TPD, it has been suggested that the peak responsible for weak acid sites consists mainly of Lewis acid sites, as they tend to desorb at low temperatures.³⁷ This peak is not always observed in literature, as these acid sites can be weakened or removed depending on the pre-treatment or calcination temperature used when preparing the catalyst.³⁸ At this stage in the testing, it became clear that $\text{SO}_4\text{-ZrO}_2$ is

the superior catalyst for the purposes of this thesis when compared to $\text{SO}_4\text{-TiO}_2$. Therefore, all tests and comparisons going forward were only carried out with zirconia-based catalysts.

In order to assess the presence and strength of specific acid sites on the material, Pyridine DRIFTS experiments were carried out on ZrO_2 and $\text{SO}_4\text{-ZrO}_2$ (Figure 26, Figure 27). Pyridine DRIFTS is able to differentiate between Lewis and Brønsted acid sites due to bonding differences between pyridine and the acid site, however quantitative analysis is notoriously difficult using this method.³⁹ As such, DRIFTS experiments were used to categorise the sites, and the results were paired with ammonia TPD in order to paint a complete picture of the surface acidity. Peak identification was carried out based on existing literature.^{38,40-42} It can be seen that plain zirconia contained no Brønsted acidity, and only Lewis acid sites were observed at 1441 cm^{-1} and 1605 cm^{-1} . A small peak was also measured at 1488 cm^{-1} , but it quickly reduced in size as the temperature increased. No temperature higher than $350\text{ }^\circ\text{C}$ was tested as the peaks greatly reduced in size compared to the room temperature spectrum. The relative size of the peaks, their retention as the temperature increases, and their position are qualitatively useful way of measuring the type and strength of the acid sites. Considering these factors suggests that plain Zirconia had only Lewis-type acid sites of moderate strength.

A similar experiment was carried out on sulfated zirconia (Figure 27). This catalyst featured several more peaks in its spectra, which were attributed to both Lewis and Brønsted-type acid sites; as such, it was confirmed that the sulfation procedure added Brønsted acidity to the material. Specifically, the peaks corresponding to Lewis-acid sites which were observed in plain zirconia were found at near-identical wavenumbers with the acidified catalyst – 1443 cm^{-1} and 1608 cm^{-1} . The small peak observed at 1488 cm^{-1} is now much more prominent as it represented both acid site types. Additionally, Brønsted-site only peaks appeared at 1540 cm^{-1} and 1638 cm^{-1} .

As the temperature was ramped up, it was noted that the peaks retained their size and shape more consistently than the non-sulfated support. In fact, the Brønsted-type peaks were easily identifiable up until 550 °C. The temperature limit of the equipment used was 575 °C, so no higher temperatures were tested. The Lewis-type peaks lost their definition in a similar fashion to the non-sulfated material. This suggests that the sulfation procedure did not have any significant effect on the Lewis acid sites. The Brønsted acid sites remained bonded to pyridine up to the maximum testing temperature – they are therefore strong sites. This is corroborated by the ammonia TPD data – a well-defined peak can be observed at 800 °C, indicating strong acid sites.

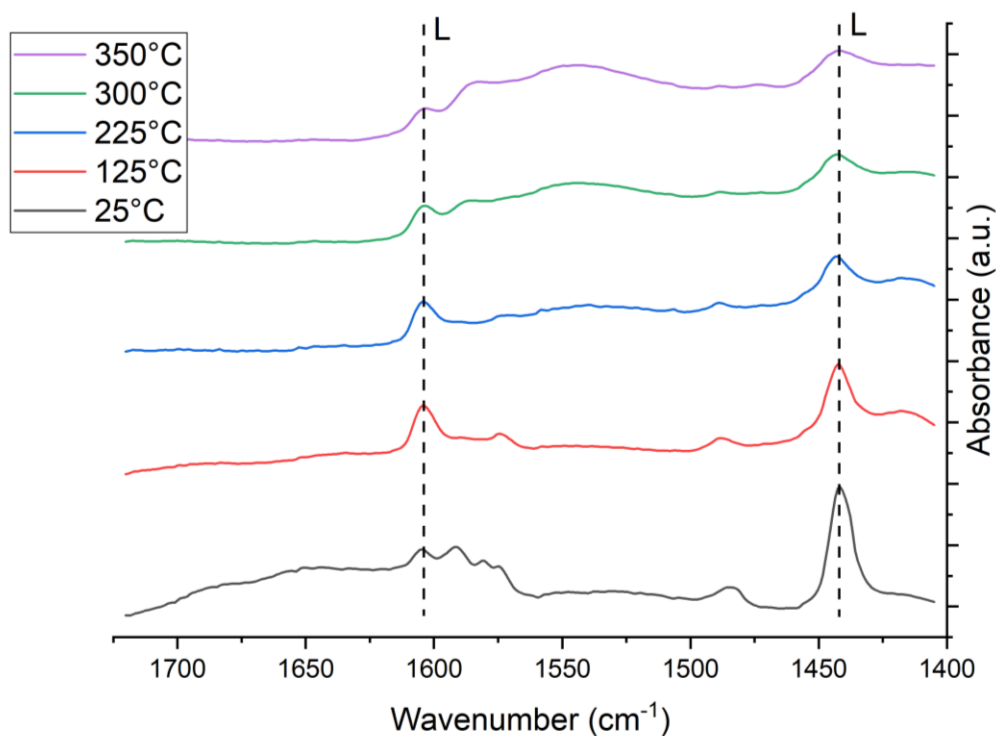


Figure 26. Pyridine DRIFTS IR of ZrO₂. L denotes Lewis-acid sites.

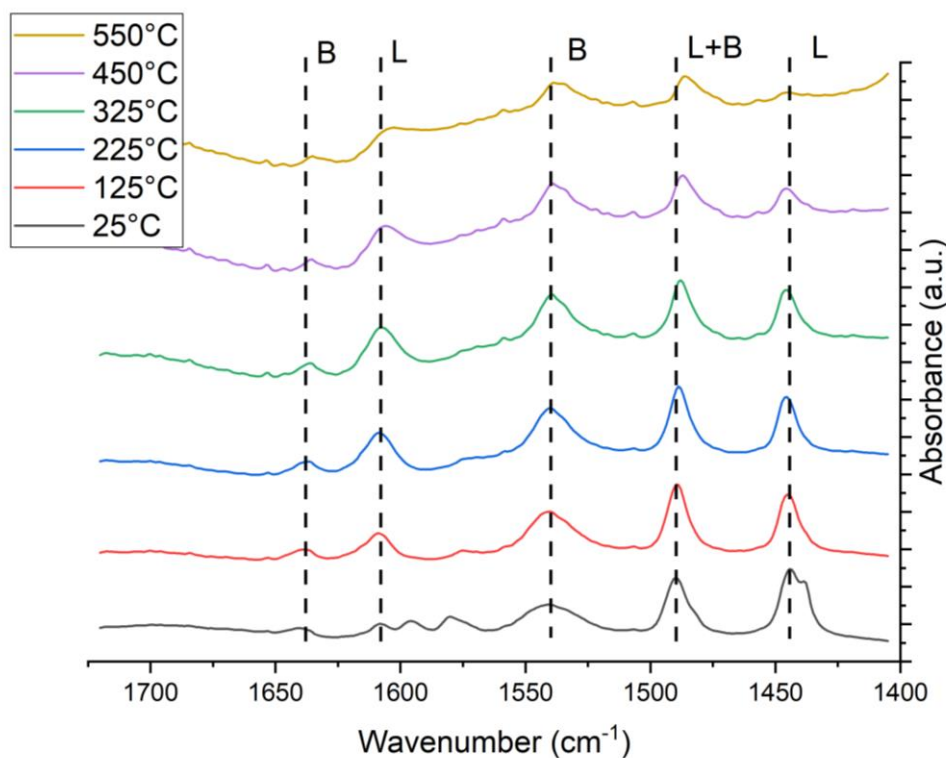


Figure 27. Pyridine DRIFTS IR for $\text{SO}_4\text{-ZrO}_2$. L denotes Lewis acid sites, B denotes Brønsted acid sites.

Having proved that the sulfation procedure did indeed add desired functionality to the catalyst, variations in loadings were explored. This was done for two reasons: to reduce the amount of material used, and to test the scalability and efficiency of sulfated zirconia for this reaction. A range of catalyst loadings were used, while keeping all other reaction conditions the same. Initially, a relatively high loading of sulfated zirconia was used in a 1:2 mass ratio of catalyst to substrate. This is because several systems reported in literature exist where weight ratios of solid acid material to substrate ranging from 40% to 100% and more were utilised, due to the perceived difficulty in carrying out dehydration reactions on cellulose, glucose, and other sugar-based molecules.^{14,29,33,36,43–46} For testing, the amount of catalyst was halved for each experiment, until no yield of ML was observable by HPLC analysis (Figure 28). With the reduction in catalyst mass a corresponding near-linear reduction in conversion and ML yield was noted. The smallest amount of $\text{SO}_4\text{-ZrO}_2$ tested was 0.04 g, at which point no ML was measured post-reaction. The linear relationship

between catalyst mass and ML yield indicates that at these conditions, the reaction was under a kinetic regime. That is to say, the main rate limiting step was the intrinsic surface reaction rather than transfer of reagents or their diffusion into catalyst pores.

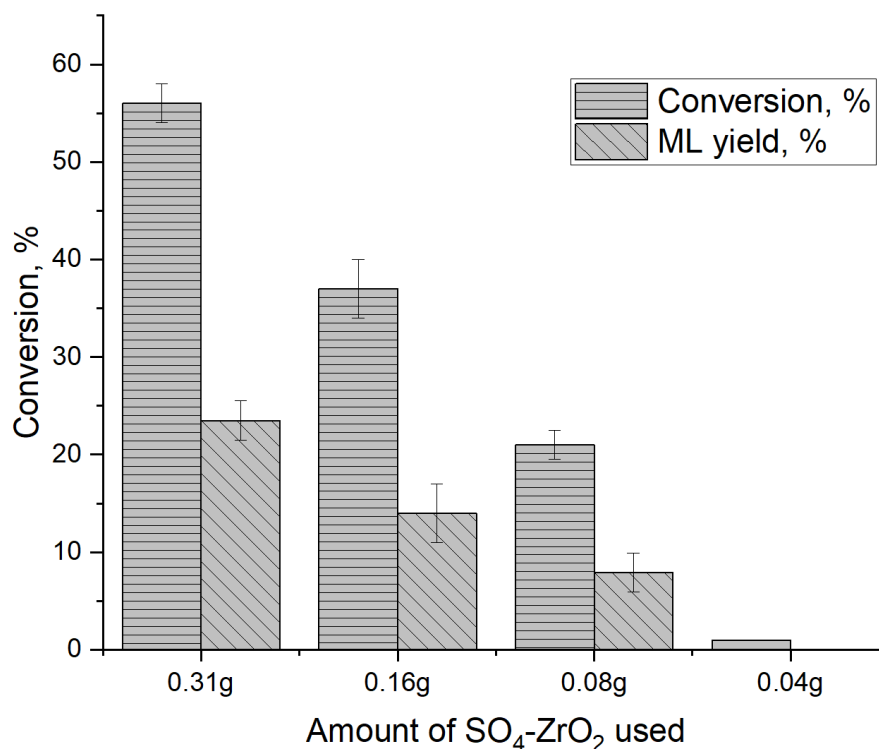


Figure 28. Conversion of alpha methyl glucoside against catalyst loading. Catalyst tested is SO₄-ZrO₂. Temp. 180°C, time 1hr, 5 bar nitrogen, 0.62 g alpha methyl glucoside, 8 g methanol

Going forward, it was decided that 0.08 g of catalyst would be used for all future reactions. The reason for this was twofold; it allowed for a more economic use of the material with the ability to scale up as the catalyst was not mass transfer limited under these conditions; additionally, perhaps as a by-product of lower conversion, the production of humins was reduced (the post-reaction solution was assessed visually) which made HPLC analysis easier. The production of humins in this reaction will be discussed further in section 3.2.4.

3.2.3. Dehydration of methyl glucoside using zeolites

Zeolites are high-surface area, porous materials generally composed of Silicon and Aluminium, which very commonly have Brønsted-acid functionality.

Due to the requirement for acid functionality in this reaction, the availability and low cost of zeolites, they were chosen as natural candidates for testing and comparison to solid-acid materials prepared in-house. Both Brønsted and Lewis-acidity in zeolites stems from the structural arrangement of silicon and aluminium atoms in the lattice. Zeolite structures are generally based upon silicate moieties, which have a tetrahedral arrangement. As aluminium atoms are introduced to the structure, they disturb and deform this arrangement, creating a charge imbalance; this must be satisfied by a cation, frequently a hydrogen atom which becomes Brønsted acidic.⁴⁷ As the number of Al atoms increases (and therefore the Si/Al ratio decreases), the number of acid sites increases due to larger amount of defects. However, each individual acid site then becomes slightly weaker due to proton crowding in the porous structure. Many types of zeolites exist, with a multitude of structures and therefore various pore sizes and acidic strengths. In this chapter, the most commonly used zeolites were tested. Several types of zeolites of various acidic strengths were tested, with Si:Al ratios from 0 to 80. The data is presented in Table 5. Arguably the most popularly used zeolite, ZSM-5, was tested first. It was found that minimal conversion was achieved, and very low ML yield was observed. Both conversion and yield dropped to 0% as the Si:Al ratio increased to 50 and 80, an indication that the acid sites in those materials were not strong or numerous enough to facilitate the reaction. Examples of dehydration of glucose or cellulose using ZSM-5 do exist in literature, however conversion to levulinate species is uncommon, or yields are low (generally less than 5-10%).⁴⁸⁻⁵¹ The yields reported in literature are still higher than the ones tested in-house – this can likely be attributed to longer reaction times and higher reaction temperatures. The low yield can be attributed to the small pore sizes of ZSM-5 compared to the glucose molecule. ZSM-5 pore sizes are about 5.5 Å in diameter due to maximum 10-member rings in the structure, notably smaller than the approximate length of the glucose molecule at 6 Å. The diffusion of the substrate throughout the material would therefore be greatly limited, or impossible;

considering that bulk of the zeolite surface area is contained within the porous structure, any chemistry would be limited to the surface interactions in this case. At the limited reaction length and temperature utilised, the conditions were likely not optimal for the formation of levulinate species, even though the catalyst is clearly capable of facilitating the dehydration of glucose.

Due to the theorised pore size issue, Zeolite β was selected as the next catalyst for testing. Due to limited commercial availability, only two Zeolite β materials were tested, with Si:Al ratios of 25 and 38. Zeolite β has larger pore size than ZSM-5 at 7.3 Å in diameter due to 12-member rings in the structure,⁵² which is sufficiently large for a methyl glucoside molecule to enter. This is reflected in the activity of the material. A similar observation was made by Moliner et. al.⁵³ Conversion and yields are considerably improved over ZSM-5. Interestingly, despite higher acidity, Beta (25) yielded the same amount of ML as Beta (38) at 12%. The difference between the catalysts could be observed in conversion, formic acid yield and carbon balance. As expected, Beta (25) had higher conversion (51% compared to 41%), but it appears that any additional acidity assisted in the side reactions and the formation of humins (hence the lower carbon balance). The post-reaction mixture was also noticeably darker with Beta (25), a typical indication of increased humin production. It can therefore be speculated that there is likely an optimal amount and strength of Brønsted acid sites which balance between achieving high activity and low production of humins.

Two additional zeolite-like materials were tested Sn- β and SBA-15. Both are silica-based materials, however with no aluminium atoms in the structure, and therefore no Brønsted acidity. SBA-15 is a high surface area, mesoporous material which was mainly used as control for these tests. As it contains no desired acidity, it was not expected to facilitate any reactions. This assumption proved true, and 0% conversion was measured with this material.

Sn- β is a zeolite material in which all the aluminium atoms have been replaced by tin, therefore removing any Brønsted acidity – only Lewis acid sites are present on Sn- β . Typically, Sn- β is prepared by hydrolysis of tetraethylorthosilicate (TEOS) alongside tin (IV) chloride around dealuminated zeolite seeds.⁵⁴⁻⁵⁶ It is the presence of tin in the zeolite structure which gives it Lewis acidity.⁵⁷ Tin-beta has been known to facilitate reactions of sugars such as isomerisation of glucose to fructose,^{53,54,58} and was therefore selected as a reactive, but non-Brønsted acidic catalyst. The catalyst was not found to produce any ML or formic acid, however it did convert the starting material. The products were not fully identified, however they appeared to be sugar isomers, as they shared similar retention times and no polymer residue was observed in post-reaction mixture.

Table 5. Catalytic testing of zeolites. Temp. 180°C, time 1 hr, 5 bar nitrogen, 0.62 g alpha methyl glucoside, 0.08 g catalyst, 8 g methanol

Catalyst (Si:Al ratio)	Conversion, %	ML yield, %	Formic acid yield, %	C bal., %
ZSM-5 (23)	5	0.5	0	95
ZSM-5 (30)	3	0.5	0	97
ZSM-5 (50)	0	0	0	100
ZSM-5 (80)	0	0	0	100
SBA-15	0	0	0	100
Zeolite β (38)	41	12	14	71
Zeolite β (25)	51	12	18	62
Sn- β	8	0	0	92

The best performing zeolite material was found to be Zeolite- β (38), and further testing was carried out with it. In order to limit the formation of humins, a silylation procedure was performed, which would cover the outside surface of the zeolite with silica, blocking surface acid sites. It was theorised that the large polymer molecules are most likely formed on the surface of the material, as they have the most room to grow there. A polymer within a zeolite pore would be greatly limited in its size due

to local sterics. Humin polymerisation is unavoidable in this reaction, but it may be limited. The required surface coverage was calculated based on some assumptions:

- Aluminium atoms make up approximately 2.6% of Zeolite- β (38) composition.
- The TEOS molecule will only interact with the zeolite surface (a reasonable assumption, given that TEOS is too large to enter the pores).
- Coverage of surface will be uniform.

Therefore, zeolite materials with 3% and 15% coverage of surface were prepared. The percentages correspond to the % wt. coverage of SiO₂, as a result of TEOS treatment. The detailed silylation procedure can be found in the experimental section. 3% SiO₂ was considered to be approximately a thin surface layer which just covered the acid sites on the surface; 15% coverage was considered excess, and a thick layer of SiO₂ would cover the surface and likely reduce pore size. These catalysts were then tested for the dehydration of methyl-glucoside (Table 6). It was found that when compared to an untreated zeolite, both 3% and 15% silylated catalysts had reduced conversion and yields, but higher carbon balance values. It appears that the additional SiO₂ at 15% coverage either did not entirely work, or the addition of further silica layers had diminishing results, as the 3% and 15% materials produced very similar results. The conversion dropped by 11 and 17 percentage points, whereas the ML yields dropped by 4 and 5 percentage points, respectively. The carbon balance has improved, but when compared alongside the reduction in conversion and yields, this was not the expected result.

Table 6. Catalytic testing of silylated zeolite beta 38. Temp. 180°C, time 1 hr, 5 bar nitrogen, 0.62 g alpha methyl glucoside, 0.08 g catalyst, 8 g methanol

Catalyst	Conversion, %	ML yield, %	Formic acid yield, %	C bal., %
Zeolite β (38)	41	12	14	71
Zeolite β (38) 3% SiO ₂	30	8	9	79
Zeolite β (38) 15% SiO ₂	24	7	11	83

The test was repeated with the untreated zeolite, but with reaction time reduced by a quarter (from 60 minutes to 45 minutes, Table 7). It was found that the results were similar to the 3% SiO₂ treated material. The conversion, yields and carbon balance were within margin of error of each other. It was therefore concluded that the silylation procedure did not produce the desired effect; it merely slowed down the rate of reaction by approximately 25%, likely due to hindered access to pores because of additional SiO₂ coverage. This was reflected in the significant reduction of surface area of the treated zeolite (Table 8). Silylation reduced the surface area by approximately 31% when compared to the untreated zeolite (H-form).

Table 7. Comparison of fresh and silylated zeolite beta 38 at equal conversions. Temp. 180°C, time 1 hr, 5 bar nitrogen, 0.62 g alpha methyl glucoside, 0.08 g catalyst, 8 g methanol

Catalyst	Time, h	Conversion, %	ML yield, %	Formic acid yield, %	C bal., %
Zeolite β (38)	0.75	31	9	8	79
Zeolite β (38) 3% SiO ₂	1	30	8	9	79

Table 8. BET surface areas for the silylated zeolite

Catalyst	BET Surface area, m ² g ⁻¹
Zeolite 38 β H form	579.2
Zeolite 38 β NH ₄ form	439.4
Zeolite 38 β 3% SiO ₂	399.3

Re-usability of the Zeolite β (38) was evaluated next (Table 9). The catalyst was subject to a re-use testing by washing the post-reaction catalyst with water and acetone, followed by drying at 110 °C for 16 hours. A decrease in conversion and yields was observed with subsequent re-uses. By the second re-use, the yield of ML has dropped to 2%; it was therefore decided that further testing was not necessary, because the yield has dropped sharply. The main reason for this decrease in activity was likely the absorption of humins onto the surface of the catalyst. After the first use, zeolite has turned brown-black with the polymer and the washing procedure did not remove the residue, likely because it is not soluble in most solvents. The humins on the surface would have blocked active sites, preventing further reactions from taking place. While it was possible to remove a portion of the polymer by re-calcination of the materials under standard conditions – essentially by burning the humins off – the activity did not improve when compared to the blackened catalyst, indicating that portion of the polymer was still located deep within the zeolite pores, blocking activity. Perhaps a long-time calcination procedure would have burned those humins off, however this was not tested due to equipment availability; additionally, there was little expectation that the material would behave as expected after this, due to carrying out prolonged pyrolysis in it. It was therefore accepted that a reduction in humin production would benefit re-usability the most, rather than attempting to salvage the used catalyst.

Table 9. Catalyst reuse of zeolite beta 38. Temp. 180°C, time 1 hr, 5 bar nitrogen, 0.62 g alpha methyl glucoside, 0.08 g catalyst, 8 g methanol

Catalyst	Conversion, %	ML yield, %	Formic acid yield, %
Zeolite β (38) first use	41	12	14
Zeolite β (38) first re-use	34	5	9
Zeolite β (38) second re-use	22	2	3

3.2.4. Humins and reaction optimisation

Humins are a major and important part of this reaction. Reducing their production would potentially improve yields, re-usability of catalysts, ease of reaction handling due to reduced filtering and reactor cleaning and improve post-reaction mixture analysis accuracy because of lower amount of intermediate products. Their production and characteristics were therefore evaluated.

A comparison of solvents was carried out between water and methanol (Table 10). Methanol is known to inhibit the formation of humins^{6,7,59,60} due to replacing the possible hydrolysis sites for polymer bonds with -OMe functionality. A near-complete conversion was observed with methanol because nearly all glucose was converted to methyl-glucoside species; this does not mean that methanol was a more active solvent for this reaction, but it's a result of glucose being the substrate in these tests. Water was found to facilitate the production of humins much better than methanol, which was reflected in the carbon balance values. Carbon balance was significantly lower when water was used as solvent; the post-reaction mixture was also observed to be much darker, with insoluble flakes of humins floating on the surface. However, both solvents yielded a similar amount of levulinate species, suggesting that perhaps the yield of levulinate is not strongly affected by polymerisation under these conditions. Interestingly, formic acid yield varied significantly between the solvents – its yield was measured at 12% in water, and 21% in methanol. This could have been a result of slightly different mechanistic

pathways. A measurable yield of 5-HMF was noted in water, but no corresponding furfural-derivative was observed in methanol. As 5-HMF is one of the major sources of formic acid in this dehydration, it is possible that this species is less stable (or more reactive) in methanol, and therefore decomposes into formic acid rapidly. The difference in furfural-species yield of 8% could approximately account for the additional 9% formic acid yield in methanol. Indeed, synthesis of 5-methoxymethyl furfural (5-MMF) in lab proved difficult, suggesting that it is not a desired product.

Table 10. Comparison of solvents for the dehydration of glucoside species. Catalyst tested is $\text{SO}_4\text{-ZrO}_2$. Temp. 180°C , time 1 hr, 5 bar nitrogen, 0.62 g glucose, 0.08 g catalyst, 8 g methanol, 600 rpm stirring

Solvent	Conversion, %	ML/LA yield, %	5-HMF yield, %	Formic acid yield, %
H ₂ O	56	10	8	12
MeOH	99	12	0	21

The next step was to attempt to reduce the polymerisation by reducing the amount of substrate available. Various amounts of substrate were tested under standard conditions with $\text{SO}_4\text{-ZrO}_2$ (Figure 29). Despite the reduction of substrate by up to four times, the conversion and yields remained almost the same, as seen in Table 11. This is indicative of first-order reaction kinetics with respect to substrate. This is because even though the yields and conversions are nearly the same, the absolute number of substrate molecules reacted increases as concentration of substrate increases.

Table 11. Conversion of alpha-methyl glucoside as a function of substrate concentration. Catalyst tested is $\text{SO}_4\text{-ZrO}_2$. Temp. 180°C , time 1 hr, 5 bar nitrogen, alpha methyl glucoside, 0.08 g catalyst, 8 g methanol

Concentration of MeGlc, mol dm ⁻³	Conversion, %	ML yield, %
0.32	21 ± 2	8 ± 2
0.16	21 ± 2	8 ± 2
0.08	20 ± 1	6 ± 1

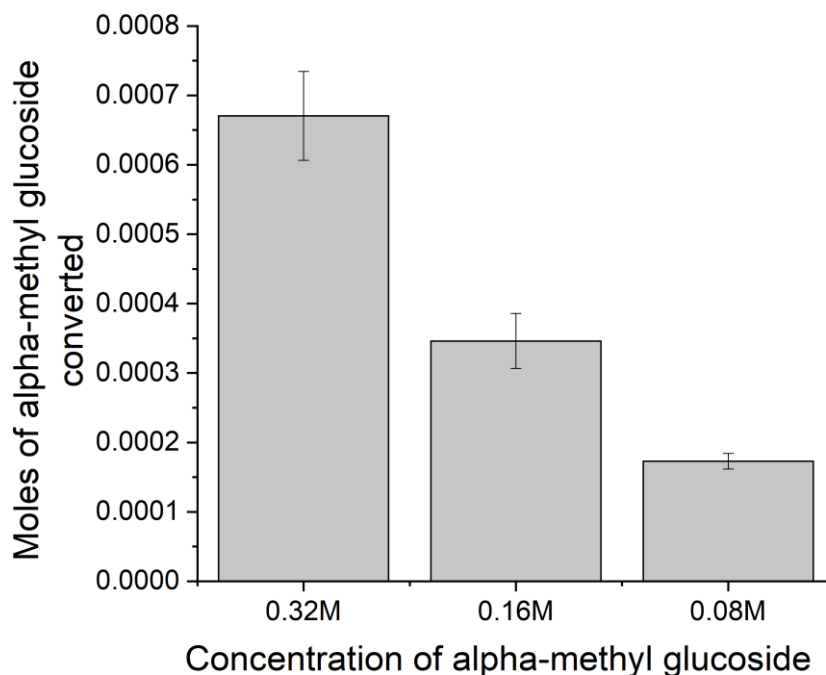


Figure 29. Converted moles of alpha-methyl glucoside against substrate concentration. Catalyst tested is $\text{SO}_4\text{-ZrO}_2$. Temp. 180°C , time 1 hr, 5 bar nitrogen, alpha methyl glucoside, 0.08 g catalyst, 8 g methanol

More likely, the reaction was pseudo-first order with respect to substrate. This is because of the apparent excess of acidic catalyst and water (even in a MeOH solvent, as this is a dehydration reaction – moreover, the methanol used was unlikely to be completely dry) which can be reduced to dependency on just the substrate. The complete kinetic rate equation can therefore be written as equation a) below; the simplified, pseudo-first rate equation is shown in equation b). Typically, a third order reaction would be very unlikely to occur due to collision theory. However, with the excess of both elements they are essentially always available.

$$a). r = k[\text{MeGlc}]^a[\text{H}_2\text{O}]^b[\text{H}^+]^c$$

$$b). r' = k'[\text{MeGlc}]^a$$

A natural log of pseudo-first equation rate b), where “a” is the order of reaction, can be taken. This results in $\ln(r') = a \ln[\text{MeGlc}] + \ln(k')$, an equation of a straight line

$y = mx + c$. Therefore plotting $\ln(r')$ against $\ln[\text{MeGlc}]$ gives a straight line with a gradient of “a” and an intercept of $\ln(k')$. This was visualised in Figure 30. The resulting plot has slope of 1.16 – indicating first order reaction.

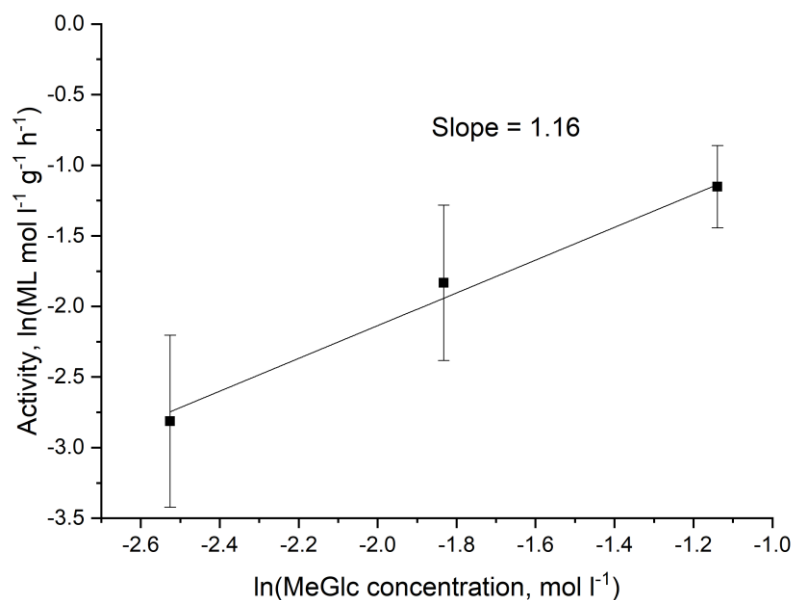


Figure 30. Effect of methyl glucoside concentration on activity of $\text{SO}_4\text{-ZrO}_2$ towards methyl levulinate. Reaction conditions: Temp. 180°C , time 1 hr, 5 bar nitrogen, alpha methyl glucoside, 0.08 g catalyst, 8 g methanol

The reduction in substrate concentration resulted in a significant reduction in reaction polymerisation. The effects can be noted by comparing the post-reaction mixtures (Figure 31). When a lower concentration of methyl glucoside was used, the post-reaction mixture was significantly clearer, with much less insoluble humins observed. At higher concentrations, the solution turned brown-black, with black, insoluble particles in suspension visible to the naked eye. The reduction in humins was achieved while maintaining yield and conversion values. This reduction can be attributed to simple collision theory. There are less molecules present in solution to collide and form the polymers. However, the amount of catalyst remained the same; in effect, the catalyst to substrate ratio increased, which allowed to maintain the yield and conversion.

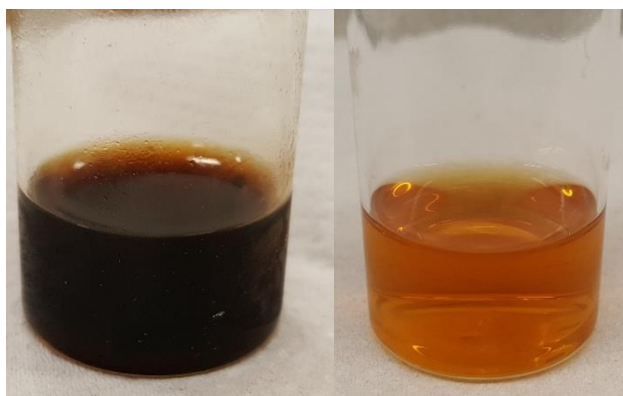


Figure 31. Comparison of post reactions solutions at 0.32M (left) and 0.08M (right) concentrations of alpha-methyl glucoside.

Analysis of humins was also carried out. To obtain a large sample of humins, a standard reaction was carried out with phosphotungstic acid as the catalyst (Table 12). Phosphotungstic acid was chosen as it is a heteropoly superacid; with a melting point of 89 °C, the acid would behave as a homogenous catalyst, maximising the conversion of substrate. The acid facilitated a near complete conversion of methyl glucoside, with a relatively high yield of ML. A large 40% yield of formic acid was observed, which corresponded to a high degree of polymerisation. The carbon balance was very low at 29%, but the desired result was achieved: large, black, insoluble flakes of humins were found in the post-reaction solution.

Table 12. Reaction with phosphotungstic acid in order to obtain humins. Reaction conditions: α glucoside 620mg, phosphotungstic acid 80mg, MeOH 8 g, temp. = 180 °C, 5b N₂, 1hr

Catalyst	Conversion, %	ML yield, %	Formic acid yield, %
Phosphotungstic acid	97	23	40

The resulting polymer was subject to analysis under IR and UV light. Due to the expected complexity of the polymer, limited analysis could be carried out. However, the test also confirmed that strong acids facilitate the polymerisation. Figure 32 shows the IR spectrum of the polymer. Several important bands were identified. The broad stretch at approximately 3400 cm⁻¹ comes from the O-H alcohol bonds. The

two stretches which have been circled in the figure correspond to C=O bonds at 1700 cm^{-1} and conjugated C=C bonds at 1600 cm^{-1} are indicative of the furan base structure in the polymer. At 1075 cm^{-1} a C-O stretch can be observed, and at 970 cm^{-1} features a stretch for a di-substituted C=C bond. The presence of all these stretches complies with the idea that humins are highly conjugated polymers of furanic structures.⁹

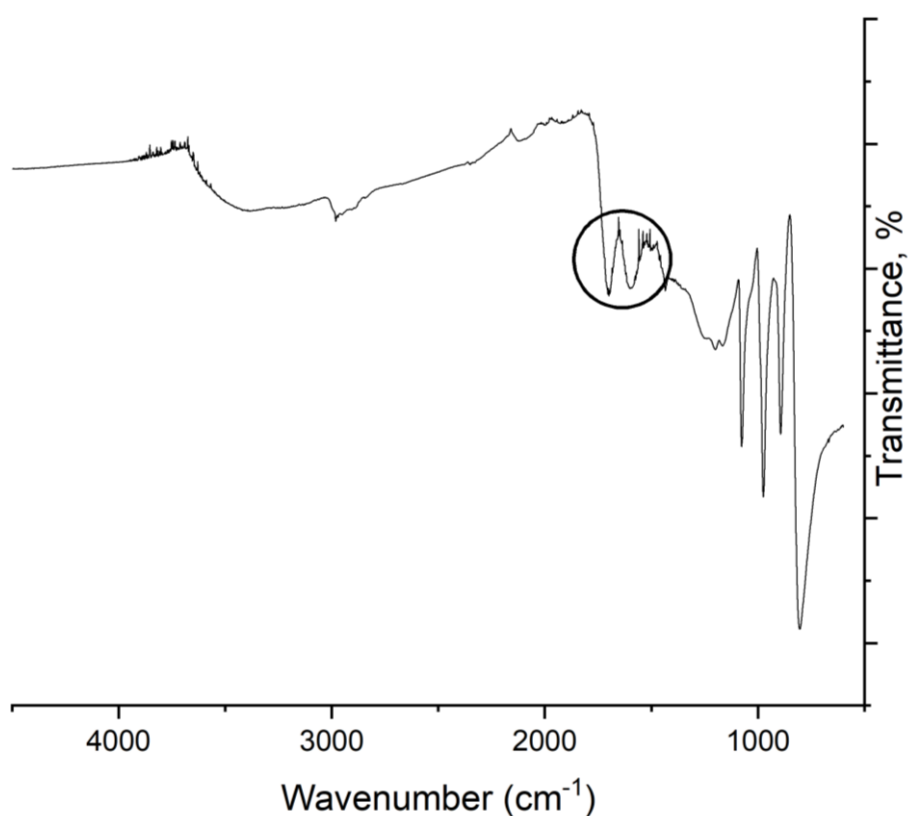


Figure 32. IR spectrum of humins obtained from phosphotungstic acid reaction. Figure 33 shows the UV spectrum of the humins. Although limited analysis can be carried out with UV in this particular case, the spectrum does show that the humins are a large, highly conjugated polymer, rather than a collection of smaller oligomers. The spectrum resembles that of a different polymer with similar features: repeating 5-member heterocyclic rings with highly conjugated structures.⁶¹ The IR and UV spectra combined strongly suggests that humins are a large, furanic polymer, however the exact structure has not been confirmed.

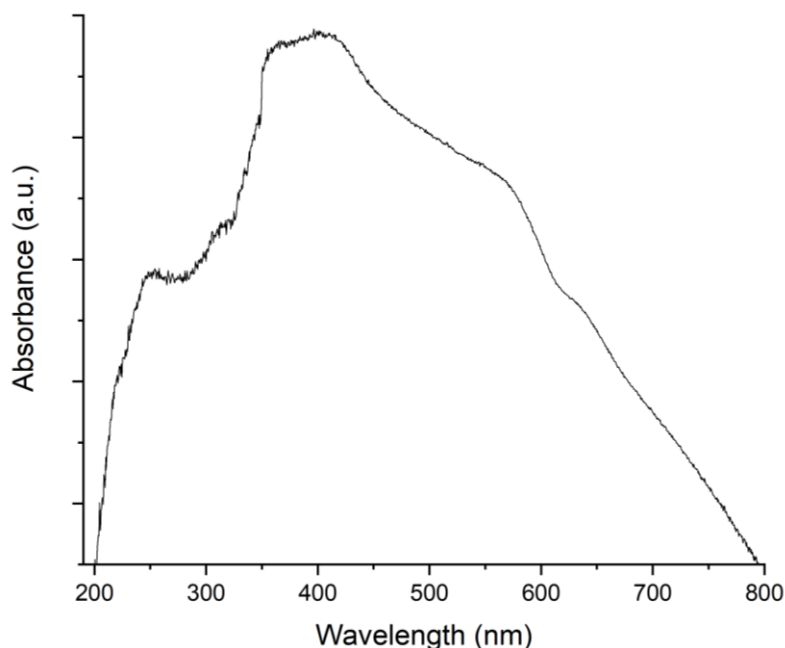


Figure 33. UV spectrum of humins obtained from phosphotungstic acid reaction.

Gas analysis of was carried out on post-reaction atmosphere to assess whether any additional products were made during the reaction, and to account for any missing carbon balance. Once the reaction has cooled down, the gas was extracted through a vent into a gas bag and injected into a GC equipped with a methanizer. The results can be found in Table 13. Majority of the gaseous mixture (nearly 82%) consisted of methyl formate and methanol (17%) with small amounts of CO and CO₂ (less than 2% combined). The CO and CO₂ likely came from decomposition of methyl formate or formic acid. Methyl formate was one of the major products from this reaction; with a low boiling point and high vapour pressure, it was expected to be found in the gas phase. Using the ideal gas law (Parameters used: $p = 5000 \text{ Pa}$, $V = 0.00005 \text{ m}^3$, $R = 8.31 \text{ J K}^{-1} \text{ mol}^{-1}$, $T = 298 \text{ K}$) to calculate the number of molecules in the gas phase returned a value of 0.001 moles. The final pressure value was estimated based on the fact that pre-reaction, the reactor was charged with 5 bar of nitrogen. Post reaction, at the same temperature, the reactor was found to be at approximately 5.5 bar on a consistent basis. Therefore, a value of 0.5 bar (5000 Pa) was used to calculate the actual amount from the reaction mixture, omitting nitrogen. The

reaction input was the substrate (0.0032 moles) and methanol (0.31 moles, solvent). The main component of the gas phase was methyl formate, which requires one molecule of methanol and one molecule of formic acid to be produced. In a standard reaction with $\text{SO}_4\text{-ZrO}_2$, 54% of the substrate converted into products, of which 31% was formic acid. This gives a value of 0.00054 moles of formic acid in the reaction mixture. At 81.7% composition of 0.001 moles in the gas phase results in 0.00082 moles of methyl formate, requiring equimolar amounts of MeOH and formic acid. This suggests that bulk of the formic acid produced is actually found in the gas phase; the total amount of formate species at the end of the reaction was approximately 0.0014 moles, increasing the yield from 31% to 44%. This would potentially account for up to 8% additional carbon balance, assuming that every molecule of substrate produces an expected amount of formic acid. It's possible that the substrate could be oxidised and form oligomers, or that not all reacted substrate goes on to follow the expected mechanistic pathway, due to complexity of the reaction. As such, it is not straightforward to state the relative impact of the gas phase compounds on carbon balance.

Table 13. GC analysis of a standard post reaction gas mixture. Catalyst tested is $\text{SO}_4\text{-ZrO}_2$. Temp. 180°C, time 1 hr, 5 bar nitrogen, 0.62 g glucose, 0.08 g catalyst, 8 g methanol, 600 rpm stirring

Gas	Composition, %
CO	0.7
CO ₂	1.0
Methyl formate	81.7
Methanol	16.6

It can be said with certainty that the results discussed up to this point were correct at the time of writing; peer reviewed; repeated multiple times for accuracy. Still, certain issues with solvent, reactor and carbon balance were discovered quite late on into the research cycle. An experiment was carried out with the aim of finding

out whether methyl levulinate is absorbed by the humin polymer; methyl levulinate was put into the reactor alongside pre-prepared humins (obtained from the reaction with phosphotungstic acid) in methanol, heated to 100 °C and stirred for 1 hour. At the end of the reaction, it was found that the concentration of ML has increased compared to baseline by approximately 20%. The humins were thoroughly washed before the reaction to make sure no residual small molecules were left on the surface, so the additional ML did not come off the polymer. It was also noted that the solvent level decreased by approximately 20% at the same time. The reactor was sealed and leak checked – the solvent did not escape the reactor. It was determined that some of the solvent was trapped in the gas inlets, outlets, under the liner, and in the pressure measuring apparatus of the reactor. Most likely due to differences in volatility, the methanol separated from the rest of the reaction mixture and therefore the mixture was not of uniform concentration across the entire reactor. As such, carbon balance is not listed in most tables, even though it was calculated for every reaction. This is because while the conversion and yield values were consistent between reactions, and can be qualitatively assessed (in the least), the difference to carbon balance was large and difficult to assess retroactively. Typical carbon balance for these reactions would be in the order of 50-80%, depending on conditions. The solvent trapped in the reactor did not affect any consecutive reactions because the reactor was thoroughly cleaned in between each experiment. As a side note, very few papers reported their carbon balance values and fewer still used an internal standard for analysis.

In consideration of the factors related to humin formation discussed in this section and the issues above, a new, better methodology was proposed. Reactions with the best performing materials, sulfated zirconia and zeolite β (38) were carried out. Mesitylene was added to these reactions as an internal standard, due to its non-volatile and unreactive (under the reaction conditions) nature. The results obtained

with these materials can be found in Table 14. A reduction in conversion and yield values was observed. This stemmed exclusively from the use of an internal standard, as the loss of methanol in previous reactions simply inflated these values on a consistent basis. Due to the inclusion of an internal standard, carbon balance values were able to be calculated.

Table 14. Reactions with best catalysts under new conditions. Each experiment was repeated three times to obtain error margins. Temp. 180°C, time 1 hr, 5 bar nitrogen, 0.2 g alpha methyl glucoside, 0.1g mesitylene, 0.08 g catalyst, 8 g methanol

Catalyst	Conversion, %	ML yield, %,	Formic acid yield, %	Carbon bal., % \pm 5%
Zeolite β (38)	18 \pm 1	7 \pm 1	3 \pm 1	89
SO ₄ -ZrO ₂	33 \pm 3	7 \pm 2	4 \pm 2	74

In order to obtain better understanding of the reaction pathways, a mechanism was proposed, found in Figure 34. The mechanism explores possible steps from the substrate to the desired product, methyl levulinate. There is a general agreement in literature that in water solvent, 5-HMF is the required intermediate for the production of levulinic acid.^{62,63} It is not uncommon to see glucose isomerisation to fructose as part of the mechanism.^{64,65} The mechanism in other solvents like methanol has been largely unexplored in literature, or an assumption is made that an identical mechanism to water takes place. While an HMF-like compound was detected in the post reaction mixtures, no evidence was found for the formation of fructose. The pathway in methanol is likely similar, but the involvement of methyl ester groups changed some of the chemistry and a new mechanism had to be proposed. Note that no labelling experiments were carried out, and the pathway was constructed solely on the observation of products in the post-reaction mixture. The mechanism is laid out with Brønsted acidity as the catalyst, though clearly the pathway can be catalysed (at least part way) with Lewis acidity as well, as evidenced by formation of 5-MMF

in Table 2. The proposed mechanism is not exhaustive, and does not account for formation of any by-products.

The first step in the mechanism is the first dehydration resulting in intramolecular rearrangement of MeGlc to a 5-member heterocycle. This leaves the previously anomeric methoxy group open to nucleophilic attack. In theory, the methoxy could be attacked by methanol or water to relieve the positive charge. They are both present in abundance in this reaction, and it can be speculated that depending on the nucleophile, the reaction can take different routes. The mechanism remains the same, however the resulting reaction intermediate, labelled “B” on the diagram, could likely be less reactive than intermediate “A” due to the nature of methoxy groups, and therefore not lead to methyl levulinate. At the same time, it is possible that this intermediate can follow the same pathway as intermediate “A”; they could also be reversibly connected if proton exchange takes place. Intermediates “A” and “B” are also likely to be the 5-MMF-like molecule detected in some of the experiments and identified by NMR. Without an isolated sample, no further analysis was carried out.

The next step in the mechanism is also likely the most important step in this pathway; it appears to determine whether methyl levulinate can be produced, or an intermediate which does not lead to the product. The distinction stems from the angle at which the nucleophile attacks this molecule. If the attack is from the di-substituted side, the mechanism reasonably allows for formation of ML. However, if the attack is carried out from the mono-substituted side, there does not appear to be a feasible way to continue the pathway. This is also likely where a portion of the divergence between conversion of substrate and yield of ML comes from, as the selectivities to ML reported in this chapter are approximately in the order of 30-50%. The pathway to ML requires attack from the di-substituted side, which is slightly more sterically hindered. The probability to continue on this pathway is therefore likely to be 50% or less.

The following steps lead to a ring opening of the heterocycle and formation of the desired product, methyl levulinate. The mechanism is distinctly different to the one in water solvent in that no fructose is produced; while furan-based compounds are key, 5-HMF is not produced; additionally, it could predict some of the methylated products from this reaction, assisting in future identification of unknown products.

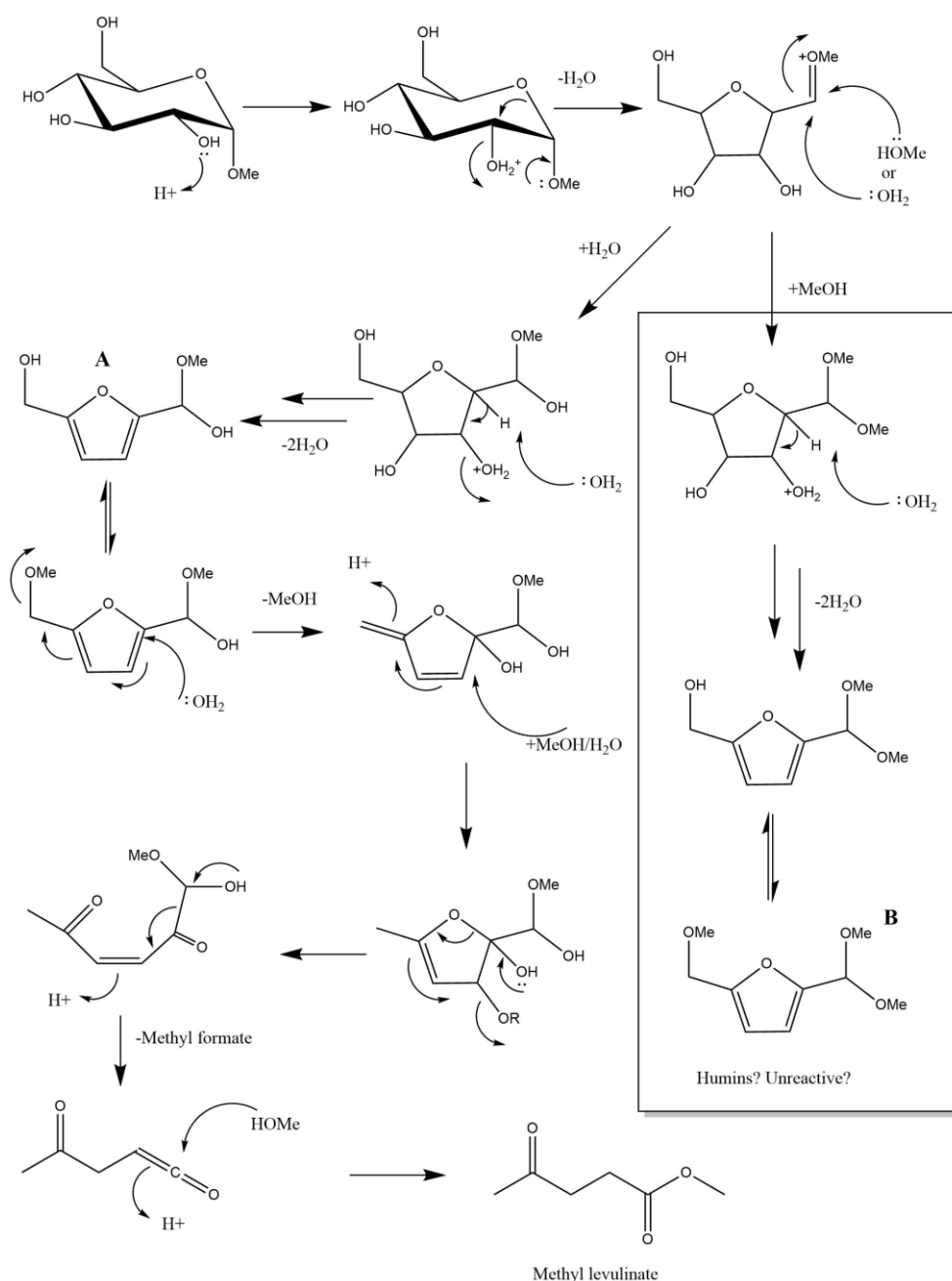


Figure 34. Suggested mechanism for the conversion of methyl glucoside to methyl levulinate

As a way to corroborate the mechanism, a series of experiments with furfural and furfural alcohol were carried out. The aim of these was to confirm the assumption from the proposed mechanism that the pathway to methyl levulinate depends on the angle of nucleophilic attack on intermediate “A”. This was achieved by approximating the two sides of the molecule to two common compounds: furfural alcohol was used to simulate the mono-substituted side; furfural was used to simulate the di-substituted side. If the assumption is correct, only furfural alcohol should have produced methyl levulinate. Unfortunately, the scope of these experiments was limited. Safety concerns arose with the use of furan compounds in the autoclave reactors because of lack of fume hoods above them. As a result, the reactions were carried out in a 50 mL glass Colaver reactor pressurised with N₂. Unlike an autoclave, the glass reactors were not airtight; as such, a moderate temperature had to be used to minimise solvent loss, alongside a 60-minute reaction time. The results can be seen in Table 15. Only one configuration yielded measurable amounts of methyl levulinate – ZSM-5 (23) with furfural alcohol. While this complies with the mechanistic assumption, Zeolite β (38) did not facilitate production of ML despite being a strongly acidic catalyst. This could be because of the low temperature. Experiments with furfural resulted in large amount of humins formed (as evidenced by the low carbon balances) but no ML was observed. This complies with the mechanism proposed in Figure 34, specifically the nucleophilic attack on intermediate A. Only the mono-substituted side of the molecule will yield levulinate species, and in these experiments only furfural alcohol has produced ML. These findings are also in line with findings reported in literature. Generally, literature yields of ML from furfural alcohol are significantly higher (ranging from 20% and as high as 98%) due to use of higher temperatures (above 100 °C).⁶⁶⁻⁷⁰ At the time of writing, no reports of furfural aldehyde to methyl levulinate could be found.

Table 15. Reactions with furfural-based substrates. Reaction conditions: 0.01 mol substrate, 80 mg catalyst, 0.1 g Mesitylene, 10 mL MeOH, 40 °C, 1.5 bar N₂, 60 minutes

Catalyst	Substrate	ML yield, %	Carbon balance \pm 5%
ZSM-5 (23)	Furfural alcohol	1.5 \pm 0.3	95
ZSM-5 (23)	Furfural	0	51
Zeolite β (38)	Furfural alcohol	0	93
Zeolite β (38)	Furfural	0	25

3.2.5. Conclusions

Solid-acid catalysed dehydration of methyl glucoside was investigated. This chapter was divided into four individual parts, each tackling a different aspect of the reaction.

The first section focused on the methylation of glucose into methyl glucoside. Different reaction conditions were tested: initially various amounts of mineral acid were utilised, alongside varying reaction times. It was found that a 1:10 ratio of mineral acid to glucose was sufficient for the methylation to take place. Initial testing used 16 h reaction time, however it was determined that the reaction progressed significantly even after the first 2 hours. Indeed, the methylation happened readily at temperatures far lower (100 °C lower) than glucose dehydration reactions discussed further in the chapter. Finally, Amberlyst-15 (w) was evaluated as a commercial solid acid catalyst. The solid acid performed slightly worse than the mineral acid, which was expected – there was an additional factor of substrate diffusion into the catalyst before a reaction could take place, which was not a significant obstacle when a mineral acid was used due to its homogenous nature. This part of the overall reaction was deemed to be the easiest to overcome, and not a limiting step in any way. Therefore, it was not explored further.

The second section explored the use of solid acid catalysts for the dehydration of MeGlc. Several metal oxides were evaluated alongside their acidified equivalents. All the materials tested, apart from P25, were synthesised in-house. It was found that superacid $\text{SO}_4\text{-ZrO}_2$ was the best performing catalyst, closely followed by $\text{SO}_4\text{-TiO}_2$. The acidity of both catalysts was explored. The total surface acidity of $\text{SO}_4\text{-ZrO}_2$ was measured at 0.76 mmol/g, over twice that of $\text{SO}_4\text{-TiO}_2$ at 0.33 mmol/g. When compared to $\text{SO}_4\text{-TiO}_2$, $\text{SO}_4\text{-ZrO}_2$ was found to be more stable at high temperatures; have much higher surface area; possess a higher concentration of acidic sulfur groups on the surface, despite identical sulfation process. The Brønsted and Lewis acid sites on sulfated zirconia proved to be relatively strong with pyridine DRIFTS. Various catalyst loadings were also explored, and a linear correlation between conversion and amount of catalyst used was found, indicating that the reaction was under a kinetic regime. This enabled the use of a lower amount of catalyst, mainly to limit the polymerisation side reactions but also for economic reasons.

The following section focused on a specific subset of solid acid materials, zeolites. A range of zeolites of various acidities were tested, alongside some Lewis-acidic zeolite materials. Only the Brønsted-acidic zeolites produced methyl levulinate. Additionally, zeolite β was significantly more active than ZSM-5. This was most likely due to the difference in pore sizes; zeolite β has slightly larger pores, which allowed the relatively big methyl glucoside molecule to diffuse through into the catalyst, where a reaction could take place. ZSM-5 features smaller pores, which are likely too small for the substrate to diffuse into. As a result, the reaction could take place on the external surface of the catalyst only, greatly limiting the reaction rate – as evidenced by the very low yields of approximately 0.5%. While the pore size limits large molecules from entering the catalyst, chemistry can still take place on the external surface, for example polymerisation reactions. Zeolite β was subject

to a silylation procedure so that the external surface acid sites would be covered with silica, but the internal acid sites would remain intact. This was done in hopes of limiting polymerisation side reactions. However, it was found that while the procedure did limit polymerisation, it also slowed the rate of reaction and reduced conversion. After closer investigation, silylation did give any real improvements to the material. Therefore, zeolite β (38) was established as the best performing zeolite, alongside the metal oxide based $\text{SO}_4\text{-ZrO}_2$. The zeolite material was tested for re-usability. Yield of methyl levulinate reduced with subsequent uses, likely due to humins covering surface of the catalyst, essentially poisoning it.

Finally, the last section of this chapter tackled the production of humins, optimisations to the reaction and the mechanistic pathway to methyl levulinate. A comparison was made between methanol and water as solvents for the reaction, concluding that despite similar yields of methyl levulinate, the reaction in water produced a great amount more of humins than in methanol. The concentration of substrate was also found to have a significant impact on the amount of polymerisation without affecting conversion or yield, due to the pseudo-first order reaction kinetics. Humins were synthesised by carrying out a reaction with phosphotungstic acid, and analysed with IR and UV. Interpretation of the spectra reveals that humins were large, highly conjugated polymers primarily consisting of C=C, C=O and C-O bonds. This fits the idea that they are made up of furan rings joined in chains. Reactor issues were discussed which meant that conversion and yield values reported in this chapter were inflated, however this was discovered at such a late stage in research that no reasonable corrections could have been made. The pathway to methyl levulinate was proposed, and mechanistic steps discussed. The proposed mechanism differs to the one which is commonly accepted in water solvent, and complies with the reaction results presented in this chapter. Initial work on confirming the mechanism was carried out by testing furfural alcohol and furfural

as starting materials for methyl levulinate. Only furfural alcohol converted into the desired product, in compliance with the proposed mechanism.

3.2.6. References

- 1 J. Wang, J. Xi and Y. Wang, *Green Chem.*, 2015, **17**, 737–751.
- 2 Z. Xue, M. G. Ma, Z. Li and T. Mu, *RSC Adv.*, 2016, **6**, 98874–98892.
- 3 T. Werpy and G. Petersen, *Top Value Added Chemicals from Biomass Volume I — Results of Screening for Potential Candidates from Sugars and Synthesis Gas*, 2004.
- 4 K. C. C. G.G. Liversidge J.F. Bishop, D.A. Czekai, 1980, **96**, 62–66.
- 5 A. Morone, M. Apte and R. A. Pandey, *Renew. Sustain. Energy Rev.*, 2015, **51**, 548–565.
- 6 X. Hu and C.-Z. Li, *Green Chem.*, 2011, **13**, 1676.
- 7 S. Kang and J. Yu, *Ind. Eng. Chem. Res.*, 2015, **54**, 11552–11559.
- 8 B. Girisuta, L. P. B. M. Janssen and H. J. Heeres, *Chem. Eng. Res. Des.*, 2006, **84**, 339–349.
- 9 I. Van Zandvoort, Y. Wang, C. B. Rasrendra, E. R. H. Van Eck, P. C. A. Bruijninx, H. J. Heeres and B. M. Weckhuysen, *ChemSusChem*, 2013, **6**, 1745–1758.
- 10 L. Yang, G. Tsilomelekis, S. Caratzoulas and D. G. Vlachos, *ChemSusChem*, 2015, **8**, 1334–1341.
- 11 H. Heeres, R. Handana, D. Chunai, C. Borromeus Rasrendra, B. Girisuta and H. Jan Heeres, *Green Chem.*, 2009, **11**, 1247.
- 12 E. Juaristi and G. Cuevas, *Tetrahedron*, 1992, **48**, 5019–5087.

- 13 Y. Chang, C. Lee and C. Bae, *RSC Adv.*, 2014, **4**, 47448–47454.
- 14 L. Peng, J. Zhuang and L. Lin, *J. Nat. Gas Chem.*, 2012, **21**, 138–147.
- 15 B. Girisuta, L. P. B. M. Janssen and H. J. Heeres, *Ind. Eng. Chem. Res.*, 2007, **46**, 1696–1708.
- 16 Q. Fang and M. A. Hanna, 2002, **81**, 187–192.
- 17 R. H. Leonard, *Ind. Eng. Chem.*, 1956, **48**, 1330–1341.
- 18 P. P. Upare, J.-W. Yoon, M. Y. Kim, H.-Y. Kang, D. W. Hwang, Y. K. Hwang, H. H. Kung and J.-S. Chang, *Green Chem.*, 2013, **15**, 2935.
- 19 T. Flannelly, M. Lopes, L. Kupiainen, S. Dooley and J. J. Leahy, *RSC Adv.*, 2016, **6**, 5797–5804.
- 20 S. S. Joshi, A. D. Zodge, K. V. Pandare and B. D. Kulkarni, *Ind. Eng. Chem. Res.*, 2014, **53**, 18796–18805.
- 21 T. D. Swift, C. Bagia, V. Choudhary, G. Peklaris, V. Nikolakis and D. G. Vlachos, *ACS Catal.*, 2014, **4**, 259–267.
- 22 R. Chong, J. Li, Y. Ma, B. Zhang, H. Han and C. Li, *J. Catal.*, 2014, **314**, 101–108.
- 23 R. M. Malaluan, H. Ohzeki, K. Arai, T. Adschiri and B. M. Kabyemela, *Ind. Eng. Chem. Res.*, 2002, **36**, 5063–5067.
- 24 and T. Z. Junying Zhang, Baolin Hou, Aiqin Wang, ZhenLei Li, Hua Wang, *AIChE J.*, 2014, **60**, 3804.
- 25 Z. Wu, A. K. P. Mann, M. Li and S. H. Overbury, *J. Phys. Chem. C*, 2015, **119**, 7340–7350.
- 26 Y. Wang, F. Wang, Q. Song, Q. Xin, S. Xu and J. Xu, *J. Am. Chem. Soc.*,

- 2013, **135**, 1506–1515.
- 27 M. L. Freedman, *Anal. Chem.*, 1960, **32**, 637–639.
- 28 M. A. Cortés-Jácome, C. Angeles-Chavez, E. López-Salinas, J. Navarrete, P. Toribio and J. A. Toledo, *Appl. Catal. A Gen.*, 2007, **318**, 178–189.
- 29 C. Yue, G. Li, E. A. Pidko, J. J. Wiesfeld, M. Rigutto and E. J. M. Hensen, *ChemSusChem*, 2016, **9**, 2421–2429.
- 30 X. Liu, X. Wu, D. Weng, Z. Si and R. Ran, *RSC Adv.*, 2017, **7**, 37787–37796.
- 31 Y. Cheng, C. Lambert, D. H. Kim, J. H. Kwak, S. J. Cho and C. H. F. Peden, *Catal. Today*, 2010, **151**, 266–270.
- 32 R. Srinivasan, R. A. Keogh, D. R. Milburn and B. H. Davis, *J. Catal.*, 1995, **153**, 123–130.
- 33 A. Osatiashtiani, A. F. Lee, M. Granollers, D. R. Brown, L. Olivi, G. Morales, J. A. Melero and K. Wilson, *ACS Catal.*, 2015, **5**, 4345–4352.
- 34 V. K. Ivanov, A. Y. Baranchikov, G. P. Kopitsa, S. A. Lermontov, L. L. Yurkova, N. N. Gubanova, O. S. Ivanova, A. S. Lermontov, M. N. Rumyantseva, L. P. Vasilyeva, M. Sharp, P. K. Pranzas and Y. D. Tretyakov, *J. Solid State Chem.*, 2013, **198**, 496–505.
- 35 L. Peng, L. Lin, H. Li and Q. Yang, *Appl. Energy*, 2011, **88**, 4590–4596.
- 36 C. H. Kuo, A. S. Poyraz, L. Jin, Y. Meng, L. Pahalagedara, S. Y. Chen, D. A. Kriz, C. Guild, A. Gudz and S. L. Suib, *Green Chem.*, 2014, **16**, 785–791.
- 37 Z. Si, D. Weng, X. Wu, J. Yang and B. Wang, *Catal. Commun.*, 2010, **11**, 1045–1048.
- 38 A. K. Shah, M. Kumar, S. H. R. Abdi, R. I. Kureshy, N. U. H. Khan and H. C. Bajaj, *Appl. Catal. A Gen.*, 2014, **486**, 105–114.

- 39 A. Platon and W. J. Thomson, *Ind. Eng. Chem. Res.*, 2003, **42**, 5988–5992.
- 40 K. Saravanan, B. Tyagi and H. C. Bajaj, *Catal. Sci. Technol.*, 2012, **2**, 2512–2520.
- 41 A. Sinhamahapatra, N. Sutradhar, M. Ghosh, H. C. Bajaj and A. B. Panda, *Appl. Catal. A Gen.*, 2011, **402**, 87–93.
- 42 S. Sinha Majumdar, G. Celik, A. M. Alexander, P. Gawade and U. S. Ozkan, *Appl. Catal. B Environ.*, 2017, **202**, 134–146.
- 43 X. Hu, S. Wang, R. J. M. Westerhof, L. Wu, Y. Song, D. Dong and C. Z. Li, *Fuel*, 2015, **141**, 56–63.
- 44 Y. Zuo, Y. Zhang and Y. Fu, *ChemCatChem*, 2014, **6**, 753–757.
- 45 N. A. S. Ramli and N. A. S. Amin, *Adv. Mater. Res.*, 2013, **699**, 155–160.
- 46 G. Morales, A. Osatiashtiani, B. Hernández, J. Iglesias, J. A. Melero, M. Paniagua, D. Robert Brown, M. Granollers, A. F. Lee and K. Wilson, *Chem. Commun.*, 2014, **50**, 11742–11745.
- 47 G. Busca, *Microporous Mesoporous Mater.*, 2017, **254**, 3–16.
- 48 D. M. Alonso, J. M. R. Gallo, M. A. Mellmer, S. G. Wettstein and J. A. Dumesic, *Catal. Sci. Technol.*, 2013, **3**, 927–931.
- 49 M. Moreno-Recio, J. Santamaría-González and P. Maireles-Torres, *Chem. Eng. J.*, 2016, **303**, 22–30.
- 50 S. Saravanamurugan and A. Riisager, *ChemCatChem*, 2013, **5**, 1754–1757.
- 51 K. Y. Nandiwale, N. D. Galande, P. Thakur, S. D. Sawant, V. P. Zambre and V. V. Bokade, *ACS Sustain. Chem. Eng.*, 2014, **2**, 1928–1932.
- 52 C. B. D. G. J.M. Newsam, M. M. J. Treacy, W. T. Koetsier, *Proc. R. Soc. L.*,

- 1988, **420**, 375–405.
- 53 M. Moliner, Y. Roman-Leshkov and M. E. Davis, *Proc. Natl. Acad. Sci.*, 2010, **107**, 6164–6168.
- 54 C. C. Chang, Z. Wang, P. Dornath, H. Je Cho and W. Fan, *RSC Adv.*, 2012, **2**, 10475–10477.
- 55 C. C. Chang, H. J. Cho, Z. Wang, X. Wang and W. Fan, *Green Chem.*, 2015, **17**, 2943–2951.
- 56 A. Corma, L. T. Nemeth, M. Renz and S. Valencia, *Nature*, 2001, **412**, 423–425.
- 57 S. Roy, K. Bakhmutsky, E. Mahmoud, R. F. Lobo and R. J. Gorte, *ACS Catal.*, 2013, **3**, 573–580.
- 58 E. Nikolla, Y. Román-Leshkov, M. Moliner and M. E. Davis, *ACS Catal.*, 2011, **1**, 408–410.
- 59 X. Hu, C. Lievens, A. Larcher and C. Z. Li, *Bioresour. Technol.*, 2011, **102**, 10104–10113.
- 60 X. Hu, R. J. M. Westerhof, L. Wu, D. Dong and C. Z. Li, *Green Chem.*, 2015, **17**, 219–224.
- 61 G. H. L. Heintges, P. J. Leenaers and R. A. J. Janssen, *J. Mater. Chem. A*, 2017, **5**, 13748–13756.
- 62 L. Qi, Y. F. Mui, S. W. Lo, M. Y. Lui, G. R. Akién and I. T. Horváth, *ACS Catal.*, 2014, 1–11.
- 63 C. M. Bohn, N. S. Mosier, G. Li, L. Yang, D. Han, Y. Jiang, J. T. Miller, M. M. Abu-Omar and H. I. Kenttämäa, *Org. Chem. Front.*, 2015, **2**, 1388–1396.
- 64 J. B. Binder, A. V. Cefali, J. J. Blank and R. T. Raines, *Energy Environ. Sci.*,

2010, **3**, 765–771.

- 65 R. Mawhood, E. Gazis, S. De Jong, R. Hoefnagels and R. Slade, *Biofuels, Bioprod. Bioref.*, 2016, 198–214.
- 66 C.-Z. Li, S. Wang, S. Jiang, L. Wu and X. Hu, *Chem. Commun.*, 2017, **53**, 2938–2941.
- 67 D. Ren, J. Fu, L. Li, Y. Liu, F. Jin and Z. Huo, *RSC Adv.*, 2016, **6**, 22174–22178.
- 68 A. M. Hengne, S. B. Kamble and C. V. Rode, *Green Chem.*, 2013, **15**, 2540–2547.
- 69 M. A. Mellmer, J. M. R. Gallo, D. Martin Alonso and J. A. Dumesic, *ACS Catal.*, 2015, **5**, 3354–3359.
- 70 I. Guzmán, A. Heras, M. B. Güemez, A. Iriondo, J. F. Cambra and J. Requies, *Ind. Eng. Chem. Res.*, 2016, **55**, 5139–5144.

Chapter 4

Conversion of levulinic acid to γ -valerolactone using Cu-ZrO₂ catalysts

All references are self-contained to within this chapter, and do not refer to any other chapters.

4.1 Introduction

Levulinic acid (LA) is one of the many chemicals derived from lignocellulose, and has been identified by the US Department of Energy as one of the top ten high-value target molecules derived from biomass.¹ LA can be further transformed into a range of useful chemicals such as γ -valerolactone (GVL)² or 2-methyl-tetrahydrofuran (2-MTHF)³; it is also one of the main products of glucose dehydration,^{4,5} which makes LA a great starting material for further studies. GVL itself has many possible applications – it can be used as a biomass-derived monomer for polymerisation;⁶ a “green solvent” to assist sugar dehydration;⁷ however, the most promising aspect of GVL is its use as a fuel additive to compete with bio-ethanol. Currently, nearly all bio-ethanol is produced by fermentation of sugars sourced from corn or sugar cane. Whilst the process itself is generally accepted as environmentally friendly, the sustainability of it is a subject of debate due to the fact that bio-ethanol is a first generation biofuel, meaning it competes for arable land with food crops.^{8,9} The technology to produce ethanol from cellulose does exist, but it is a relatively expensive process that accounts for a fraction of global bio-ethanol production.¹⁰ GVL possesses many attractive properties that make it a potential replacement for bio-ethanol – lower vapour pressure, high energy density, high

boiling point and lack of azeotrope with water (for easy separation), to name a few.^{11,12} It is also possible to produce liquid alkenes (C₈-C₁₆ chains) for conventional fuel uses from GVL.¹³ Finding a cheap, efficient catalyst for the production of GVL is crucial if these applications are to be realised on an industrial scale.

In this chapter, we demonstrate a novel catalyst synthesis method based on previous work with Cu-ZrO₂ by the Hutchings group.^{14,15} Previously prepared catalysts contain a large amount of copper within the ZrO₂ lattice, as well as CuO and Cu species on the surface. The aim of using the new method is to reduce the amount of copper in the catalyst (particularly the Cu species in the bulk lattice of ZrO₂) while retaining activity, and therefore increasing the efficiency and reducing the cost of Cu-ZrO₂ for hydrogenation of LA to GVL, making it more competitive against ruthenium-based catalysts. This work explores new catalyst preparation methodology, effect of pre-treatment on activity of the new material, reaction kinetics and characterisation to explain the activity trends.

4.2. Results and discussion

4.2.1. Manual preparation

Catalysts synthesised with the new pH gradient method were tested for the hydrogenation of LA to GVL. All of the reactions were selective to GVL and no side products were formed. Carbon mass balance was within 95-100% in all of the reactions. The novel catalyst preparation method was developed on the basis of the difference in the initial precipitation point for copper and zirconia. In testing, it was found that zirconia precipitates started appearing when pH of the solution reached 3-4. Copper precipitates did not start appearing until slightly higher pH of 4-5 was reached, and they did not fully precipitate until strongly alkaline pH (above 9) was reached.¹⁶ Therefore, by ramping the pH slowly over time, we could in theory create nanoparticles with a compositional gradient, where the core was predominately zirconia, and surface consisted mainly of copper-rich species. It was found that a

mixed phase Cu-Zr interface promoted higher activity of Cu-ZrO₂ catalysts.¹⁵ Development of the pH gradient method is a way to minimise the amount of those mixed metal phases in the bulk lattice, where they cannot be involved in the reaction, and ensure that they are closer to the surface.

Initially, the materials were prepared manually, by dropping base from a burette into a stirred solution of copper and zirconia nitrates in a beaker. Aging time was monitored with a stopwatch. The first catalyst that was prepared was 50% Cu-ZrO₂, and it was tested for hydrogenation of LA to GVL after calcination (Figure 35). The catalyst offered modest activity, especially when contrasted with 50% Cu-ZrO₂ prepared without pH ramping, which produced approximately 77% GVL yield.¹⁴ Batch 1 gave a slightly higher GVL yield of 35% after two hours reaction compared to 25% and 28% for batches 2 and 3, respectively.

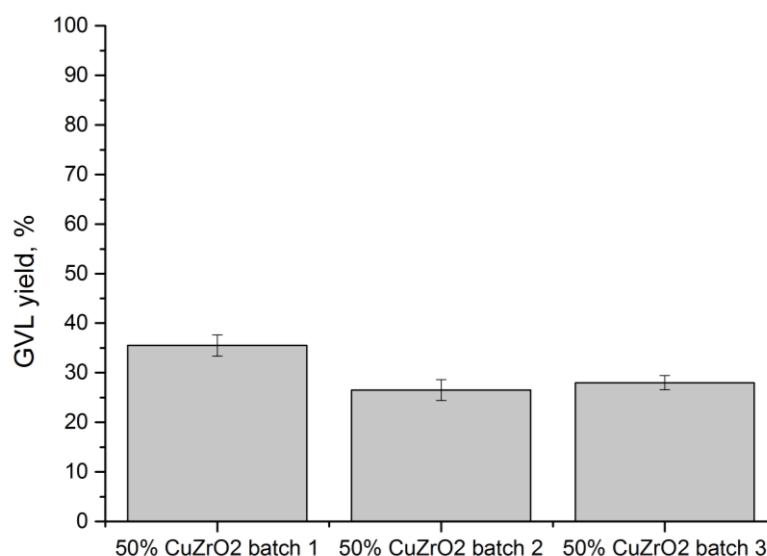


Figure 35. Catalytic activity of calcined 50% Cu-ZrO₂ catalyst prepared manually. Reaction conditions: 200 °C, H₂ 27 barg, 2 h, Substrate 5 wt.% LA/H₂O (10 g), catalyst (0.05 g).

In order to understand the small, but non-negligible difference in activity between batch 1 and batches 2 and 3 presented in Figure 35, TPR was obtained for each catalyst (Figure 36). In the case of batch 2 and batch 3, two maxima can be observed – one at 210 °C and the second, more intense peak at about 240 °C. These

peaks are generally accepted to represent different species of copper (II) oxide; small, well-dispersed nanoparticles on the surface are most easily reduced and they showed up at 210 °C. The species of relatively larger copper nanoparticles with strong metal-support interactions are harder to reduce, and therefore undergo reduction at a slightly higher temperature of 240 °C.^{17,18} However, the slightly more active batch 1 featured a third reduction event at approximately 220 °C. This suggests that, while batch 1 contained the well-dispersed surface nanoparticles and the large particles with strong metal-support interactions, it also contained an intermediate species; perhaps nanoparticles which were close to the surface, but that were not labile, and interacted with the support meaningfully. This raises the possibility of the intermediate species being responsible for the increased activity, which will be studied in more detail in section 4.2.3. There was a small reduction event recorded at roughly 550 °C, which can be attributed to hydrogen spillover from copper onto the zirconia support.¹⁹ Hydrogen spillover onto zirconia is a well-documented phenomenon,²⁰⁻²² and it is very likely that it was conducive to the hydrogenation reaction. Hydrogen adsorbs and dissociates on the surface of copper, whereas LA adsorbs on zirconia; as the hydrogenation of LA happens on the interface between copper and zirconia, it is therefore important that dissociated hydrogen is within close proximity to the adsorbed LA on zirconia sites. Hydrogen spillover guarantees that there will be hydrogen atoms on the zirconia surface, facilitating the hydrogenation reaction.

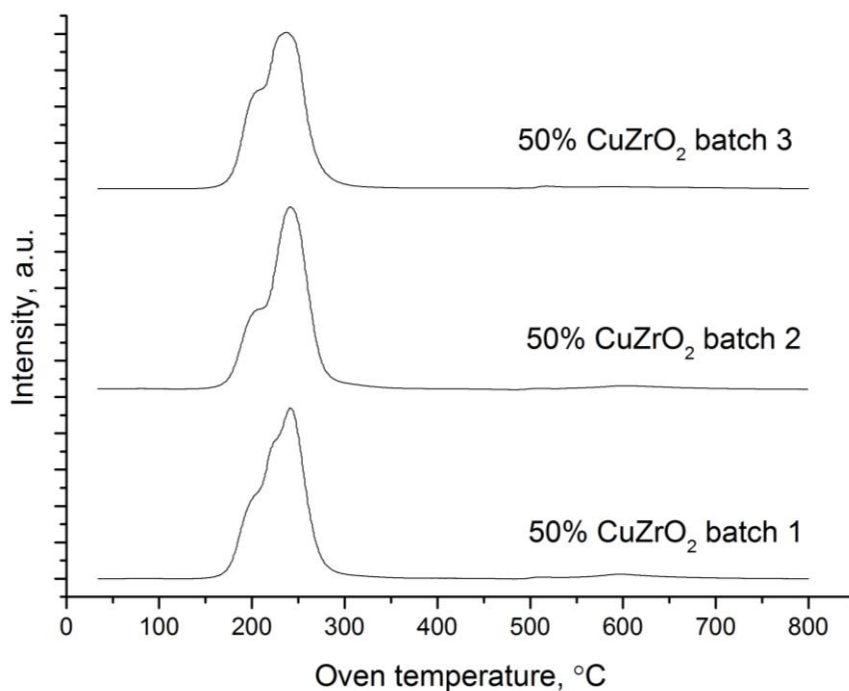


Figure 36. TPR for calcined 50% Cu-ZrO₂ catalysts. Reduction treatment carried out under 10% H₂/Ar (25 mL min⁻¹), ramp rate 10 °C min.

BET surface areas of the 50% Cu catalysts were also measured (Table 16). There was minimal variation between them. Although the slightly more active batch 1 featured the lowest BET surface area, the inherent error in the BET measurement (estimated to be around $\pm 5\%$ on average) discounts the small variability in BET surface area between the batches.²³

Table 16. BET surface areas of 50% Cu-ZrO₂ catalysts prepared manually. Measurements were obtained using a 5-point analysis.

Catalyst	BET Surface area (m ² g ⁻¹)
50% Cu-ZrO ₂ batch 1	95
50% Cu-ZrO ₂ batch 2	97
50% Cu-ZrO ₂ batch 3	104

In order to accurately assess activity of these catalysts, further copper loadings were tested. The next series of catalysts featured 40 mol% loading of

copper. Despite a lower copper content, 40% Cu-ZrO₂ performed significantly better than 50% Cu-ZrO₂ (Figure 37).

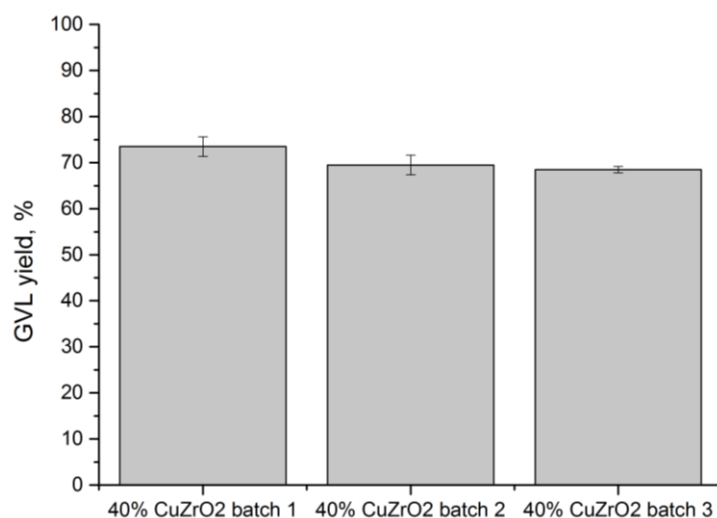


Figure 37. Catalytic activity of calcined 40% Cu-ZrO₂ catalyst prepared manually. Reaction conditions: 200 °C, H₂ 27 barg, 2 h, Substrate 5 wt.% LA/H₂O (10 g), catalyst (0.05 g).

BET surface area of 40% Cu-ZrO₂ catalysts was measured. The surface area was slightly higher than 50% Cu-ZrO₂ material, however it did not correspond to a linear correlation between activity and BET surface area. 40% Cu catalysts gave over twice the yield of GVL at two hours than 50% Cu catalysts, however the corresponding increase in BET surface area was only 13% on average. This means that the total surface area of the material was not a significant factor in determining activity.

Table 17. BET surface areas of 40% Cu-ZrO₂ catalysts prepared manually. Measurements were obtained using a 5-point analysis.

Catalyst	BET Surface area (m ² g ⁻¹)
40% Cu-ZrO ₂ batch 1	115
40% Cu-ZrO ₂ batch 2	108
40% Cu-ZrO ₂ batch 3	112

There was a difference in copper oxide reflection size between 50% and 40% Cu catalysts in XRD, which could mean two things: either copper oxide crystallite

size was smaller in the 40% Cu catalyst (and therefore had smaller particles), or the 40% Cu copper oxide was more amorphous; it is not clear which was the case, however both can account for the differences in activity, shown in Figure 37 and Figure 38, respectively. 50% Cu-ZrO₂ shows clear CuO reflections at 36° and 39°, whereas 40% Cu-ZrO₂ are largely amorphous materials. However, 40% Cu-ZrO₂ batch two shows some very small CuO reflections. This inconsistency is likely due to the difficulty in perfect reproducibility of the catalyst synthesis stage. The manual preparation was subject to a myriad of uncontrolled (or poorly controlled) variables, such as temperature of the mixture, base addition speed, and differences in solution agitation stemming from variance in beaker and stirrer bar size; for example beaker size varied at times between 500 mL and 1000 mL, and stirrer bar size varied between medium and large. This could have affected the rate of agitation of the metal nitrate mixture. All care was taken to make the method as reproducible as possible, however because of the nature of laboratory working space, use of the same reaction vessel every time was not always possible. Additionally, temperature of the mixture was not controlled externally through the use of a water or oil bath, so the mixture itself was susceptible to temperature changes in the laboratory itself; the “room temperature” can vary by as much as 10 °C depending on whether its summer or winter. Nonetheless, both the 50% and 40% Cu-ZrO₂ catalysts produced consistent hydrogenation results despite the small differences in XRD.

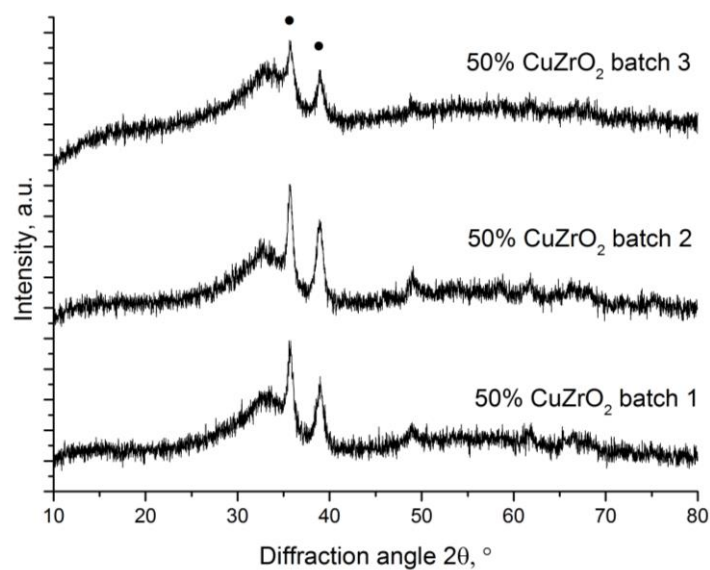


Figure 38. XRD patterns for 50% Cu-ZrO₂ calcined catalysts prepared manually. • CuO

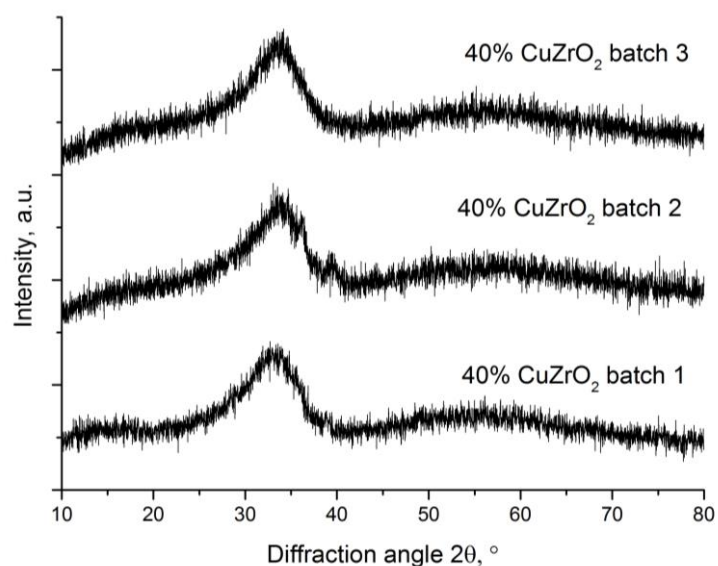


Figure 39. XRD patterns for 40% Cu-ZrO₂ calcined catalysts prepared manually

Material synthesis and testing was continued with 30% Cu-ZrO₂ catalysts. Figure 40 shows GVL yield after two hour runs for 5 batches of the 30% Cu-ZrO₂ catalyst. GVL yield of batch 1 was slightly lower than 40% Cu catalysts, likely due to the lower amount of copper in the catalyst. However, with further testing, the activity has decreased over subsequent batches. This lack of reproducibility underlines the major downside to manual preparation with the pH gradient method – despite careful

preparation, results varied across different batches. Batches 1 to 4 were prepared using the same conditions. As a result of the high variability these results, it was thought that a slower, more controlled addition of base to metal nitrate solution would improve consistency of synthesis. Therefore, batch 5 was prepared with very slow changes in pH, so that it took approximately 30 minutes to increment the pH value by one point. This had the side effect of increasing the total aging time by 2 hours, which could have potentially affected activity of this batch. Batch 5 was the worst performing batch so far.

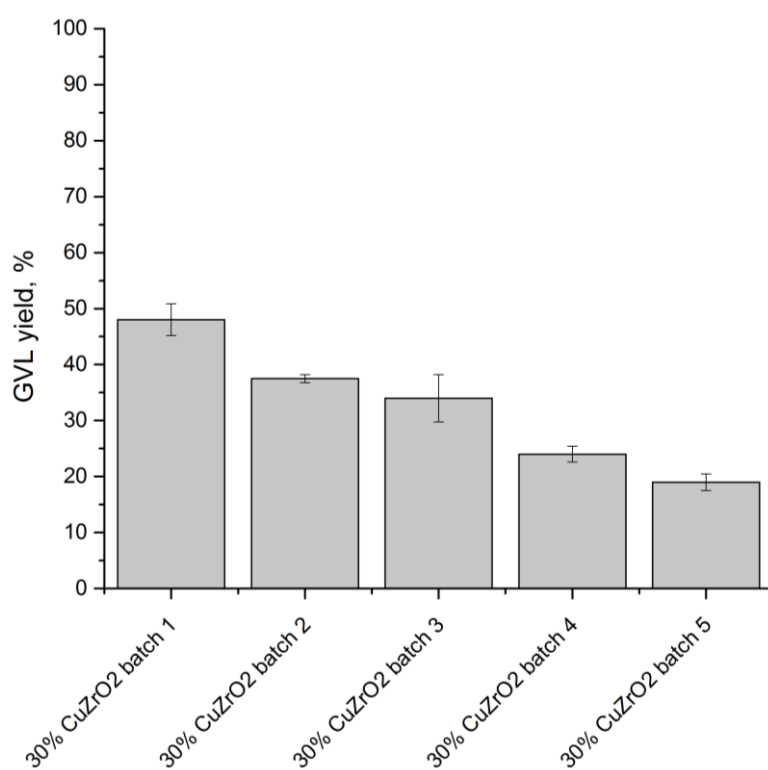


Figure 40. Catalytic activity of calcined 30% Cu-ZrO₂ catalyst prepared manually. Reaction conditions: 200 °C, H₂ 27 barg, 2 h, Substrate 5 wt.% LA/H₂O (10 g), catalyst (0.05 g).

In light of these results, an attempt was made to prepare the 30% and 40% Cu-ZrO₂ catalysts with an autotitrator. An autotitrator is a piece of equipment which can be used to automate the material synthesis process. It controlled pH value with high accuracy, controlled temperature, stirring rate and timings. Several batches were prepared, seen in Figure 41, and the batch-to-batch variation was much lower than

with manually prepared materials. 30% Cu-ZrO₂ has retained the activity shown by batch 1, however activity of 40% Cu-ZrO₂ has decreased when compared to manual preparation. This has made the 30% and 40% Cu directly comparable in activity. The drop in activity could have been caused by the fact that an autotitrator was capable of much more specific pH control, which possibly resulted in more thorough mixing of the metal precursors. This in turn could have caused more copper to be found in the bulk lattice where it remains inactive. Regardless of the effect on activity an autotitrator preparation had on these catalysts, the automatic synthesis proved more consistent and reproducible, and as such it was chosen as the main way to prepare these catalysts. No further materials were prepared manually, and therefore the 10% and 20% copper-content catalysts were only explored as prepared automatically.

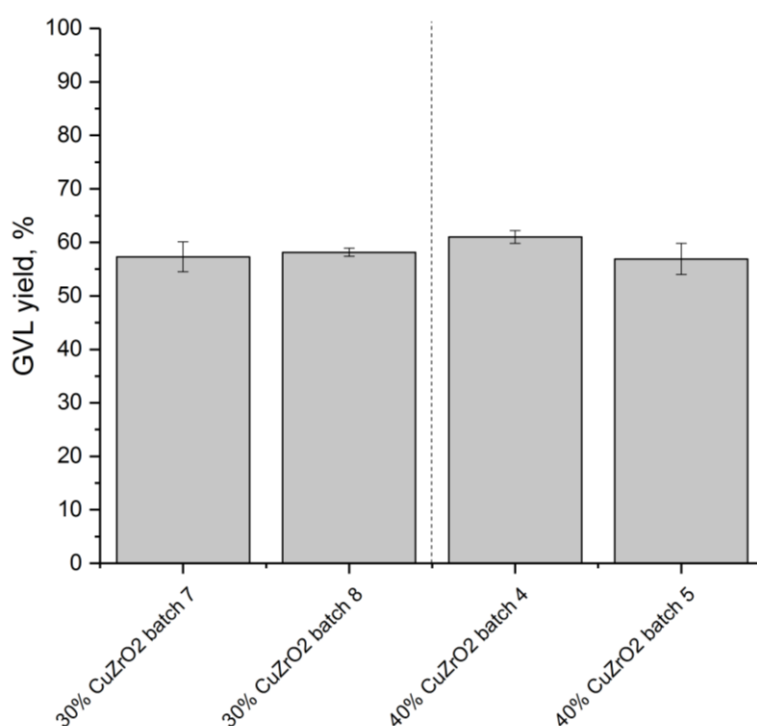


Figure 41. Catalytic activity of calcined 30% and 40% Cu-ZrO₂ catalysts prepared with an autotitrator. Reaction conditions: 200 °C, H₂ 27 barg, 2 h, Substrate 5 wt.% LA/H₂O (10 g), catalyst (0.05 g).

4.2.2. Automated preparation

As a conclusion of findings from section 4.2.1, all further material synthesis was carried out with the use of an autotitrator. Activity testing was carried out with calcined catalyst materials and a range of copper loadings was explored (Figure 42). The yield of GVL increased rapidly when the copper loading was increased from 10% to 30%. Material with 40% Cu provided yield slightly higher than 30% Cu catalyst, whereas 50% Cu loading showed a notable decrease in catalytic activity of 45% when compared to 40% Cu results.

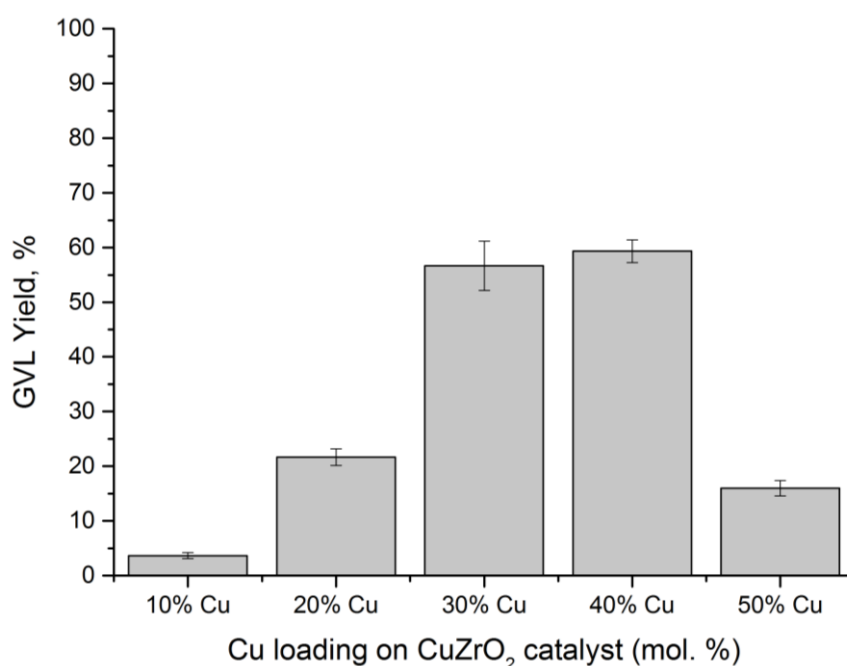


Figure 42. Catalytic activity of various catalysts prepared by variation of Cu loading. *Reaction conditions:* 200 °C, H₂ 27 barg, 2 h, Substrate 5 wt.% LA/H₂O (10 g), catalyst (0.05 g).

BET Surface area of all of the materials prepared by variation of Cu loading followed a similar pattern, however it was not linear. There was a steady increase in surface area as the copper content increased from 10% to 30%, where a plateau is reached (see Table 18). The surface area and activity for catalyst with 40% Cu was within experimental error of 30% Cu-ZrO₂, indicating that activity and surface area are closely related. This is a trend we observed in our previous work with similar Cu-ZrO₂ catalysts.¹⁴ There was a sharp decrease in yield when 50% Cu-ZrO₂ was

used, accompanied by a small decrease in surface area. However, as the activity of 50% Cu-ZrO₂ decreased below that of 20% Cu-ZrO₂, only a small decrease in surface area was observed.

Table 18. BET surface areas for calcined Cu-ZrO₂ catalysts prepared by variation of Cu content.

Catalyst	BET surface area, m ² g ⁻¹
10% Cu-ZrO ₂	48
20% Cu-ZrO ₂	84
30% Cu-ZrO ₂	107
40% Cu-ZrO ₂	108
50% Cu-ZrO ₂	92

Powder XRD patterns for the calcined catalysts are shown in Figure 43. Lower copper content materials (10-30% Cu) appeared to be amorphous and no distinct reflections were observed because the size of copper crystallites was below the 5 nm detection limit. At 40% Cu loading, three CuO (ICDD = 01-089-2529) reflections faintly emerged at 2θ values of 36°, 39° and 49°, indicating crystallite size growth most likely caused by the increased concentration of copper atoms in solution during synthesis.²⁴ At 50% Cu loading, several new CuO reflections appeared prominently at 2θ values of 59°, 62°, 67°, 68°, and 75°. Furthermore, a small tetragonal zirconia (t-ZrO₂, ICDD = 01-080-3783) reflection appeared at 31°.

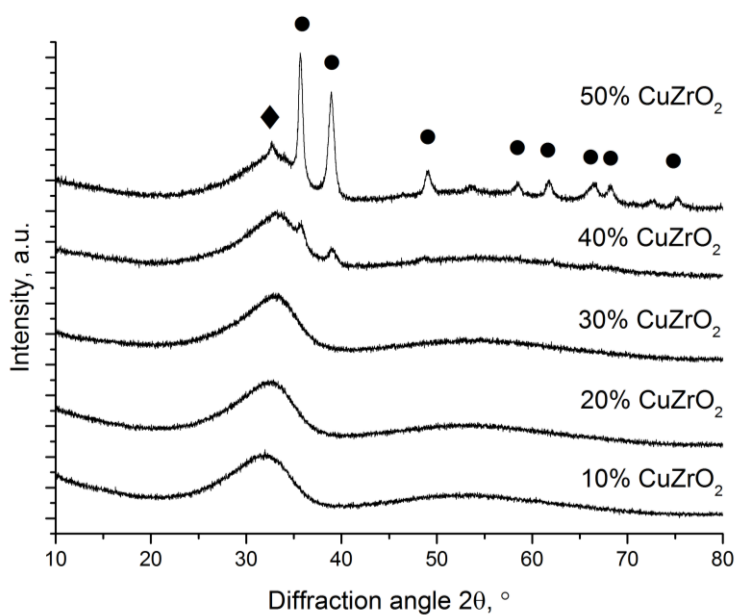


Figure 43. XRD patterns for various Cu loadings of calcined catalysts. • CuO; ♦ t-ZrO₂

Analysis of the surface elemental composition with XPS (Table 19) revealed information about the surface composition of these materials. The amount of Cu atoms on the surface steadily increased with rising Cu loading on the catalyst, whereas the amount of Zr atoms on the surface decreased marginally between 10-40% Cu, and showed a large decrease in the 50% Cu catalyst. However, by calculating Cu/Zr ratio on the surface, it is evident that the surface species very closely corresponded to the theoretical molar ratios of copper and zirconia. The initial rationale in preparing the materials with pH gradient method was that the surface of the catalyst would become more copper-rich, and copper would not be precipitated in the bulk, where it does not participate in the reaction. While it is still likely that there has been less copper incorporation into the bulk lattice, XPS data suggests that the catalysts contain well-mixed phases on the surface. We have found Cu/ZrO₂ catalysts prepared by deposition-precipitation (DP) to have very poor activity for the hydrogenation of LA, achieving yield of 2.26 ± 0.52 . In DP catalysts, there was a clear separation between two metal phases and surface consisted of

almost entirely copper. Therefore, it appears that a certain degree of mixing of CuO and ZrO₂ phases is beneficial to the reaction and desirable in a good catalyst. An appreciable quantity of carbon was also detected on the surfaces, which means there may have been some left over K₂CO₃ from catalyst preparation on the surface. Presence of oxygen was expected, as the materials themselves are oxides.

Table 19. Surface atom coverage derived from XPS for various Cu loadings on calcined catalysts.

Cu loading, mol. %	Surface elemental concentrations, atom %				Cu/Cu+Zr ratio
	Cu 2p	O 1s	C 1s	Zr 3d	
10%	2.32	50.57	24.15	22.97	0.09
20%	5.47	53.02	18.27	23.24	0.19
30%	9.21	54.58	14.17	22.04	0.29
40%	12.93	54.88	11.80	20.39	0.39
50%	19.74	51.65	12.69	15.91	0.55

In consideration of the relatively low copper content and high activity, 30% Cu-ZrO₂ was chosen as the material for all further testing due to the compromise between low copper loading and high activity. The catalyst was subject to time-on-line testing, shown in Figure 44. No significant induction period was observed. In fact, when the catalyst was subject to *in-situ* reduction with no substrate present, the catalyst was reduced (observed in XRD, SEM and visual inspection) even after a 5 minute reduction period, indicating that the reduction process was rapid and not a limiting process in the reaction. The GVL yield scaled with time almost linearly up to two hours, at which point it started to plateau off. . This behaviour is expected, as a lot of catalysts will give lower reaction rates once most of the substrate has been reacted, in accordance with collision theory. There are less substrate particles available for reaction, and therefore the probability of catalyst-substrate interaction decreases – as such, the rate of reaction decreases as well. Hence, two hour reaction

time was selected as a fair measure of catalytic activity. Leaching studies (MPAES) were carried out for each reaction time, and less than 0.3% of copper was found in the post-reaction solution. Therefore, the catalyst were stable and the reaction was catalysed heterogeneously.

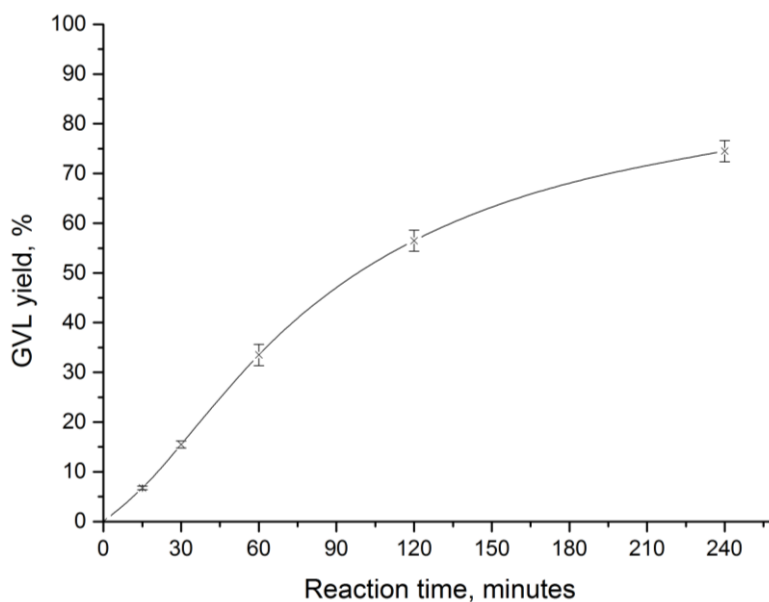


Figure 44. Time on line testing of 30% Cu-ZrO₂ catalyst (calcined). *Reaction conditions:* 200 °C, H₂ 27 barg, Substrate 5 wt.% LA/H₂O (10 g), catalyst (0.05 g).

The same catalyst was subject to several cycles of reactions in order to test its reusability (Figure 45). There was no loss in activity upon first reuse, and only a small decrease in yield after second and third uses.

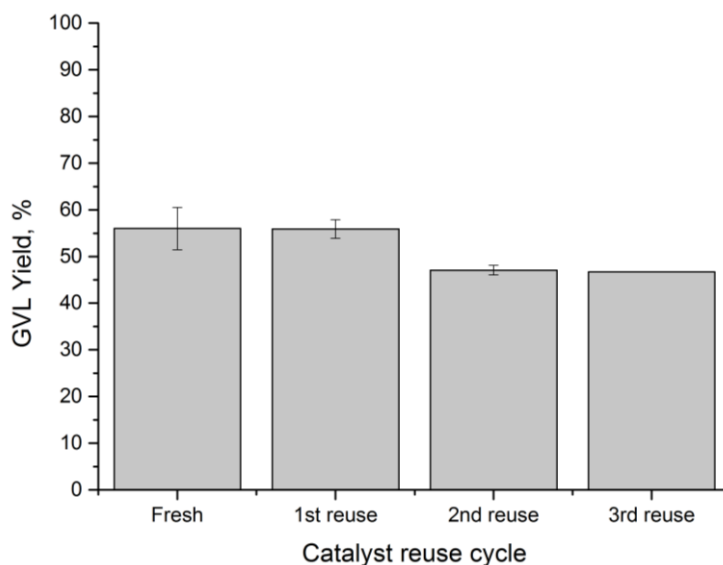


Figure 45. Reuse testing. *Reaction conditions:* 200 °C, H₂ 27 barg, 2 h, Substrate 5 wt.% LA/H₂O (10 g), catalyst (0.05 g).

Due to high temperature and pressure of pure H₂ in the reactor, the catalysts were reduced *in-situ* after the first use, and copper remained in metallic form throughout the following uses (Figure 46). It is worth noting that a small Cu₂O reflection was observed in all post-use samples, with a large reflection visible in the sample used thrice. This is due to the fact that the instrument used for these measurements suffered significant downtime for maintenance, which has caused the samples to oxidise in air a bit. From previous work on Cu-ZrO₂ catalysts by the Hutchings group,¹⁵ it is known that reduction of copper catalysts can significantly improve their hydrogenation activity. When a fresh pH gradient catalyst was subject to *in-situ* reduction with no substrate present, whether the reduction time was fifteen minutes or two hours (200 °C, 27 barg H₂, 10 g H₂O), a moderate increase in activity from 55% to 66% GVL yield was observed when tested. However, any *in-situ* treatment of the material resulted in copper agglomeration (observed by SEM), increased crystallite size (from XRD), and various degrees of phase separation between copper and zirconia, all of which had a negative effect on catalyst activity. Therefore, there are two major effects responsible for no loss in activity on first reuse: the *in-situ* reduction of the catalyst which generally increases activity of Cu-

ZrO₂, and agglomeration of copper into relatively large crystallites (Table 20) which makes the catalyst less active. These two effects effectively cancelled each other out, so that the conversion stayed the same. Upon second and third reuse, approximately 10% yield was lost.

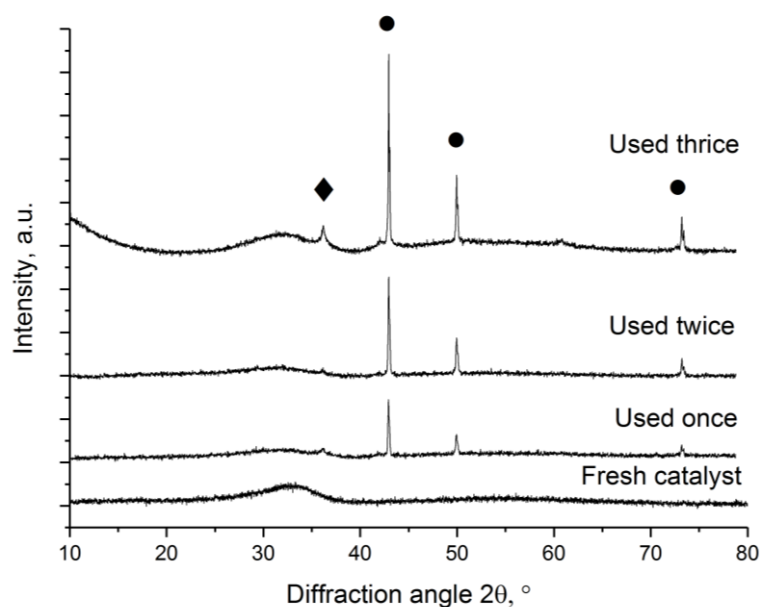


Figure 46. XRD patterns of re-used 30% Cu-ZrO₂ catalyst. • metallic Cu ♦ Cu₂O

Table 20. Copper crystallite size for reused catalysts calculated from Cu reflection at $2\theta = 35^\circ$.

Catalyst	Metallic Cu particle size (Scherrer equation), nm
30% Cu used once	63
30% Cu used twice	74
30% Cu used three times	92

The decreased activity after second reuse can be related to the morphological changes in the catalyst (Figure 47). There was a significant amount of phase separation between Cu and ZrO₂. A solid block of ZrO₂ was observed, with large clumps of copper agglomerating on the surface of the particle. However, no real

change in activity or morphology was observed between second and third uses, indicating that the material has reached a stable state. The agglomeration of copper crystallites is unavoidable at the temperature this reaction has been carried out at, due to the low Hüttig temperature of the metal (approximately 179 °C) – that is, the temperature at which surface atoms become significantly mobile. Another likely factor in morphological changes is how the H₂ gas was introduced to the reactor. As the internal reactor temperature reached 200 °C, 27 barg of H₂ was vented into the chamber, exposing the catalyst to extreme conditions over a short amount of time. Internal testing has shown that CuO on the calcined catalyst was fully reduced within minutes of introduction of H₂ to the reactor. This is in contrast to a typically utilised furnace reduction, where not only the concentration of H₂ was much lower, the flow of gas, ramp rate, and time were all controllable variables. These relatively harsh conditions likely promote particle agglomeration and growth in an uncontrollable manner.

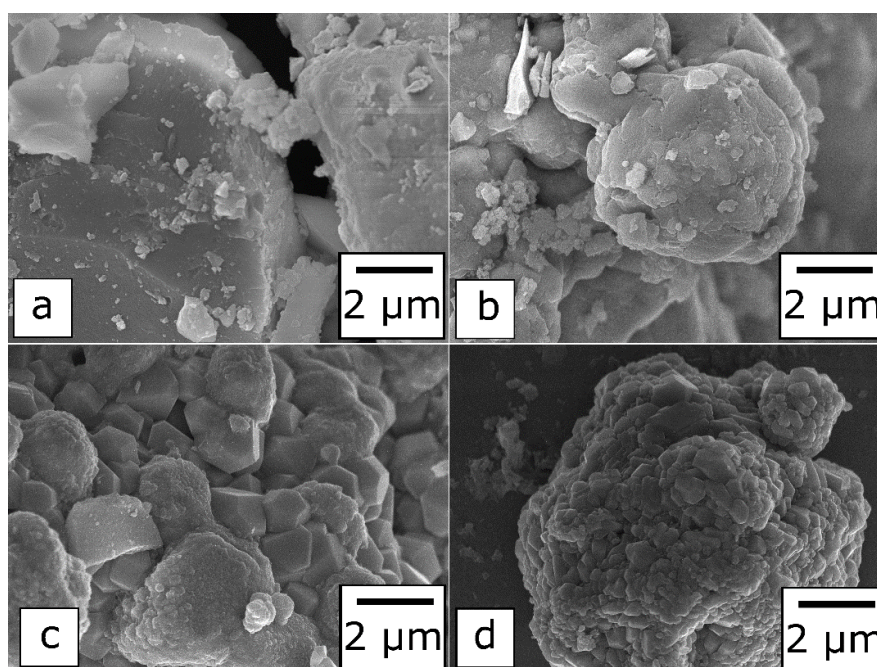


Figure 47. SEM images of a) fresh (calcined) 30% Cu-ZrO₂ catalyst b) the same catalyst after 1 use c) after 2 uses d) after 3 uses.

4.2.3. Acid wash of the catalyst

In order to determine the active species on the catalyst, they were subject to acid treatment with 0.5M HNO₃. The acid treatment stripped the surface of any labile copper species, and exposed the underlying copper with strong metal-support interactions. To confirm that all the labile species have been washed off, some of the acid-treated catalysts were subjected to a second acid wash, after which negligible amount of Cu was found in solution. Following the acid treatment, the catalysts were tested for hydrogenation of LA to GVL under standard conditions (Figure 48). It was found that the catalysts retained their activity completely. The amount of copper metal washed off the catalyst was calculated from MPAES analysis of the post-acid wash solutions. As much as 77% of copper originally loaded on the 50% Cu-ZrO₂ was washed off, demonstrating that a large amount of metal acted as spectator species. The lowest metal loading of 10% Cu leached only 1.3% of metal, with the 20% Cu catalyst leaching significantly more at 28.2%. This shows that during catalyst synthesis, copper species first saturate the bulk lattice before precipitating on the surface. The point of lattice saturation appeared to be roughly around 10% Cu loading. Approximately the first 15-20% of the loaded copper appears to have strong metal-support interactions (Table 21). As the surface copper was not involved in the reaction, it was therefore the metal with strong metal-support interactions that was the active species. The resilience of the active species towards acid treatment underlines stability of the catalyst, which was further underlined by the negligible leaching of the zirconia support.

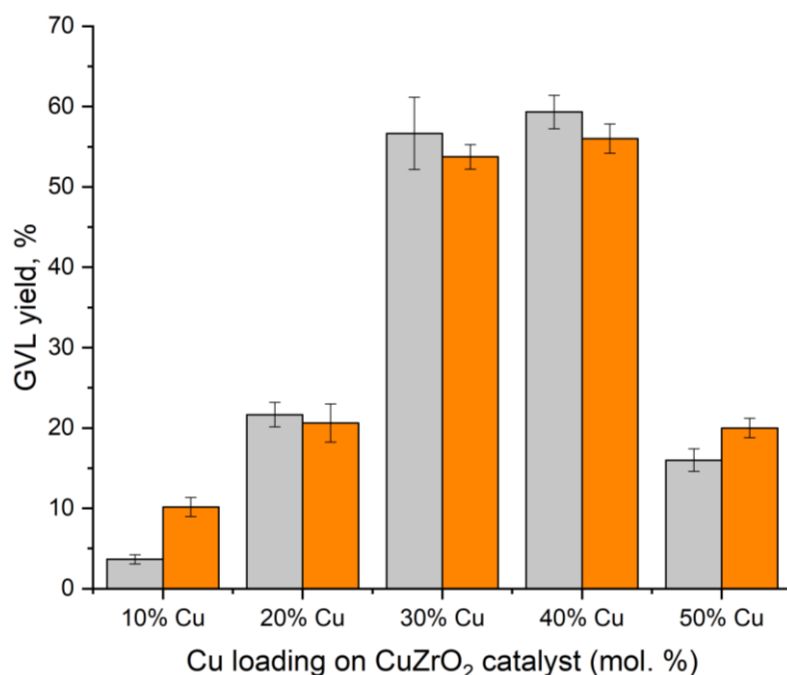


Figure 48. Activity of calcined Cu-ZrO₂ catalysts in relation to acid washing. **Grey:** before acid wash; **Orange:** after acid wash. Reaction conditions: 200 °C, 50 mg catalyst, 5% LA/H₂O, 27 barg H₂, 2 hours

Table 21. Calculated amounts of metallic copper and zirconia lost upon acid washing the catalysts. Percentages calculated from MPAES data.

Catalyst	Copper lost upon acid treatment, %	Zirconia lost upon acid treatment, %	Cu loading before treatment, %	Cu loading after treatment, %
10% Cu-ZrO ₂	1.3	0.2	10	9.9
20% Cu-ZrO ₂	28.2	0.4	20	14.4
30% Cu-ZrO ₂	28.9	0.3	30	21.3
40% Cu-ZrO ₂	48.4	0.6	40	20.6
50% Cu-ZrO ₂	76.6	0.4	50	11.7

Powdered XRD patterns for the acid washed catalysts can be seen in Figure 49. The pattern for 30% CuZrO₂ did not change drastically due to the acid treatment, as the material appeared amorphous in XRD when freshly calcined. However, a large change was observed in the pattern for 50% CuZrO₂. All the crystalline CuO reflections observed before have disappeared (2θ values of 59°, 62°, 67°, 68°, and 75°), in agreement with the 77% loss of copper from MPAES. Despite the large loss

of copper and disappearance of copper oxide reflections from XRD, acid washed 50% CuZrO₂ remained active for the hydrogenation of LA. This suggests that it is the metal with strong metal-support interactions which were highly important for this reaction.

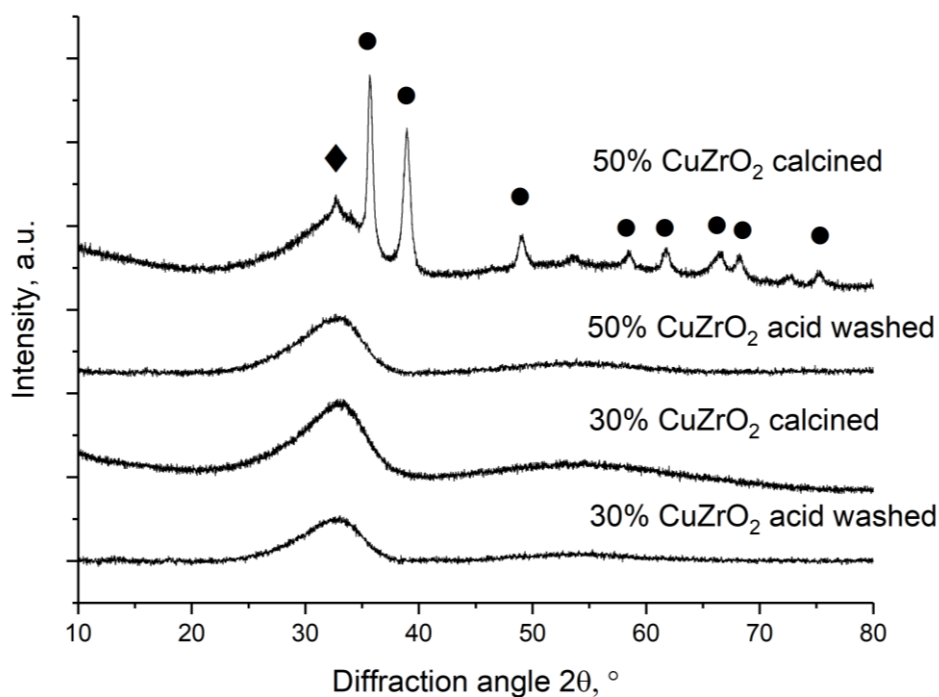


Figure 49. XRD patterns for acid-treated catalysts compared to untreated catalysts. • CuO; ◆ t-ZrO₂

However, the testing carried out in Figure 48 was carried out with 50 mg of catalyst, which means that the data is not directly comparable with pre-acid wash results; that is, if 50 mg of fresh catalyst were acid washed, there would be less than 50 mg of material left at the end of the process. Therefore a certain amount of catalyst was acid washed so that there was 50 mg of acid-washed catalyst available for reaction. As the acid wash removed any large copper particles and spectator species from the surface, it would leave behind mostly active sites. Therefore, 50 mg of acid washed catalyst had more active sites than 50 mg of fresh catalyst. To rationalise this data, dependence of catalyst TOF on moles of copper on the catalyst was plotted (Figure 50). It was found that the acid washed catalysts had higher TOFs than their fresh counterparts. This confirmed the idea that the leached copper acted purely as

spectator species. It was found that the acid-washed catalysts with the same amount of copper had near identical activities, and their TOFs overlapped. Two such groups were identified, 30% and 40% Cu-ZrO₂, and 20% and 50% Cu-ZrO₂ (labelling based on pre-acid wash quantities). This means that activity of the catalysts was very closely related to the amount of copper which had strong metal-support interactions (and therefore did not leach during the acid-wash).

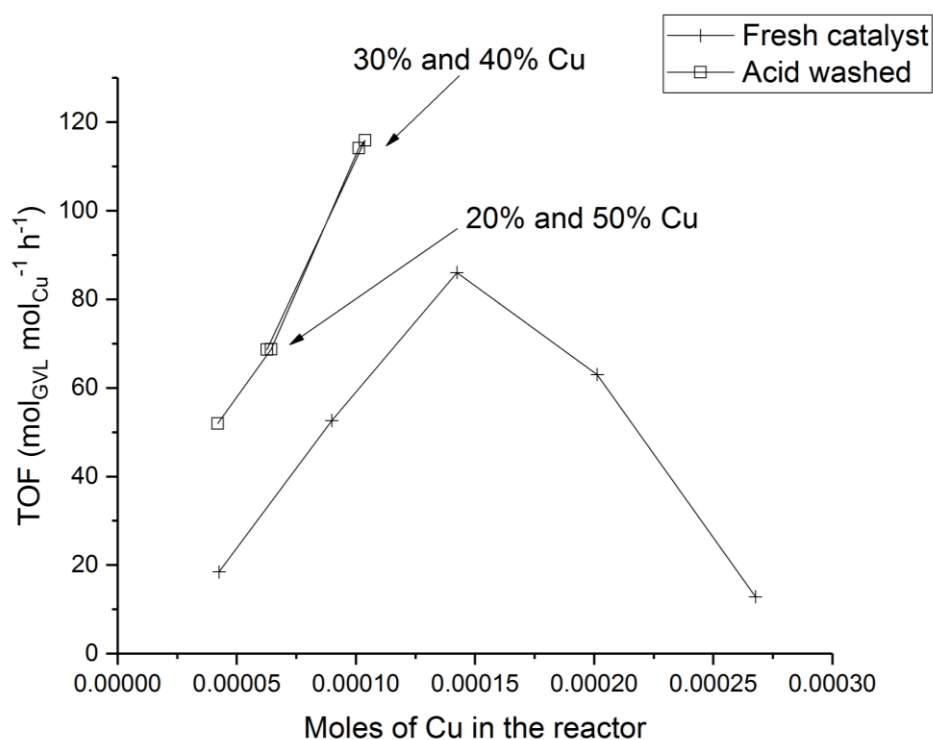


Figure 50. Catalyst TOF dependence on moles of Cu present in the reactor. Comparison between fresh and acid washed materials.

SEM images of the materials were also obtained (Figure 51). A significant difference was observed for all the catalysts. At all loadings, the biggest and most copper-rich particles from the surface were washed off. At 40% and 50% Cu, significant holes started to form due to the high loadings of metal. The holes appeared to be relatively uniform in size and distribution, and are remnants of where the most copper-rich particles were located. Interestingly, despite the fact that large holes were formed on 50% Cu material, the activity did not decrease, and TOF improved drastically, from 12.85 mol_{GVL} mol_{Cu}⁻¹ h⁻¹, to 68.64 mol_{GVL} mol_{Cu}⁻¹ h⁻¹. This shows that there was

excess copper-rich spectator species on the surface of 50% Cu catalyst which covered, or obscured, the strong metal-support interaction active sites.

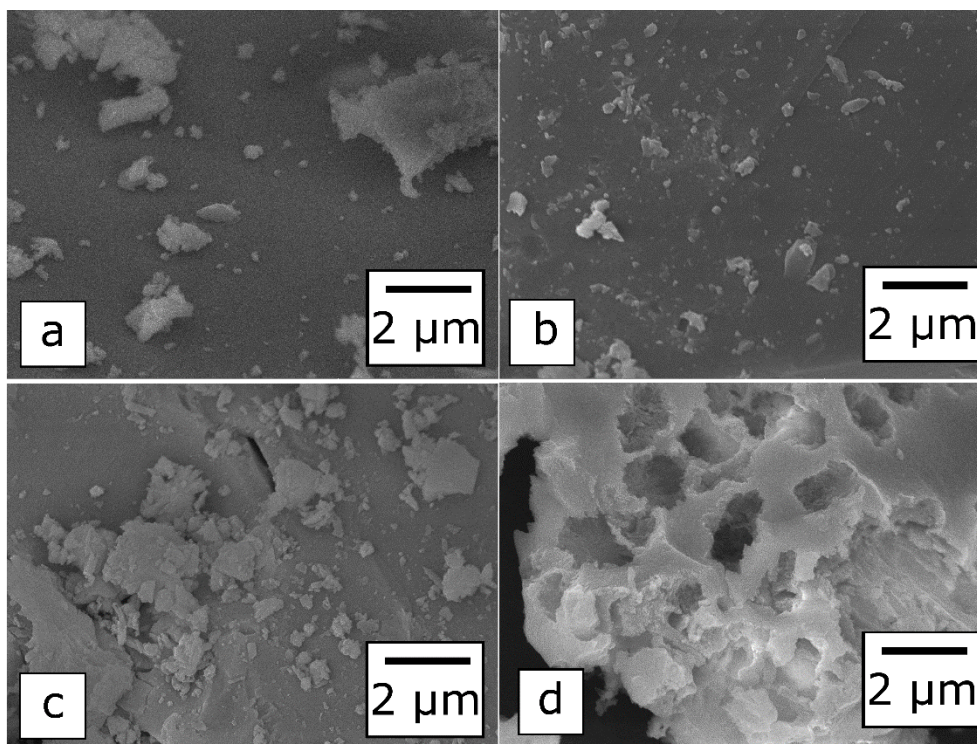


Figure 51. SEM images of a) fresh (calcined) 10% Cu-ZrO₂ catalyst b) 10% Cu-ZrO₂ after acid wash c) fresh (calcined) 50% Cu-ZrO₂ catalyst d) 50% Cu-ZrO₂ after acid wash

4.2.4. Effect of reduction treatment on catalyst activity

Reducibility of the calcined materials prepared by autotitrator was measured by TPR. It was found that the copper was fully reduced at around 150 °C (Figure 52). This is in contrast to the TPR data presented in section 4.2.1 (Figure 36), where the reduction event was still happening up to about 280 °C. The main reason for this difference is the refinement in methodology of how the TPR was carried out. Spectra shown in Figure 36, were ran with a ramp rate of 10 °C min⁻¹, whereas the spectra in Figure 52 were ran with a ramp rate of 1 °C min⁻¹. The lower ramp rate allowed not only for a more detailed spectra due to essentially a higher resolution, but also it showed the true reduction event of copper (II) oxide. This is because at high ramp rates, the oven would have rapidly continued heating whilst the material was still

being reduced, often overshooting the true reduction event – therefore the reported reduction temperature was inflated by the ramp rate. Two reduction profiles were present, indicating two species of copper in the catalysts. The lower temperature profile is typically attributed to well-dispersed surface CuO, whereas larger, bulk particles of CuO are responsible for the higher temperature profile.^{25,26} The proximity of these peaks, and their relatively low temperature indicates that a large portion of the copper in the catalyst was either on the surface, or close to the surface.

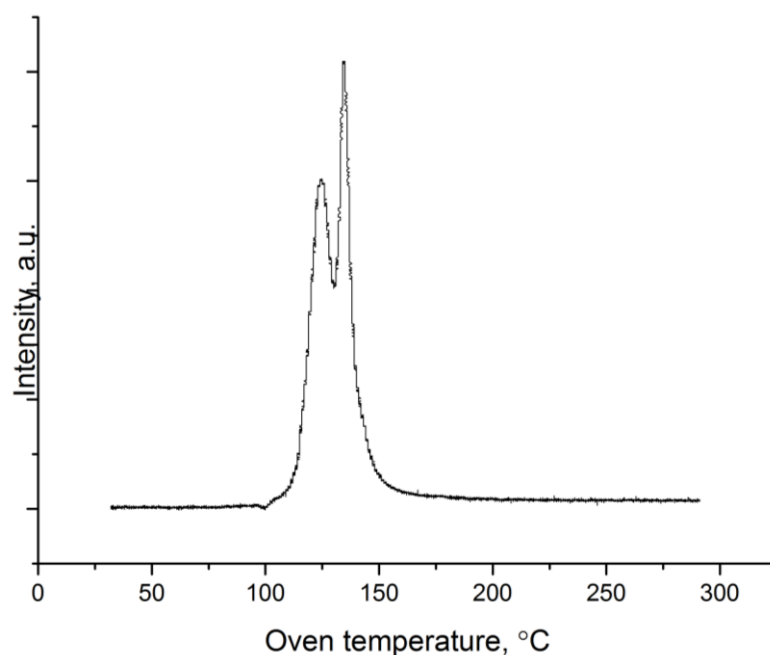


Figure 52. TPR for calcined 30% Cu-ZrO₂ catalysts. Reduction treatment carried out under 10% H₂/Ar (25 mL min⁻¹), ramp rate 1 °C min.

Reduction treatment was carried out on calcined 30% Cu-ZrO₂ catalysts at various temperatures, and the materials were then tested for the hydrogenation of LA to GVL (Figure 53). All of the reactions were selective to GVL and no side products were formed. Carbon mass balance was within 95-100% in all of the reactions. It was found that the lowest reduction temperature, 150 °C, produced the highest yield of GVL. Activity of the catalyst decreased when higher reduction temperatures were used. The lowest GVL yield was obtained with catalyst reduced at 500 °C (higher reduction temperatures were not tested).

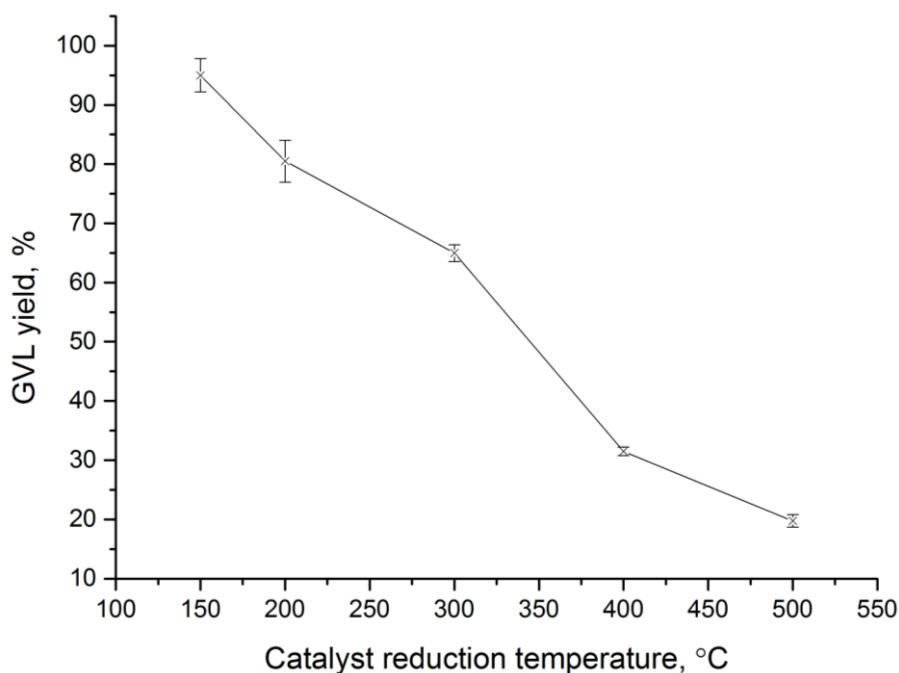


Figure 53. Catalytic activity of 30% Cu-ZrO₂ catalyst as a function of reduction temperature. *Reaction conditions:* 200 °C, H₂ 27 barg, 2 h, Substrate 5 wt.% LA/H₂O (10 g), catalyst (0.05 g). n.b. the error margins at 400 °C and 500 °C are small enough that are obscured by the average.

The trend in activity can be explained by looking at particle size trends. XRD (Figure 55) showed rapid growth in metallic Cu crystallite size with increasing reduction temperatures (Table 22). Catalyst with the smallest Cu crystallites produced the highest GVL yield, however the yield did not scale linearly with particle size differences. As evidenced by calcined XPS data, well-mixed copper and zirconia phase in a catalyst promotes hydrogenation of LA to GVL. Indeed, EDX analysis of the reduced materials showed almost homogeneous mixing of metal phases at low reduction temperatures; catalyst reduced at 500 °C displayed a noticeable degree of phase separation as well as particle growth (Figure 55). Due to the fact that small crystallite size and good mixing of phases resulted in better LA hydrogenation yields, it can be concluded that it is the interface between copper and zirconia where the reaction takes place. In fact, such interactions have been suggested before in literature.^{27,28} Zirconia atoms at the edges where metal particle and support meet create Zr⁴⁺/Zr³⁺ sites with incomplete coordination, which have

oxophilic properties.²⁹ Levulinic acid binds to those sites with its carboxylic acid group. Additionally, zirconia possesses amphoteric properties – levulinic acid can bind to the weak base sites on the support.³⁰ On the copper side of this interaction, hydrogen is adsorbed and dissociated.^{27,31,32} Dissociated hydrogen and levulinic acid are able to meet at the copper-zirconia interface, and thus a hydrogenation reaction is able to take place. One can consider different copper species for this reaction: surface copper, copper with access to the surface but interacting with the zirconia support, and copper embedded under the surface. Surface copper can adsorb and dissociate hydrogen, however it needs LA to proceed; as LA adsorbs on zirconia defect sites, the easily reducible surface copper species will not participate in the reaction because they are mainly surrounded by other copper atoms. The copper which interacts with zirconia will be the optimal type for hydrogenation of LA, as it has many interface sites where adsorbed LA and H₂ can meet for the reaction to proceed. The last type of copper, which is embedded under the surface, cannot interact with any substrates and therefore does not participate in the reaction – in fact this type of copper was the basis of developing the pH gradient catalyst synthesis method, as one of the goals was to reduce the amount of sub-surface copper which does not contribute towards activity.

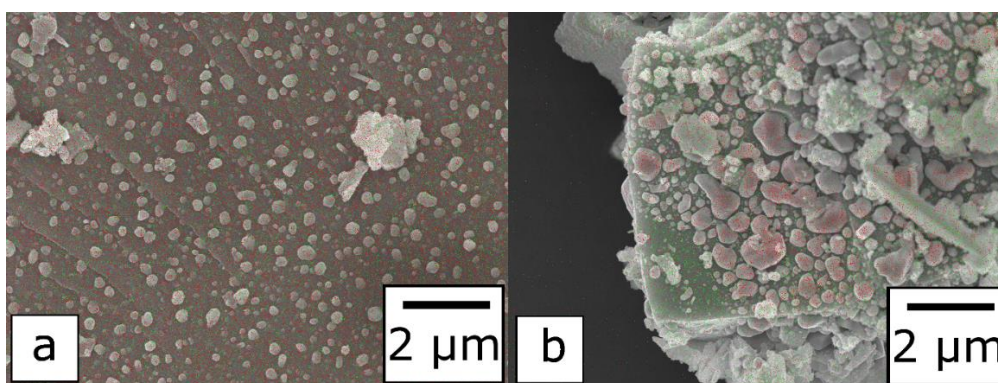


Figure 54. EDX data superimposed on SEM images of 30% Cu-ZrO₂ catalysts a) reduced at 150 °C, b) reduced at 500 °C. Red is copper, green is zirconium.

XRD patterns for the reduced catalysts are shown in Figure 55. All of the reduced catalyst featured metallic copper phase with peaks at $2\theta = 43^\circ$, 51° and 74° (ICDD = 01-070-3038). The copper crystallites increased in size at higher reduction temperatures (Table 22). No zirconia peaks were observed at temperatures below 500°C due to the amorphous nature of the oxide. At 500°C , tetragonal zirconia was observed with reflections appearing at $2\theta = 31^\circ$, 35° , 60° , and 63° (t-ZrO₂, ICDD = 01-080-3783). The phase change of zirconia from amorphous to crystalline tetragonal contributed to the phase separation observed in EDX (Figure 54). As zirconia crystallised in the bulk, it pushed out majority of copper towards the surface where it agglomerated.

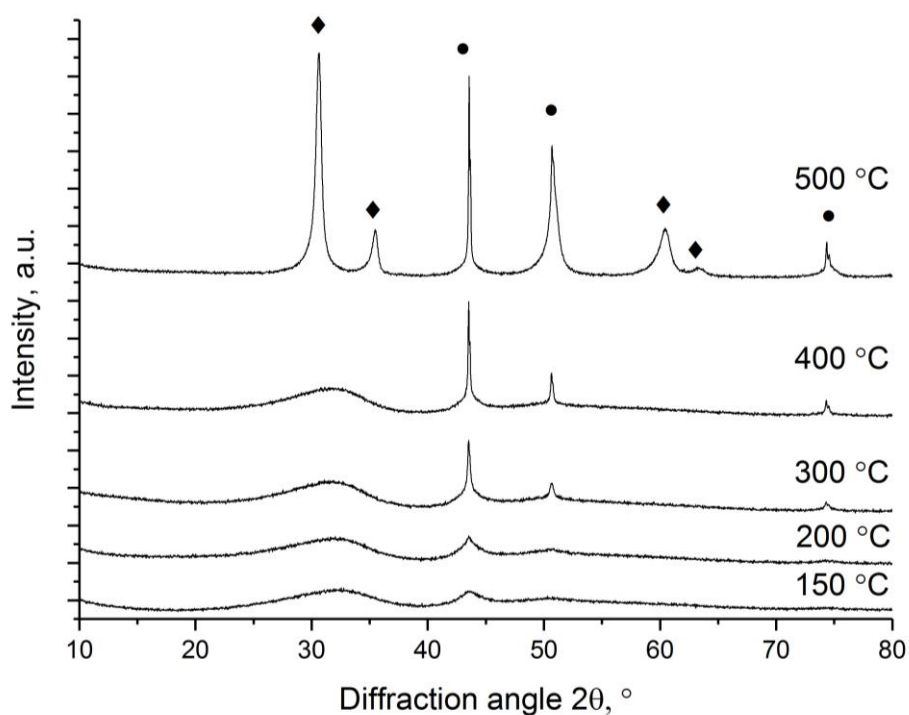


Figure 55. XRD patterns of reduced 30% Cu-ZrO₂ catalyst. • metallic Cu ♦ tetragonal Zirconia

Table 22. Cu crystallite size for 30% Cu-ZrO₂ catalysts reduced at various temperatures

Reduction temperature, °C	Cu crystallite size (Scherrer equation, $2\theta = 43^\circ$), nm
150	4.5
200	6
300	25
400	75
500	87

BET surface areas of the reduced materials were obtained, displayed in Table 23. Catalysts with relatively large particles had smaller surface areas. However, just like the trend in crystallite size, GVL yield did not scale linearly with BET surface area, and no trend was observed when yield was normalised to it. However, there was a correlation between higher surface area and higher GVL yield.

Table 23. 5-point BET surface areas for reduced Cu-ZrO₂ catalysts prepared by variation of reduction temperature

Reduction temperature, °C	BET surface area, m ² g ⁻¹
150	62
200	50
300	28
400	9
500	11

Copper surface area (Cu SA) of the reduced catalysts was obtained by N₂O titration for catalysts reduced at different temperatures (Table 24). Copper surface area did not reflect the large differences in activity. The most active catalyst, reduced at 150 °C, had marginally more copper surface area than the least active one, reduced at 500 °C. Despite the fact that clear differences between these materials could have been observed in SEM: phase mixing, particle size, and dispersion, no significant variance can be observed between the Cu SAs. If the assumption made earlier in this section is correct, that the interface sites catalyse this reaction, one would assume that the most active catalysts had the highest Cu SA. This is because a higher Cu SA allows for more Cu-Zr interface sites, and therefore higher activity. However, the apparent lack of correlation between Cu SA and activity can be explained with results from the acid-washed catalysts in section 4.2.3. In terms of the 30% Cu catalyst, at least 28% of the original copper content was washed off without affecting the activity adversely. This means that at least 28% of the copper on the catalysts acts as spectator species. Therefore, a large percentage of the measured copper surface area in presented in Table 24 did not participate in the reaction. It can be inferred that the catalysts reduced at lower temperatures would have higher “usable” copper surface area (that is, copper with strong metal-support interactions) than the catalysts reduced at high temperatures.

Table 24. Copper surface areas for 30% Cu-ZrO₂ catalyst as a variation of reduction temperature.

Material	Copper surface area, m ² g ⁻¹	GVL yield, %
30% Cu-ZrO ₂ 150 °C	6.2	95
30% Cu-ZrO ₂ 300 °C	5.3	65
30% Cu-ZrO ₂ 500 °C	5.1	20

4.2.5. Kinetic analysis of 30% Cu-ZrO₂

Kinetic analysis was carried out on the 30% Cu-ZrO₂ catalyst reduced at 200 °C in order to determine reaction orders. Note that the pressure of hydrogen was normalised to the actual partial pressure of hydrogen present in the autoclave, as the reaction reached an autogenous pressure of about 8 bar before any hydrogen was introduced to the system. The autogenous pressure was subtracted from the total pressure to calculate the actual pressure of hydrogen. Reaction order with respect to levulinic acid was found to be approximately zero, and an order of approximately 1 was found with respect to hydrogen pressure. This means that there is essentially an excess of levulinic acid available, and surface of the catalyst was saturated with substrate – there was no shortage of levulinic acid at any point in the reaction. However, yield of GVL was directly related to the pressure of hydrogen present in the reactor. The generally accepted mechanism for conversion of LA to GVL is the hydrogenation of LA into 4-hydroxypentanoic acid (4-HPA), followed by a subsequent cyclisation to GVL.³³ The hydrogenation of LA to 4-HPA is therefore the limiting step in this reaction.

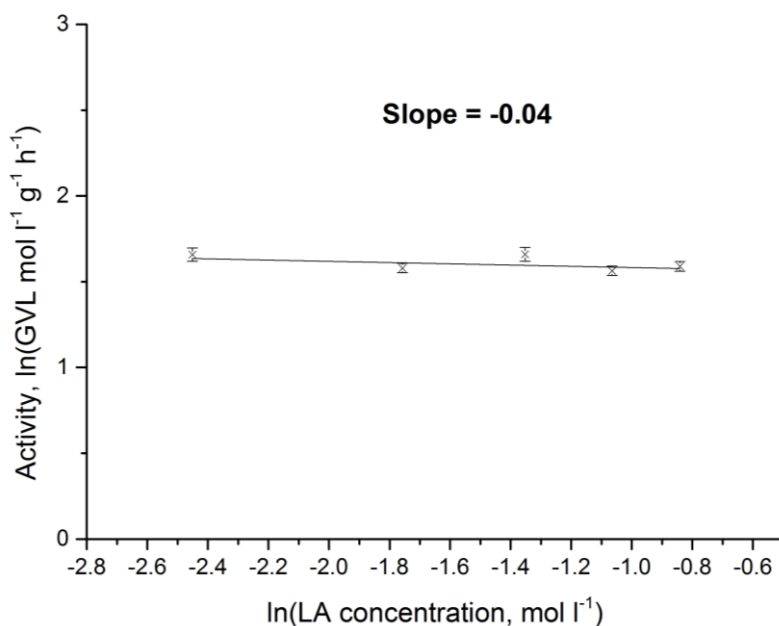
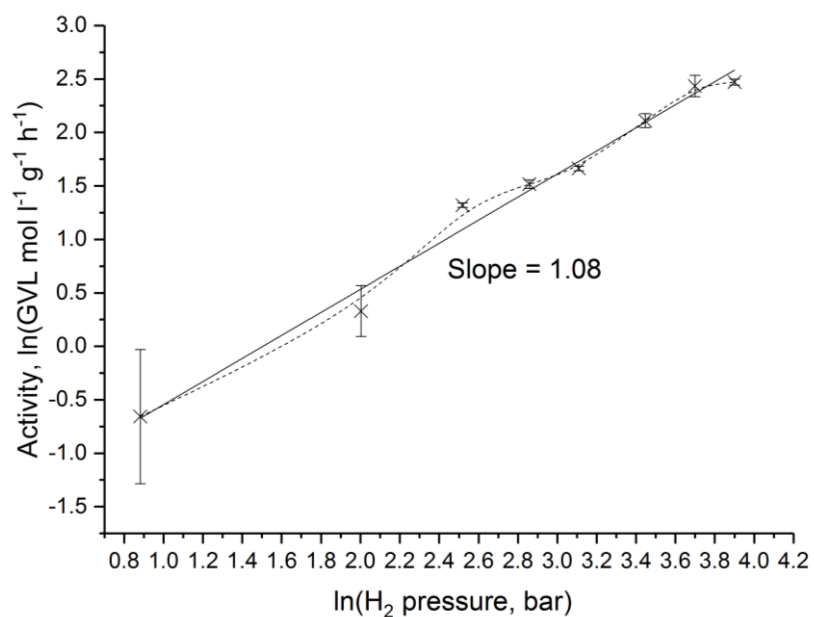


Figure 56. Effect of hydrogen concentration (top) and levulinic acid concentration (bottom) on activity of 200 °C reduced 30% Cu-ZrO₂. *Reaction conditions:* 200 °C, H₂ 7 – 54 barg, 15 min, Substrate 1 - 5 wt.% LA/H₂O (10 g), catalyst (0.05 g).

There was a linear increase in GVL yield with hydrogen pressure, with an order of approximately 1. The gradient of the line never became flat, or approached zero, indicating that the diffusion limit of hydrogen was not reached even at 54 barg pressure.

4.2.6. Mechanistic studies

A recent paper by the Li group suggested that water is involved in the mechanism of hydrogenating levulinic acid to γ -valerolactone.³⁴ However, ruthenium-based catalysts are known to be much more active for this reaction. In order to explore whether Cu-ZrO₂ catalysts follow the same hydrogenation mechanism, deuteration studies were carried out using 5% Ru/Al₂O₃, 50% Cu-ZrO₂ and 1% Mn/Cu-ZrO₂. Ruthenium catalyst was used as a control, and to reproduce results published by the Li group. The 50% Cu-ZrO₂ and 1% Mn/Cu-ZrO₂ were prepared by the oxalate gel method, and not the pH gradient method. This is because the work was carried out to supplement a paper regarding doping oxalate-gel prepared materials. However, it has been observed that both the pH gradient and oxalate gel materials follow similar kinetic orders. Therefore, these catalysts can be compared in terms of their activity and mechanistic behaviours despite different preparation methods. Doping studies were carried out with the first row of transition metals, using 1 wt. % loadings on 50% Cu-ZrO₂. Manganese was found to be the best performing dopant, and so 1 wt. % Mn/Cu-ZrO₂ was selected for further testing. Discussion of dopant effect, their characterisation and activity data is contained within the paper by Jun *et al.*, whereas this section focuses deuteration studies.

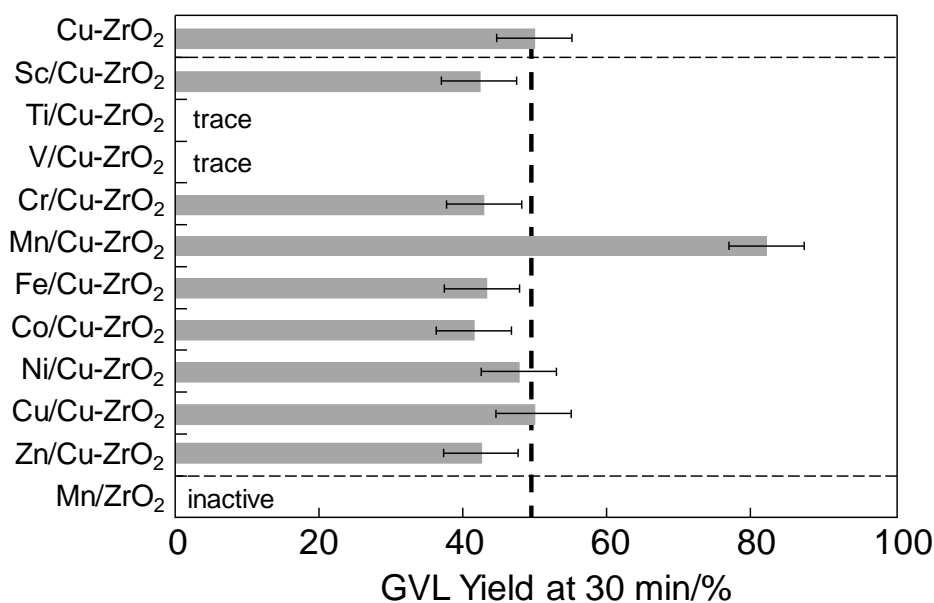


Figure 57. Testing of first row transition metals as 1 wt. % dopants to 50% Cu-ZrO₂. Reaction conditions: 200 °C, H₂ 27 barg, 30 min, Substrate 5 wt.% LA/H₂O (10 g), catalyst (0.05 g). Figure adapted from a Hutchings group paper in submission (with permission).

Initial testing was focused on reproducing the activity data from Li and Hutchings groups. For this purpose, 5% Ru/Al₂O₃ was used as a readily available catalyst from within the research group. It featured slightly higher Ru loading than the ones reported in the paper (0.5 – 2 wt. %), which may have enhanced activity of the material, but for the purposes of a mechanistic studies it was an appropriate loading. 50% Cu-ZrO₂ and 1% Mn/Cu-ZrO₂ were re-synthesised and re-tested. Figure 58 shows the GVL yields obtained with these catalysts. Doping Cu-ZrO₂ with Mn enhanced the activity of the catalyst as expected, increasing GVL yield from 50% to 66%. 5% Ru/Al₂O₃ was the most active catalyst, producing 95% GVL yield. However, the testing conditions for Ru and Cu-based catalysts were different, due to the fact that Ru-based materials are much more active for this reaction than Cu materials. As such, testing conditions for 5% Ru/Al₂O₃ were reproduced from literature, whereas 50% Cu-ZrO₂ and 1% Mn/Cu-ZrO₂ were tested under standard experimental conditions used so far in this thesis. To account for different reaction conditions, moles of substrate converted can be compared. Ruthenium catalyst has

converted approximately fifteen times more levulinic acid, with a tenfold reduction in metal loading.

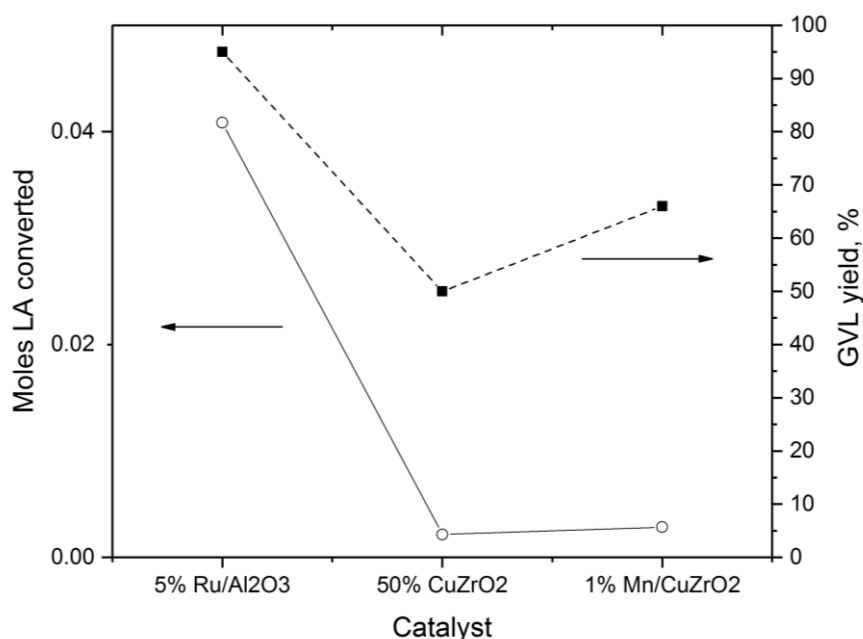


Figure 58. Conversion of LA to GVL using various catalysts. Reaction conditions: Ru/Al₂O₃: 0.1 g catalyst, temp. 130 °C, time 30 min, 40 bar H₂, 5 g levulinic acid, 10 g H₂O. Cu catalysts: 0.05 g catalyst, temp 200 °C, time 30 min, 27 barg H₂, 10 g 5% LA/H₂O.

All three materials presented above have been subject to reactions in both H₂O and D₂O. It was found that when 5% Ru/Al₂O₃ was used, deuteration only affected one proton, located at position G4 in the spectra below. This proton was gained in the hydrogenation process from levulinic acid. This effect can be visible by comparing ¹³C NMR in Figure 59. Peak integrals have been normalized to the carbonyl signal at 181ppm (G1); the carbon at that position is unique within the GVL molecule, and has no protons attached to it. Its signal size will therefore remain constant in relation to the other peaks. Integral of that peak was calibrated to 100. The signal corresponding to G4 at 80ppm decreases in size from 278 to 145, with all the other signals remaining unchanged. Due to the fact that signals in ¹³C NMR are directly affected by neighbouring protons, deuteration effects manifest themselves in reduction of the size of the carbon signal to which the affected proton is attached to. The presence of deuterium in that position can signify two things: either the proton

came directly from the D₂O solvent, and therefore water is involved in the hydrogenation reaction; or the proton was added after GVL was formed, through an exchange mechanism. However, when GVL was subject to reaction conditions under D₂O (temp 200 °C, time 30 min, 27 barg H₂, 10 g 5% LA/H₂O, 0.05 g Cu-ZrO₂, or no catalyst), no deuteration products were observed in NMR. This means that GVL did not exchange protons with the solvent, and that water must be part of the hydrogenation reaction.

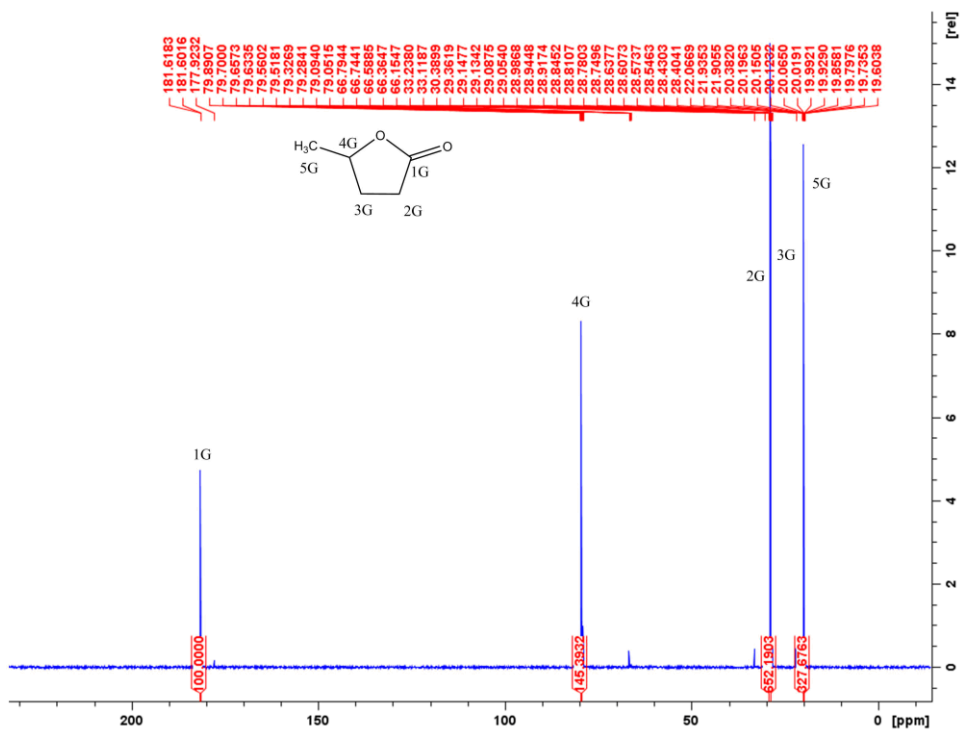
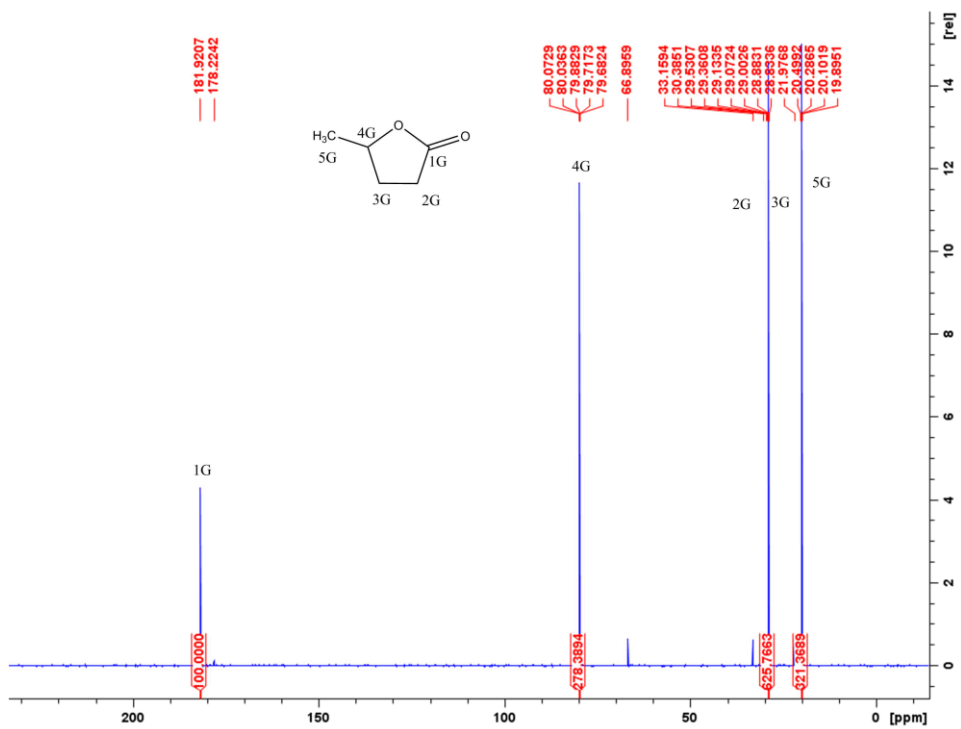


Figure 59. ^{13}C NMR of post reaction mixture from LA to GVL hydrogenation reaction catalysed by 5% $\text{Ru}/\text{Al}_2\text{O}_3$. The reaction was conducted using top) H_2O and bottom) D_2O as the solvent. Carbon numbers include G for GVL. For top) ^{13}C NMR (500 MHz, D_2O) δ 181.9, 80.1, 37.7, 29.6, 28.8, 27.8, 20.5

For bottom) ^{13}C NMR (500 MHz, D_2O) δ 181.6, 79.8, 29.4, 28. 19.9

The proposed mechanism involving water can be seen in Figure 60. The process begins with a hydrogen molecule dissociating on the surface of the catalyst. It is known that hydrogen dissociation can happen on Cu-ZrO₂, because hydrogen spillover has been observed to happen from Cu to Zr.¹⁹ Following the dissociation, a nearby water molecule (with the proton of interest circled) can exchange a hydrogen atom with the catalyst surface. Hydrogen diffusion across the surface of the catalyst can be mediated by this mechanism, called “proton hopping”. Water-mediated proton hopping can lower the energy barrier for hydrogen diffusion.³⁵ The exchanged hydrogen species (very likely in the hydride form) can then attack the ketone carbonyl in levulinic acid, adsorbed on a nearby Zr-site, and carry out the concerted hydrogenation reaction. As a result, hydrogen atom from solvent water can end up on the GVL product. It is important to note that the exchange can happen, but does not have to; the hydrogenation reaction can easily happen before the exchange reaction takes place.

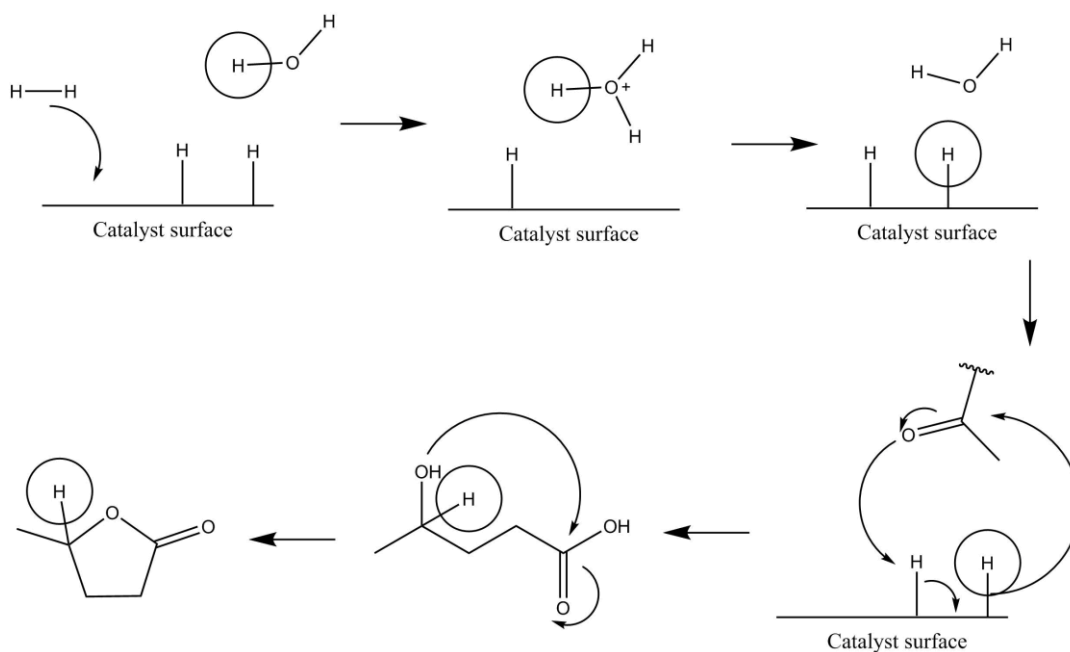


Figure 60. Proposed mechanism for the involvement of water into the final product.

The post-reaction solutions were injected into GC-MS to confirm the deuteration effect. The results can be seen in Figure 61. A standard reaction in H₂O as solvent resulted in the heaviest fragment m/z = 100, corresponding to a GVL molecule. When a deuterated solvent was used, the heaviest fragment m/z was observed to be 101, corresponding to a GVL molecule with one hydrogen atom substituted for a deuterium atom. Therefore, together with NMR data, it was conclusively shown that water can be involved in the hydrogenation reaction.

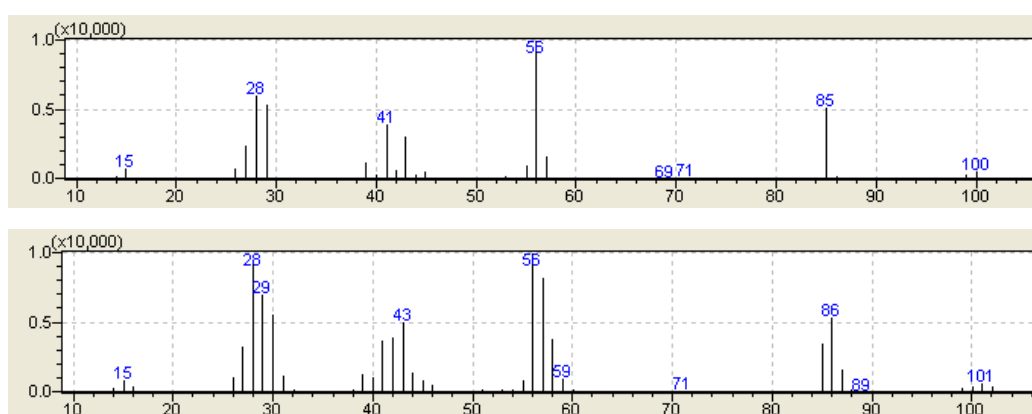


Figure 61. GC-MS of post-reaction solutions in H₂O (top) and D₂O (bottom). Testing carried out with 5% Ru/Al₂O₃. The fragment analysis was carried out on GVL only.

Following the ruthenium testing, 1% Mn/Cu-ZrO₂ was subject to deuteration experiments. When deuterated solvent was used, identical effect was observed as with the ruthenium catalyst. In ¹³C NMR spectra (Figure 62), the G4 signal at 80ppm reduced in size from 310 to 194. Again, the integrals were normalized to G1 signal. Therefore, 1% Mn/Cu-ZrO₂ follows the same or very similar mechanistic pathway as the ruthenium catalyst – water seems to play an important role in the hydrogenation process; perhaps it enables the diffusion of hydrogen from copper-rich sites to Cu-Zr interfaces with the previously mentioned water-hopping mechanism.

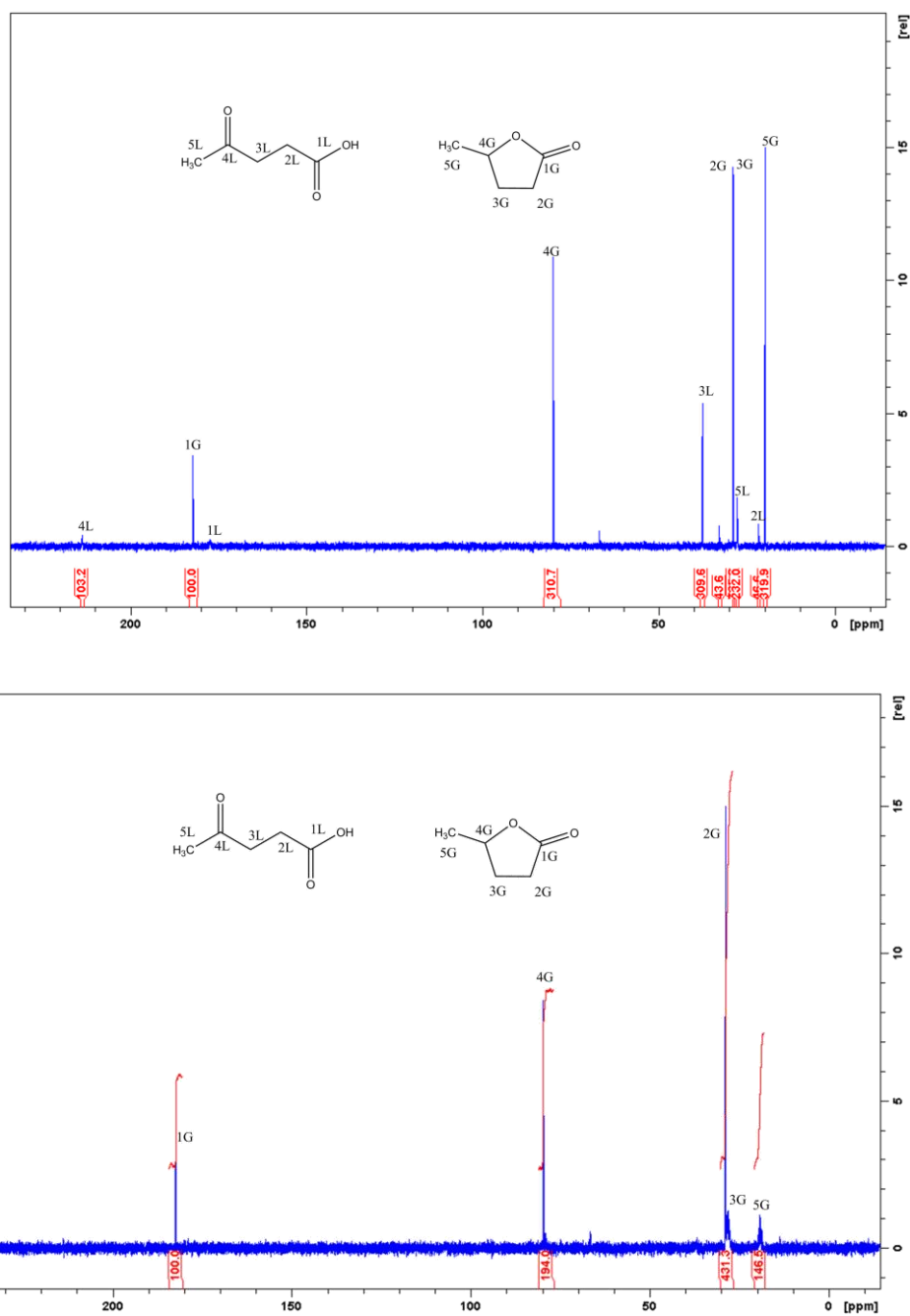


Figure 62. ¹³C NMR of post reaction mixture from LA to GVL hydrogenation reaction catalysed by MnCu-ZrO₂. The reaction was conducted using top) H₂O and bottom) D₂O as the solvent. Carbon numbers include letters L for levulinic acid and G for GVL.

For top) ¹³C NMR (500 MHz, D₂O) δ 213.7, 182.2, 177.6, 79.9, 37.7, 29.1, 28.8, 27.8, 21.7, 19.9

For bottom) ¹³C NMR (500 MHz, D₂O) δ 182.4, 79.8, 29.1 – 27.9 (m due to deuteration), 19.9 – 18.7 (m due to deuteration). Carbons 1L-5L not observable due to high conversion and deuteration of the substrate.

Conversely, the G4 signal was not the only one which decreased in size. Despite incomplete conversion, levulinic acid all but disappeared from the spectrum. Furthermore, GVL carbons 3G and 5G greatly reduced in size, indicating that they were deuterated. 2G has retained its integral size. Deuteration of $-\text{CH}_2$ and $-\text{CH}_3$ groups is unusual, and so ^1H NMR analysis was carried out in order to confirm these findings. Proton NMR has shown the same effect, with many protons decreasing in integral size and losing their multiplicity, a sure sign of deuteration.

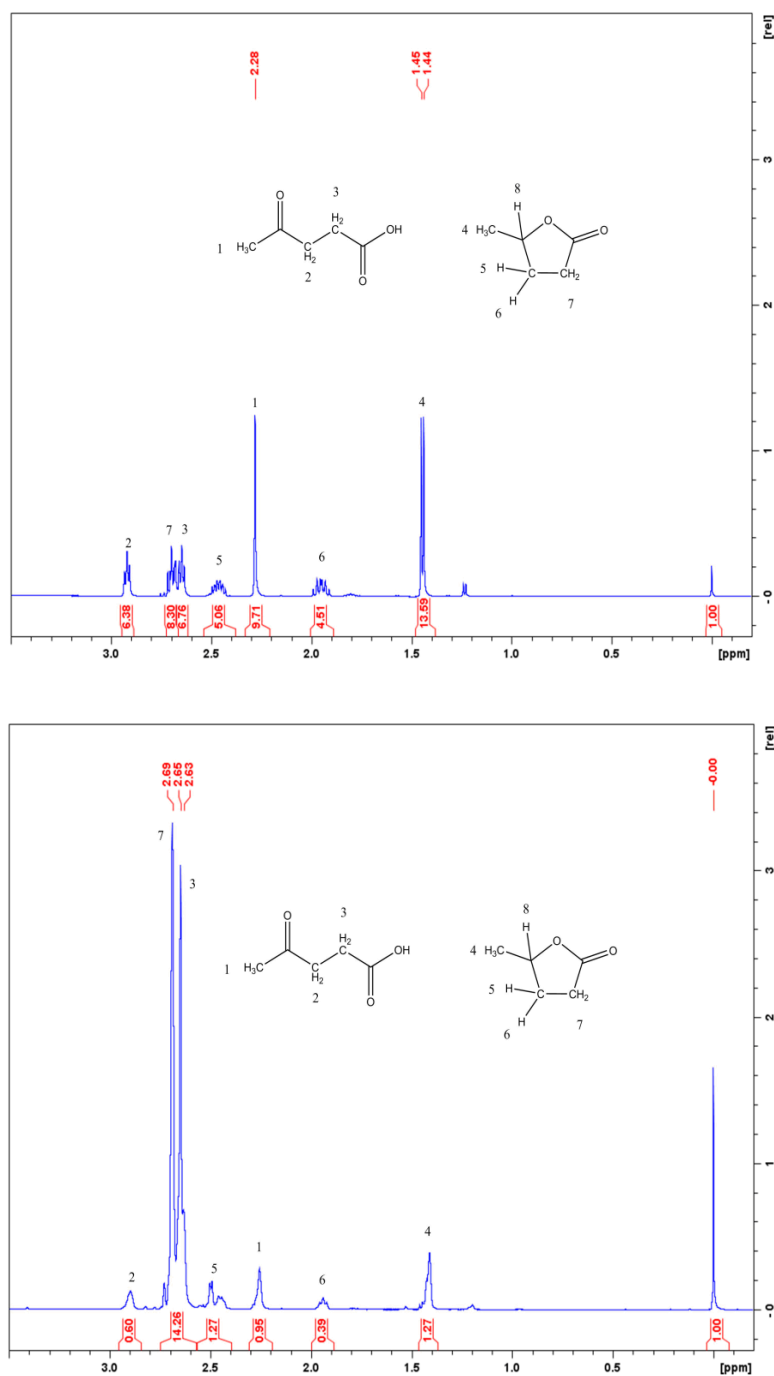


Figure 63. ¹H NMR of post reaction mixture from LA to GVL hydrogenation reaction catalysed by Mn/Cu-ZrO₂. The reaction was conducted using top) H₂O and bottom) D₂O as the solvent. In both cases, spectra were referenced against a tetramethylsilane (TMS) insert (δ 0). Note proton 8 would be expected to give a peak around 4 ppm, but this region of the spectrum is dominated by resonances from water.

For top) ¹H NMR (500 MHz, D₂O) δ 2.94 – 2.91 (t, *J* = 12.7 Hz, 6.4 Hz, 2H), 2.72 – 2.67 (m, 2H), 2.67 – 2.63 (t, *J* = 12.7 Hz, 6.3 Hz, 2H), 2.52 – 2.43 (m, 1H), 2.28 (s, 3H), 1.99 – 1.91 (m, 1H), 1.45 – 1.44 (d, *J* = 6.4 Hz, 3H), 0.00 (s, 12H)

For bottom) ¹H NMR (500 MHz, D₂O) δ 2.90 (s, 2H), 2.74 – 2.62 (m, 4H), 2.50 – 2.40 (m, 1H), 2.25 (s, 3H), 1.98 – 1.91 (m, 1H), 1.46 – 1.40 (m, 3H), 0.00 (s, 12H)

The list of NMR signals and their integrals can be found in Table 25. Extent of deuteration was calculated by comparing sizes of the normalised integrals. For majority of the protons, the deuteration exchange rate was above 90%, showing that it was a very favourable process that happened readily.

Table 25. List of integrals normalized to the TMS peak at δ 0.00 from Figure 63. Corresponding peaks from both spectra are matched the extent of deuteration compared.

C atom	Proton position	Corresponding peaks δ		Normalised integrals		Extent of deuteration
		H ₂ O	D ₂ O	H ₂ O	D ₂ O	
3 LA	2	2.94 – 2.91	2.90	6.38	0.60	91%
2 GVL	7	2.72 – 2.67	2.74 –	8.30	14.26	5%
2 LA	3	2.67 – 2.63	2.62	6.76		
3 GVL	5	2.52 – 2.43	2.50 – 2.40	5.06	1.27	75%
5 LA	1	2.28	2.25	9.71	0.95	90%
3 GVL	6	1.99 – 1.91	1.98 – 1.91	4.51	0.39	91%
5 GVL	4	1.45 – 1.44	1.46 – 1.40	13.59	1.27	91%
		0.00	0.00	1.00 (TMS)	1.00 (TMS)	-

GC-MS studies (Figure 64) agree with these findings. When the GVL signal was inspected, several heavy fragments were seen which can only be attributed to deuterated species. In water, the heaviest fragment observed had $m/z = 100$, which correlates to GVL. In deuterated water, the heaviest fragment had $m/z = 106$, corresponding to GVL molecule with six hydrogen atoms substituted for deuterium atoms. Since GVL does not exchange with D₂O at all, the deuteration must have

taken place before GVL was formed. This implies a possibility of a different reaction mechanism to the ruthenium catalyst.

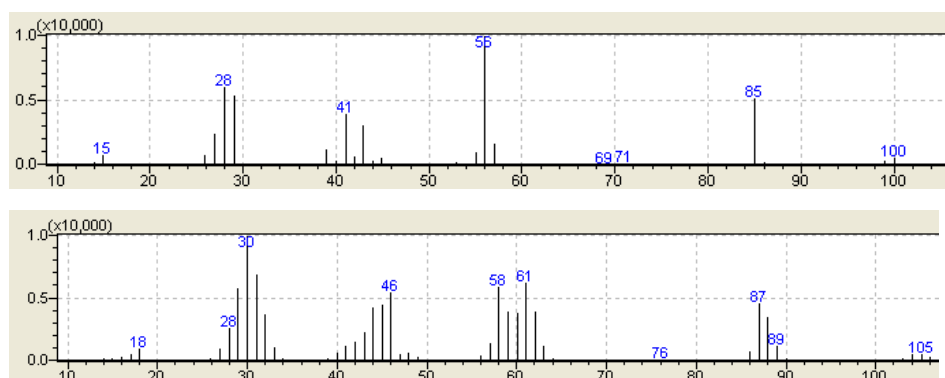


Figure 64. GC-MS of post-reaction solutions in H₂O (top) and D₂O (bottom). Testing carried out with MnCu-ZrO₂. The fragment analysis was carried out on GVL only.

In order to determine the stage of reaction in which levulinic acid is deuterated, three control experiments were carried out: levulinic acid in H₂O with no catalyst, levulinic acid in D₂O with no catalyst, and levulinic acid in D₂O with MnCu-ZrO₂ in inert atmosphere (N₂). Expectedly, when no catalyst was used in H₂O, levulinic acid did not react in any way, as evidenced by Figure 65 and confirmed by GC. The heaviest observed fragment in GC-MS had $m/z = 116$, which was unaltered LA. However, when a reaction was carried out with no catalyst, LA in D₂O, the heaviest fragment observed in GC-MS had $m/z = 122$. This increase of 6 in the fragment size was identical to the increase in fragment size in GVL. The same result was obtained when MnCu-ZrO₂ was used in an inert atmosphere. This means that the deuteration occurred spontaneously, and was not a mechanistic pathway into GVL.

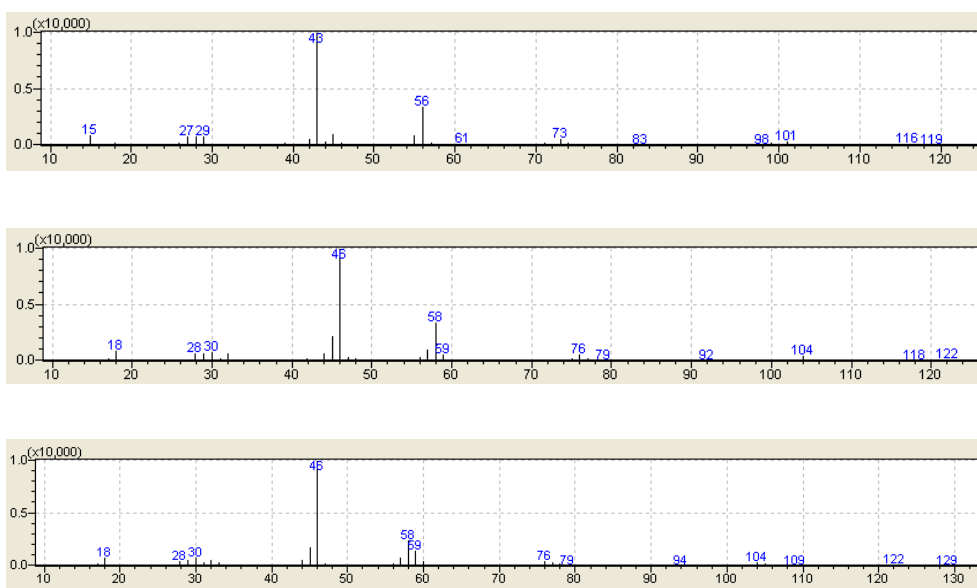


Figure 65. (Top) 10 g 5% LA in H₂O with no catalyst. Temp 200 °C, time 30 min, 27 barg H₂; (Middle) 10 mL 5% LA in D₂O with no catalyst. Temp 200 °C, time 30 min, 27 barg H₂; (Bottom) 10 mL 5% LA in D₂O with 0.05 g MnCu-ZrO₂. Temp 200 °C, time 30 min, 27 barg N₂.

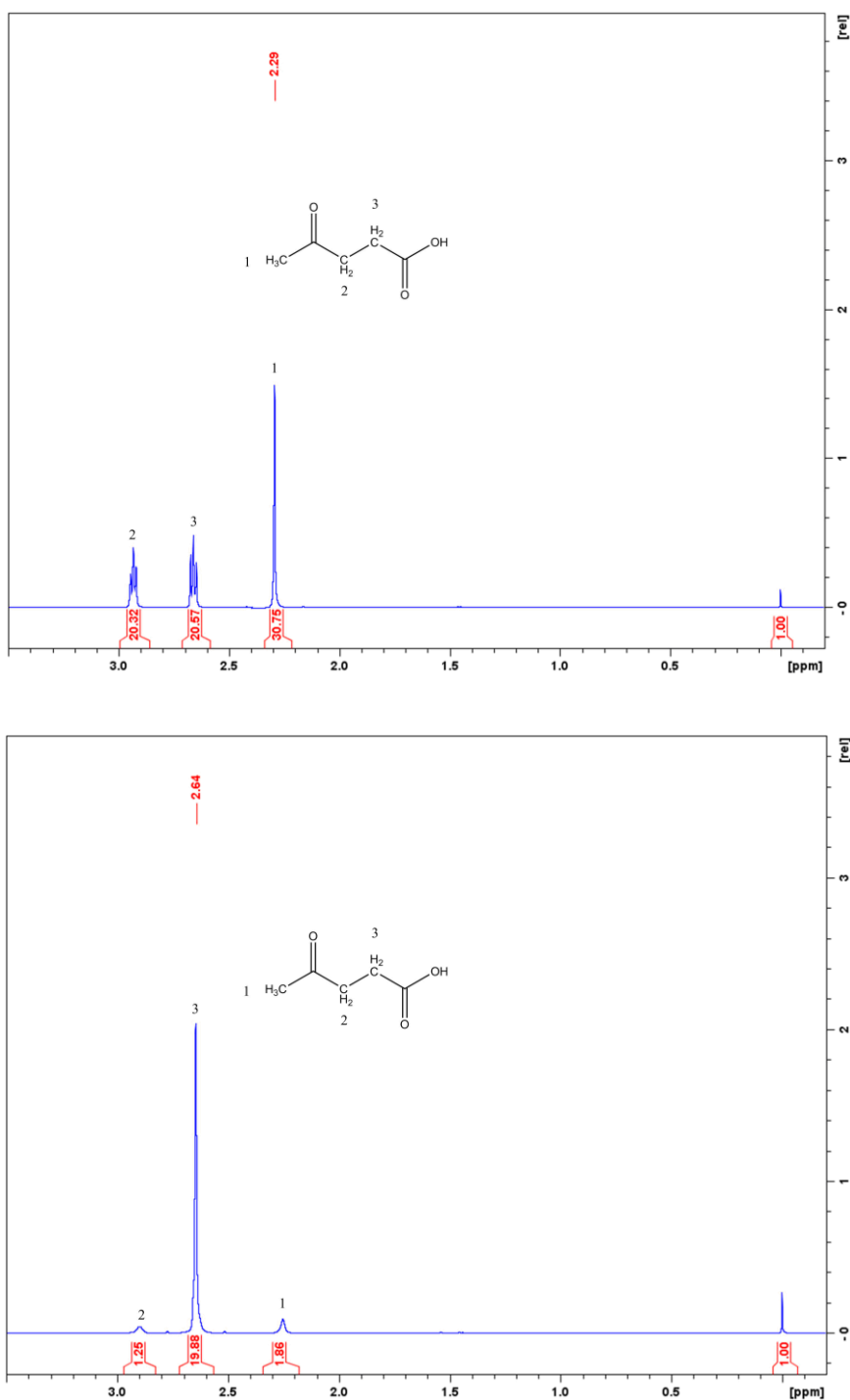


Figure 66. ¹H NMR of LA following treatment under reaction conditions but without catalyst present as a blank reaction test. The reaction was conducted using top) H₂O and bottom) D₂O as the solvent. In both cases, the spectra were referenced against a tetramethylsilane (TMS) insert (δ 0).

For top) ¹H NMR (500 MHz, D₂O) δ 2.95 – 2.91 (t, *J* = 12.3 Hz, 5.9 Hz, 2H), 2.68 – 2.64 (t, *J* = 12.3 Hz, 5.9 Hz, 2H), 2.29 (s, 3H), 0.00 (s, 12H)

For bottom) ¹H NMR (500 MHz, D₂O) δ 2.89 (s, 2H), 2.64 (s, 2H), 2.50 (s, 3H) 0.00 (s, 12H)

Since the deuteration of LA was a spontaneous event, the most likely reason for why it was not observed when 5% Ru/Al₂O₃ was tested, was that the proton exchange on levulinic acid had a high energy barrier, which was not reached at 130 °C (reaction temperature for Ru-catalyst), but 200 °C provided enough thermal energy for the process to occur. To confirm this, 5% Ru/Al₂O₃ was tested under the same conditions as MnCu-ZrO₂, with the catalyst mass reduced from 50 mg to 17.5 mg in order to bring the conversion values in line (as Ru is much more active than the MnCu catalyst). Data from those experiments is shown in Figure 67.

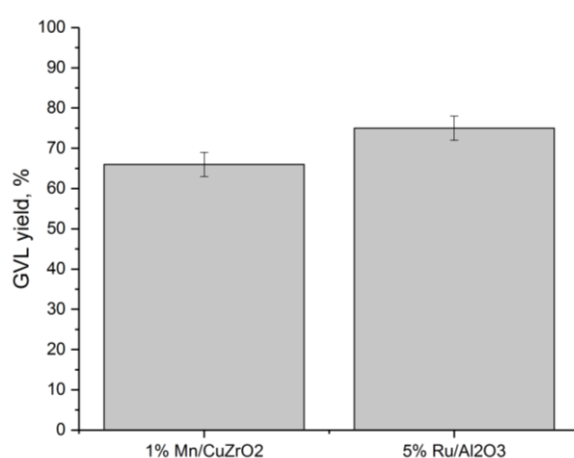


Figure 67. Conversion of LA to GVL in D₂O. Reaction conditions: temp 200 °C, time 30 min, 27 barg H₂, 10 mL 5% LA/D₂O, 0.05 g Mn/Cu-ZrO₂ or 0.0175 g Ru/Al₂O₃

Post reaction solution was analysed by ¹³C NMR (Figure 68). As with MnCu-ZrO₂, there was a significant reduction in peak size of 5G. Levulinic acid peaks have also reduced in size. This demonstrates that deuterium exchange with levulinic acid was a spontaneous event, and happened as soon as the thermal energy barrier has been reached.

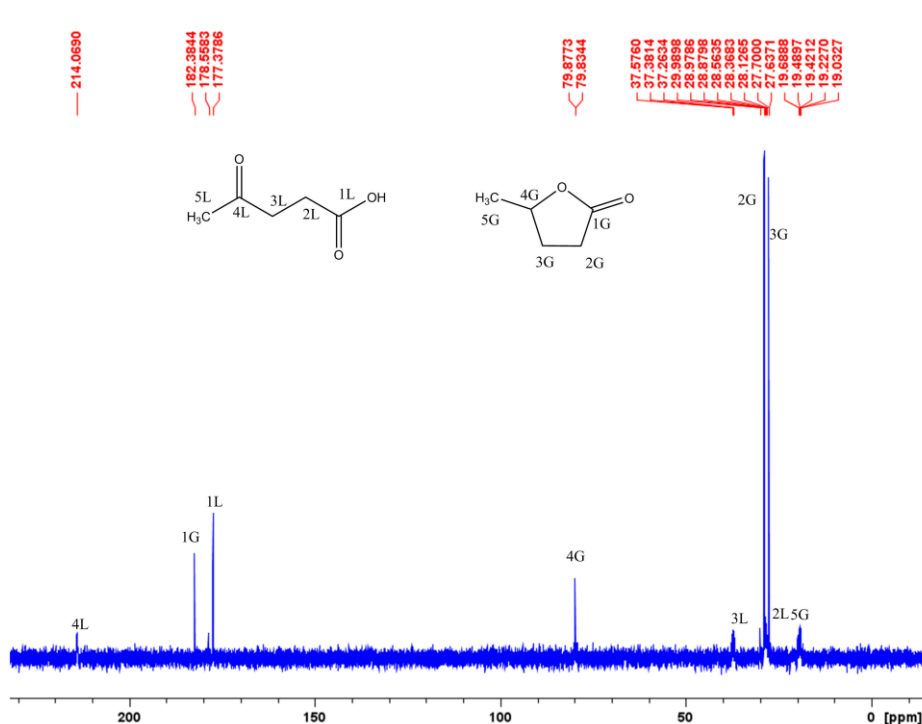


Figure 68. ^{13}C NMR of post reaction mixture from LA to GVL hydrogenation reaction catalysed by $\text{Ru}/\text{Al}_2\text{O}_3$. The reaction was conducted using D_2O as the solvent. Carbon numbers include letters L for levulinic acid and G for GVL.

^{13}C NMR (500 MHz, D_2O) δ 214.1, 182.4, 177.4, 79.9, 37.6, 29.9, 28.8, 27.7, 19.7

The most likely mechanism for this exchange is through an enol formation of levulinic acid, shown in Figure 69. The process was self-catalysed by the substrate, and no catalyst was necessary for the exchange to take place. Hydrogen atoms at positions 1 and 3 can undergo alpha-deprotonation. The reverse process takes up protons from solvent in order to reform levulinic acid, and so deuteration of the substrate happened. At the same time, exchange of protons on position 4 was mechanistically impossible, as the enolate could not have formed there. This was confirmed by all NMR experiments, as the signal of that carbon in ^{13}C NMR or proton in ^1H NMR has always retained its integral size, regardless of the test carried out.

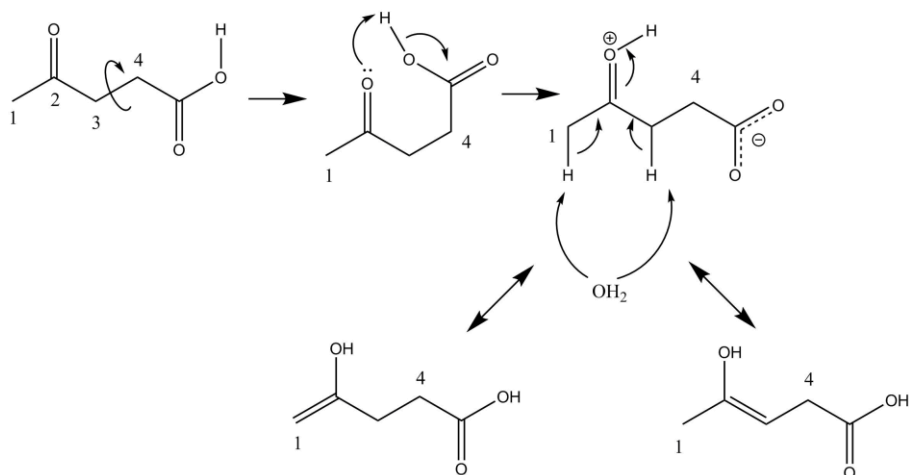


Figure 69. Proposed mechanism for the self-catalysed deuteration of levulinic acid, proceeding through an enolate.

4.3. Conclusions

This chapter has explored a novel catalyst synthesis method of copper zirconia materials, and characterisation thereof. This body of work resulted in publication of results in two papers.^{36,37}

Two distinct methods of preparation were investigated, manual and automatic. Manual preparation proved to be an inconsistent method, most likely due to the difficulty in precise, yet quick addition of base into the metal solution with the use of a burette. As such, automatic preparation was used.

A range of Cu-ZrO₂ catalysts with different copper contents were synthesised. Their activity was related to the amount of copper found in the material and the degree to which the Cu and Zr phases were mixed. Catalysts with better phase mixing performed better, indicating that Cu/Zr interface sites were the active sites for this reaction. In order to confirm this, the catalysts were acid washed and again tested for the hydrogenation of LA. All of the acid-washed catalysts had higher TOFs, and showed a very strong dependence on the amount of copper left on the catalyst. Acid treatment has washed off any labile species off the surface and left

behind copper with strong metal-support interactions, proving that the Cu/Zr interface sites were the active sites.

The effect of reduction treatment on the 30% Cu-ZrO₂ was investigated. TPR analysis was carried out and it was found that the catalyst was fully reduced at 150°C. The activity of reduced catalysts had a direct relationship with the reduction temperature. Activity decreased as the temperature increased, with the highest activity catalyst reduced at 150°C, in agreement with TPR data. Inspection of the catalyst surface with SEM and EDX showed that the most active reduced catalyst featured almost homogeneously mixed Cu/Zr phases, and the least active catalyst had phase separated.

Mechanistic and kinetic aspects of the system were explored. The reduced 30% Cu-ZrO₂ catalyst showed first reaction order with respect to hydrogen, and zeroth reaction order with respect to levulinic acid. This was in agreement with literature data on similar systems. Mechanistically, it was found that water plays a role in the hydrogenation process, possibly facilitating it by providing an alternate pathway for the hydrogen to travel. This was confirmed by deuteration studies analysed with ¹³C and ¹H NMR alongside GC-MS, and deuterium was observed in the GVL product.

The findings in this chapter provide an insight into use of non-critical metals as a replacement for the widely used noble metals for the hydrogenation of LA to GVL. The main issue with these catalysts remains the high content of copper, which is likely less economically feasible than the low loadings required for noble metals. Still, the work represents a step forward in the direction of cheaper catalysis of renewable fuel sources.

4.4. References

- 1 T. Werpy and G. Petersen, *Top Value Added Chemicals from Biomass Volume I — Results of Screening for Potential Candidates from Sugars and Synthesis Gas*, 2004.
- 2 Q. Xu, X. Li, T. Pan, C. Yu, J. Deng, Q. Guo and Y. Fu, *Green Chem.*, 2016, **18**, 1287–1294.
- 3 X.-L. Du, Q.-Y. Bi, Y.-M. Liu, Y. Cao, H.-Y. He and K.-N. Fan, *Green Chem.*, 2012, **14**, 935.
- 4 P. P. Upare, J.-W. Yoon, M. Y. Kim, H.-Y. Kang, D. W. Hwang, Y. K. Hwang, H. H. Kung and J.-S. Chang, *Green Chem.*, 2013, **15**, 2935.
- 5 Y. Zuo, Y. Zhang and Y. Fu, *ChemCatChem*, 2014, **6**, 753–757.
- 6 L. E. Manzer, *Appl. Catal. A Gen.*, 2004, **272**, 249–256.
- 7 L. Qi, Y. F. Mui, S. W. Lo, M. Y. Lui, G. R. Akien and I. T. Horváth, *ACS Catal.*, 2014, 1–11.
- 8 D. Pimentel, *Nat. Resour. Res.*, 2003, **12**, 127–134.
- 9 R. Rathmann, A. Szklo and R. Schaeffer, *Renew. Energy*, 2010, **35**, 14–22.
- 10 M. B. Sainz, *Biofuels Glob. Impact Renew. Energy, Prod. Agric. Technol. Adv.*, 2011, 237–264.
- 11 I. T. Horváth, H. Mehdi, V. Fábos, L. Boda and L. T. Mika, *Green Chem.*, 2008, **10**, 238–242.
- 12 D. M. Alonso, S. G. Wettstein and J. A. Dumesic, *Green Chem.*, 2013, **15**, 584.
- 13 J. Q. Bond, D. M. Alonso, D. Wang, R. M. West and J. a Dumesic, *Science*

- (80-), 2010, 1110–1114.
- 14 D. R. Jones, S. Iqbal, S. Ishikawa, C. Reece, L. M. Thomas, P. J. Miedziak, D. J. Morgan, J. K. Edwards, J. K. Bartley, D. J. Willock and G. J. Hutchings, *Catal. Sci. Technol.*, 2016, **6**, 6022–6030.
- 15 S. Ishikawa, D. R. Jones, S. Iqbal, C. Reece, D. J. Morgan, D. J. Willock, P. J. Miedziak, J. K. Bartley, J. K. Edwards, T. Murayama, W. Ueda and G. J. Hutchings, *Green Chem.*, 2017, **19**, 225–236.
- 16 J. W. Patterson, R. E. Boice and D. Marani, *Environ. Sci. Technol.*, 1991, **25**, 1780–1787.
- 17 S. Velu, K. Suzuki, M. Okazaki, M. P. Kapoor, T. Osaki and F. Ohashi, *J. Catal.*, 2000, **194**, 373–384.
- 18 J. Sloczynski, R. Grabowski, A. Kozłowska, P. K. Olszewski and J. Stoch, *Phys. Chem. Chem. Phys.*, 2003, **5**, 4631.
- 19 K. D. Jung and A. T. Bell, *J. Catal.*, 2000, **193**, 207–223.
- 20 H.-Y. T. Chen, S. Tosoni and G. Pacchioni, *ACS Catal.*, 2015, **5**, 5486–5495.
- 21 D. L. Hoang, H. Berndt and H. Lieske, *Catal. Letters*, 1995, **31**, 165–172.
- 22 T. Takeguchi, S. N. Furukawa and M. Inoue, *J. Catal.*, 2001, **202**, 14–24.
- 23 V. A. Hackley and A. B. Stefaniak, *J. Nanoparticle Res.*, 2013, **15**, 1742.
- 24 N. T. K. Thanh, N. Maclean and S. Mahiddine, *Chem. Rev.*, 2014, **114**, 7610–7630.
- 25 K. V. R. Chary, G. V. Sagar, C. S. Srikanth and V. V. Rao, *J. Phys. Chem. B*, 2007, **111**, 543–550.
- 26 S. Lomate, A. Sultana and T. Fujitani, *Catal. Letters*, 2018, **148**, 348–358.

- 27 S. C. Patankar and G. D. Yadav, *ACS Sustain. Chem. Eng.*, 2015, **3**, 2619–2630.
- 28 I. Ro, Y. Liu, M. R. Ball, D. H. K. Jackson, J. P. Chada, C. Sener, T. F. Kuech, R. J. Madon, G. W. Huber and J. A. Dumesic, *ACS Catal.*, 2016, **6**, 7040–7050.
- 29 P. M. de Souza, R. C. Rabelo-Neto, L. E. P. Borges, G. Jacobs, B. H. Davis, D. E. Resasco and F. B. Noronha, *ACS Catal.*, 2017, **7**, 2058–2073.
- 30 J. Wang, S. Jaenicke and G.-K. Chuah, *RSC Adv.*, 2014, **4**, 13481–13489.
- 31 G. Fuchsel, K. Cao, S. Er, E. W. F. Smeets, A. W. Kleyne, L. B. F. Juurlink and G. J. Kroes, *J. Phys. Chem. Lett.*, 2018, **9**, 170–175.
- 32 T. Abdollahi and D. Farmanzadeh, *J. Alloys Compd.*, 2018, **735**, 117–130.
- 33 M. Al-Naji, A. Yopez, A. M. Balu, A. A. Romero, Z. Chen, N. Wilde, H. Li, K. Shih, R. Gläser and R. Luqueb, *J. Mol. Catal. A Chem.*, 2016, **417**, 145–152.
- 34 J. Tan, J. Cui, T. Deng, X. Cui, G. Ding, Y. Zhu and Y. Li, *ChemCatChem*, 2015, **7**, 508–512.
- 35 F. B. Lindsay R. Merte, Guowen Peng, Ralf Bechstein, Felix Rieboldt, Carrie A. Farberow, Lars C. Grabow, Wilhelmine Kudernatsch, Stefan Wendt, Erik Lægsgaard, Manos Mavrikakis, *Science (80-.)*, 2012, **889**, 889–894.
- 36 J. Hirayama, I. Orłowski, S. Iqbal, M. Douthwaite, S. Ishikawa, P. J. Miedziak, J. K. Bartley, J. Edwards, Q. He, R. L. Jenkins, T. Murayama, C. Reece, W. Ueda, D. J. Willock and G. J. Hutchings, *J. Phys. Chem. C*, 2018, **123**, 7879–7888.
- 37 I. Orłowski, J. Hirayama, T. E. Davies, S. Iqbal, J. K. Bartley, D. J. Morgan,

M. Douthwaite, D. J. Willock, P. J. Miedziak, G. J. Hutchings and J. S. Hayward, *J. Energy Chem.*, 2019, **36**, 15–24.

Chapter 5

All references are self-contained to within this chapter, and do not refer to any other chapters.

Conclusions and future work

This thesis has explored the reaction pathway from glucose to γ -valerolactone using a range of materials. The entire body of work presented in this thesis was part of the international NOVACAM project, tasked with finding cheap, novel ways of converting biomass to useful chemicals. This chapter re-evaluates conclusions drawn from the work done and discusses additional research which would complement the findings.

The work in this thesis contributed towards two publications:

- “The hydrogenation of levulinic acid to γ -valerolactone over Cu–ZrO₂ catalysts prepared by a pH-gradient methodology”¹
- “The Effects of Dopants on the Cu–ZrO₂ Catalyzed Hydrogenation of Levulinic Acid”²

“Green catalysis by design” school and conference were attended on the 22nd and 23rd of February 2017 in Padova, Italy, as a final meeting of the NOVACAM consortium.

5.1. Conversion of methyl glucoside to methyl levulinate using solid acid catalysts

In this chapter, a range of metal oxide-based materials was prepared and tested for the dehydration of methyl glucoside to methyl levulinate. Initially, the esterification of glucose to methyl glucoside was investigated. It was found that the esterification reached 100% yield after 16 hours with mineral acid, and conversion of 77% was obtained after 2 hours. At the relatively mild temperature of 80 °C, the only products were the two anomers of methyl glucoside, α (the thermodynamic product) and β (the kinetic product). As the esterification step was found to readily take place at much lower temperatures than the temperature planned for the overall reaction (180 °C), further research was focused on conversion of methyl glucoside to methyl levulinate. It was found that $\text{SO}_4\text{-ZrO}_2$ was the best performing material (yielding 24% ML after one hour) and the sulfation process was crucial to adding desired catalyst functionality. ZrO_2 on its own did not produce any methyl levulinate. Only two other materials were found to yield ML, $\text{SO}_4\text{-TiO}_2$ (15% yield after one hour, and 35% yield after two hours) and $\text{WO}_3\text{-ZrO}_2$ (1.5% yield). Other metal oxides, such as CeO_2 and P25 were acidified, however they did not yield any ML despite converting some of the substrate. This was speculated to be due to lack of amphoteric effect of these oxides. Acidity profiles of $\text{SO}_4\text{-ZrO}_2$ and $\text{SO}_4\text{-TiO}_2$ were measured using NH_3 TPD. Sulfated zirconia was found to be over twice as acidic as sulfated titania, at 0.77 mmol g^{-1} and 0.33 mmol g^{-1} , respectively. This likely correlated with the increased BET surface area of $\text{SO}_4\text{-ZrO}_2$ at 157 m^2g^{-1} compared to 80 m^2g^{-1} for $\text{SO}_4\text{-TiO}_2$, and increased sulfur content on the surface (measured with XPS), indicating higher sulfation rate – and therefore higher number of acid groups. Pyridine DRIFTS was used to further elucidate the effects of sulfation procedure on ZrO_2 . The untreated metal oxide only contained weak Lewis acid sites, unstable above approximately 350 °C. However, the sulfation treatment resulted in a material

with both Lewis, and strong Brønsted-type acid sites. The Brønsted sites were stable at 550 °C, near the instruments' maximum temperature range of 575 °C.

The next section of the chapter focused on testing of zeolites for dehydration of methyl glucoside. Zeolite β (38) was found to be the best performing zeolite material, yielding 12% ML after one hour. Despite higher acidity, zeolite β (25) did not produce more ML, but it did result in a higher number of side-reactions, and as such, a lower carbon balance. ZSM-5 produced negligible amounts of ML due to its smaller pore size when compared to the β -material.³ In an effort to reduce the polymerisation side-reactions, a silylation procedure was carried out on Zeolite β (38), covering the surface acid sites; the assumption was made that the polymerisation takes place on the surface of the catalyst rather than the pores due to size of the polymer and available space on the surface. The procedure slowed the reaction rate down to approximately 75% rather than limiting the polymerisation reactions.

The analysis of humins in this chapter has led to a new set of experimental conditions focused on reducing the polymerisation. During the process of polymer analysis, it became apparent that there were solvent issues causing the reported values to be slightly inflated. This was rectified with the addition of an internal standard into the reaction mixture before the reaction takes place. This has resulted in a drop in reported conversion and yield values; however, the new set of conditions also proved to minimise humin formation.

A reaction mechanism was proposed at the end of the chapter, stemming from the known product profile and corroborated with a short section of mechanistic studies of furfural and furfural alcohol. The results of these experiments agreed with the proposed mechanism; however, the conditions utilised were very mild when compared to the conditions used in the dehydration reaction. This was due to safety concerns surrounding use of furans at high temperatures in an unventilated area,

where the autoclave reactors were located. A set of further experiments with furfural and furfural alcohol at standard reaction conditions would complement the results greatly, but literature reports were in agreement with the findings in this chapter.⁴⁻⁸

5.2. Conversion of levulinic acid to γ -valerolactone using Cu-ZrO₂ catalysts

Chapter 4 centred on the conversion of levulinic acid to γ -valerolactone using copper-zirconia catalysts. This chapter builds on the findings from the previous one, by taking the levulinic acid product and hydrogenating it to a potential fuel additive. The link is not direct, i.e. in chapter 3 methyl levulinate in methanol was the product whereas in chapter 4 it is levulinic acid in water is used; this is because the research is a continuation of previous work established within the Hutchings group on Cu-ZrO₂ materials.^{9,10} The focus of this chapter was on developing a novel catalyst synthesis method. The aim was to prepare a novel Cu-ZrO₂ material with lower Cu loading than previous catalysts developed within the group, while retaining high activity.

Initially, the catalysts were prepared manually with a hand-controlled burette dropping base into the metal mixture. This methodology was soon replaced by an automatic preparation using an autotitrator, due to inconsistencies between different batches. A range of materials with different copper loadings (10% - 50% mol.) were prepared and tested for the hydrogenation reaction. It was found that the best performing catalysts were those with well-mixed Cu - Zr phases (strong metal-support interactions), and small, well-dispersed particles. This was achieved with a 30% Cu-ZrO₂ catalyst reduced at 150 °C. Images obtained with SEM and EDX of catalysts reduced at a range of temperatures from 150 °C to 500 °C showed as the reduction temperature increased, so did the separation of copper and zirconia phases. The copper crystallite size also increased drastically, from approximately 4.5 nm at 150 °C to approximately 87 nm at 500 °C. The phase separation and increase in Cu crystallite size was the likely cause of decreased activity.

The catalysts were then subject to an acid wash procedure. This was done to remove any labile species of copper from the surface and expose the particles with strong metal-support interactions. It was found that a significant amount (up to 77% for 50% Cu-ZrO₂) of the original copper was washed off in the process. However, it was found that the acid washed catalysts had notably higher TOF values than the non-treated catalysts. This suggests that the active species on this catalyst was indeed the copper that had strong metal-support interactions.

Mechanistic studies were carried out to assert if water is involved in the hydrogenation mechanism when a copper catalyst is present, as reported by Tan *et al.* when ruthenium-catalyst was used.¹¹ Hydrogenation of LA to GVL using 5% Ru/Al₂O₃, 50% Cu-ZrO₂ and 1% Mn/Cu-ZrO₂ was investigated using GC-MS, ¹³C and ¹H NMR. The experimental results were in agreement with literature – deuterated protons from the solvent were found to be incorporated into GVL at the position where hydrogenation takes place. However, with copper catalysts the deuteration took place in several other sites on the molecule when compared to ruthenium catalyst. Ultimately, this was found to be the result of high temperature utilised (200 °C). LA self-catalysed the formation of LA enolate at high temperatures, an event which did not occur at temperatures used with the ruthenium catalyst (130 °C). When ruthenium was used at 200 °C, an identical effect was found. In summary, water was involved in the hydrogenation mechanism.

5.3. Future work

5.3.1. Conversion of methyl glucoside to methyl levulinate using solid acid catalysts

The scope of materials tested for the conversion of MeGlc to ML could be expanded. Several materials were tested, and an attempt was made to acidify them. Reactions were carried out with the goal of yielding ML. If a material did not produce

any, it was not investigated further. However, it is possible that all the materials were acidified successfully – perhaps the strength of the acid was too weak to facilitate the reaction. Likewise, the acidification procedure could have failed. For example, phosphated zirconia was not active at all, however literature reports production of levulinic acid with this material.¹² Ammonia TPD and pyridine DRIFTS studies were carried out on selected materials only, however in order to fully understand the pattern of activity, the analysis should be carried out on all the tested catalysts.

Interestingly, $\text{WO}_3\text{-ZrO}_2$ was also found to produce ML. Tungsten has been known to display acidic behaviour.¹³⁻¹⁵ Zhang *et al.* reported synthesis of a tungsten-tellurium oxide catalyst capable of producing 8.5% yield LA from cellulose after 2 hours at 175 °C in water solvent.¹⁶ Liu *et al.* reported 21% yield of levulinic acid from glucose at 180 °C in a 60 minute reaction with $\text{WO}_3\text{-Ta}_2\text{O}_5$.¹⁷ Despite the catalyst's ability to complete the reaction pathway, tungsten was not investigated further because of additional costs associated with use of tungsten and the guidelines outlined at the start of the NOVACAM project. However, further investigation into preparation procedures and metal support variation could have resulted in a well-performing catalyst. Similar, other potentially active metals were not investigated due to assertions made at the beginning of the project. Niobium, reported to be effective for the conversion of methyl glucoside to methyl levulinate by Ding *et al.* in the form of niobium phosphate solid acid catalyst.¹⁸ Chromium which was found not only facilitating the dehydration of glucose to 5-HMF as a CrCl_2 salt paired with *N,N*-dimethylacetamide solvent (81% yield)¹⁹, or directly to LA in water as $\text{CrCl}_2\cdot 6\text{H}_2\text{O}$,²⁰ it was also effective for the hydrogenation of LA to GVL as Cr-Cu oxide.²¹ Like tungsten, these materials were outside of the scope of NOVACAM. However, exploration of these metals could potentially lead to more effective catalysts.

A limited variety of acidification techniques was tested. There is potential in using more varied acid sources apart from H₂SO₄. For example, Sun *et al.* reported a solid heteropoly-acid based material functionalised with lysine, Ly_{0.5}H_{2.5}PW (based on phosphotungstic acid, H₃PW₁₂O₄₀).²² They obtained 53% yield of LA after 30 minutes at temperature of 130 °C. One of the key points in their work is the use of choline chloride (ChCl) as a solvent – in conjunction with glucose, ChCl formed a deep eutectic solvent, that is a mixture of a solid salt (ChCl) and a hydrogen-bond donor (in this case glucose) in specific ratios.²³ The reasoning for the use ChCl as solvent was two-fold: it is a cheap, abundantly available molecule, and reportedly it limited the formation of HMF while not hindering formation of LA. This highlights another area of future interest: testing of different solvents. While the NOVACAM project focused on water and methanol-based systems, a multitude of solvent systems can potentially be effective for this reaction. Ionic liquids can be functionalised with acidic groups,²⁴ and have been reported as effective catalysts and solvents for the conversion of glucose to LA. Komal *et al.* reported 47% yield of LA from glucose using 1-(4-Sulfonic acid)butyl-3-methylimidazolium chloride (IL-SO₃H) after 5 hours at 155 °C.²⁵ The ionic liquid formed *in situ* HCl, which then catalysed the reaction. Amin *et al.* reported 68% yield by weight using 1-sulfonic acid-3-methylimidazoliumtetrachloroferrate ([SMIM][FeCl₄]) after 4 hours at 150 °C.²⁶ Apart from ionic liquids, GVL has been investigated as a solvent. Dumesic *et al.* reported 66% yield of LA from corn stover using 0.2M H₂SO₄ and 80% GVL solvent.²⁷ Horvath reported 52% yield of LA from glucose in GVL solvent using 5M H₂SO₄.²⁸ There is therefore precedent to explore different solvents, especially if they could potentially solubilise humins.

Additional work could also be carried out on zeolites. Zeolite Y was not tested, even though it is known to be comparable in activity to zeolite β for this reaction.²⁹ This was the case because of supply issues. Secondly, all the zeolites

should have their acidity assessed and quantified with ammonia TPD and pyridine DRIFTS. This would help paint a complete picture of how acidity impacts activity. The silylation procedure was not explored in enough depth. There was room to explore various silylating agents in different loadings. The silylated materials structure was also not quantitatively or qualitatively assessed. Perhaps a surface acidity measurement would give an indication of the change in structure. If the assumption that humins are largely formed on the surface of the catalyst rather than the pores is correct, developing the silylation procedure has potential to have significant impact on catalyst re-usability, yields, and limiting polymerisation.

Chapter 3 would also benefit from more detailed reaction mixture analysis. There were only several identified peaks in HPLC or GC spectra, with many side-products and intermediates not identified. This would not only help with accounting for much of the missing carbon balance, but also assist in a better understanding of the reaction mechanism. This could be achieved with LC-MS or GC-MS equipment, paired with 2D-NMR experiments. 1D-NMR was attempted on the post-reaction mixture, however due to the abundance of overlapping peaks, only major products were able to be identified.

5.3.2. Conversion of levulinic acid to γ -valerolactone using Cu-ZrO₂ catalysts

Chapter 4 outlined a novel catalyst synthesis method. However, only one methodology of catalyst preparation was evaluated; the preparation method relies heavily on accurate control of pH of the metal mixture over time. Perhaps a slower, more gradual addition of the precipitant would have resulted in a more active catalyst due to better mixing of Cu – Zr phases. Secondly, the catalysts were only tested for the hydrogenation of levulinic acid in water. Other solvents such as methanol could be explored. This would not only tie in with chapter 3, providing a better understanding of possible yields from a theoretical one-pot system; but also help elucidate the mechanism, as it was reported that water plays an important role in the

hydrogenation reaction.² The reaction is known to proceed in methanol, but with reduced yields and a different pathway utilising levulinate esters.³⁰

The copper catalysts were acid washed, and it was found that a large portion of the copper only plays a spectator role, and it is the small, well-dispersed copper particles with strong metal-support interactions which catalyse the hydrogenation of LA. An experiment that would further help explain this phenomenon would be the measurement of BET and Cu-surface areas of the materials. It would reveal a trend (if any exist) between surface area, dispersion of particles and activity.

With the knowledge that it is possible to limit the amount of copper in the catalyst while retaining activity, doping the pH-gradient prepared materials would be a promising avenue to explore. Hutchings group has previously reported that mixing copper-zirconia with other metals such as nickel³¹ or manganese can enhance the catalyst's activity for hydrogenation of LA.² Preparation of such mixed and doped materials by the pH-gradient method could not only reduce the amount of metal necessary (and therefore reducing cost) but also provide greater control over structure of the material. Perhaps a Cu-ZrO₂ material could be prepared by pH gradient method, acid washed to remove the spectator species, and then subsequently doped. Such materials could potentially be very effective for the hydrogenation of LA.

5.4. References

- 1 I. Orłowski, J. Hirayama, T. E. Davies, S. Iqbal, J. K. Bartley, D. J. Morgan, M. Douthwaite, D. J. Willock, P. J. Miedziak, G. J. Hutchings and J. S. Hayward, *J. Energy Chem.*, 2019, **36**, 15–24.
- 2 J. Hirayama, I. Orłowski, S. Iqbal, M. Douthwaite, S. Ishikawa, P. J. Miedziak, J. K. Bartley, J. Edwards, Q. He, R. L. Jenkins, T. Murayama, C. Reece, W. Ueda, D. J. Willock and G. J. Hutchings, *J. Phys. Chem. C*, 2018,

- 123**, 7879–7888.
- 3 M. Moliner, Y. Roman-Leshkov and M. E. Davis, *Proc. Natl. Acad. Sci.*, 2010, **107**, 6164–6168.
- 4 C.-Z. Li, S. Wang, S. Jiang, L. Wu and X. Hu, *Chem. Commun.*, 2017, **53**, 2938–2941.
- 5 D. Ren, J. Fu, L. Li, Y. Liu, F. Jin and Z. Huo, *RSC Adv.*, 2016, **6**, 22174–22178.
- 6 A. M. Hengne, S. B. Kamble and C. V. Rode, *Green Chem.*, 2013, **15**, 2540–2547.
- 7 M. A. Mellmer, J. M. R. Gallo, D. Martin Alonso and J. A. Dumesic, *ACS Catal.*, 2015, **5**, 3354–3359.
- 8 I. Guzmán, A. Heras, M. B. Güemez, A. Iriondo, J. F. Cambra and J. Requies, *Ind. Eng. Chem. Res.*, 2016, **55**, 5139–5144.
- 9 D. R. Jones, S. Iqbal, S. Ishikawa, C. Reece, L. M. Thomas, P. J. Miedziak, D. J. Morgan, J. K. Edwards, J. K. Bartley, D. J. Willock and G. J. Hutchings, *Catal. Sci. Technol.*, 2016, **6**, 6022–6030.
- 10 S. Ishikawa, D. R. Jones, S. Iqbal, C. Reece, D. J. Morgan, D. J. Willock, P. J. Miedziak, J. K. Bartley, J. K. Edwards, T. Murayama, W. Ueda and G. J. Hutchings, *Green Chem.*, 2017, **19**, 225–236.
- 11 J. Tan, J. Cui, T. Deng, X. Cui, G. Ding, Y. Zhu and Y. Li, *ChemCatChem*, 2015, **7**, 508–512.
- 12 W. C. Conner, G. A. Tompsett, A. Fernández, G. W. Huber, R. Weingarten, Y. T. Kim, E. W. Hagaman, K. S. Han and J. A. Dumesic, *J. Catal.*, 2013, **304**, 123–134.

- 13 M. L. Freedman, *Anal. Chem.*, 1960, **32**, 637–639.
- 14 M. A. Cortés-Jácome, C. Angeles-Chavez, E. López-Salinas, J. Navarrete, P. Toribio and J. A. Toledo, *Appl. Catal. A Gen.*, 2007, **318**, 178–189.
- 15 C. Yue, G. Li, E. A. Pidko, J. J. Wiesfeld, M. Rigutto and E. J. M. Hensen, *ChemSusChem*, 2016, **9**, 2421–2429.
- 16 Z. Zhang, M. Sadakane, N. Hiyoshi, A. Yoshida, M. Hara and W. Ueda, *Angew. Chemie - Int. Ed.*, 2016, **55**, 10234–10238.
- 17 Q. Liu, F. Yang, H. Yin and Y. Du, *RSC Adv.*, 2016, **6**, 49760–49763.
- 18 D. Ding, J. Xi, J. Wang, X. Liu, G. Lu and Y. Wang, *Green Chem.*, 2015, **17**, 4037–4044.
- 19 J. B. Binder and R. T. Raines, *J. Am. Chem. Soc.*, 2009, **131**, 1979–1985.
- 20 C. Loerbroks, J. Van Rijn, M. P. Ruby, Q. Tong, F. Schüth and W. Thiel, *Chem. - A Eur. J.*, 2014, **20**, 12298–12309.
- 21 Z. Li, X. Tang, Y. Jiang, Y. Wang, M. Zuo, W. Chen, X. Zeng, Y. Sun and L. Lin, *Chem. Commun.*, 2015, **51**, 16320–16323.
- 22 Z. Sun, S. Wang, X. Wang and Z. Jiang, *Fuel*, 2016, **164**, 262–266.
- 23 P. Domínguez de María and Z. Maugeri, *Curr. Opin. Chem. Biol.*, 2011, **15**, 220–225.
- 24 N. A. S. Ramli and N. A. S. Amin, *Adv. Mater. Res.*, 2013, **699**, 155–160.
- 25 K. Kumar, F. Parveen, T. Patra and S. Upadhyayula, *New J. Chem.*, 2018, **42**, 228–236.
- 26 N. A. S. Ramli and N. A. S. Amin, *J. Mol. Catal. A Chem.*, 2015, **407**, 113–121.

- 27 D. M. Alonso, S. G. Wettstein, M. A. Mellmer, E. I. Gurbuz and J. A. Dumesic, *Energy Environ. Sci.*, 2013, **6**, 76–80.
- 28 L. Qi, Y. F. Mui, S. W. Lo, M. Y. Lui, G. R. Akien and I. T. Horváth, *ACS Catal.*, 2014, 1–11.
- 29 S. Saravanamurugan and A. Riisager, *ChemCatChem*, 2013, **5**, 1754–1757.
- 30 A. M. Hengne and C. V. Rode, *Green Chem.*, 2012, **14**, 1064.
- 31 D. R. Jones, S. Iqbal, L. Thomas, S. Ishikawa, C. Reece, P. J. Miedziak, D. J. Morgan, J. K. Bartley, D. J. Willock, W. Ueda and G. J. Hutchings, *Catal. Struct. React.*, 2018, **4**, 12–23.